Development of A Novel Casting Alloy Composed of Aluminum and Cerium with other Minor Additions

A Dissertation Presented for the

Doctor of Philosophy

The University of Tennessee Knoxville

Zachary Cole Sims

December 2020

Dedication

To my wife and parents,

Melinda, Paul, and Carla

I would have never been able to succeed without the solid footing on which you have kept me throughout this process and my life.

Acknowledgements

It goes without saying that I would not have had the capability to craft and execute the research contained below without the support of many individuals. Dr. Orlando Rios my advisor was willing to let me grow as a metallurgical material scientist with no background in metals prior to starting work on the Al-Ce alloy project five years ago. Thank you for the opportunity and guidance on my pathway to success. Also, Orlando's flexibility in allowing me to pursue additional extracurricular interests such as policy making and community development must be acknowledged. During my time with the Bredesen Center, I have been able to assist in the formation of several important organizations at the department, collegiate, and state level. I would have never had these opportunities were it not for Orlando's understanding of my varied interests. Also, thanks must be afforded to everyone who is a part of my committee and the clarity they have provided during my dissertation research and preparation.

Next, I must thank the numerous collaborators without whose help I would have no progress to show. Firstly, to David Weiss at Eck industries for opening the way to cast numerous compositions and thousands of pounds of material, perform hundreds of mechanical tests, X-ray many cast pieces, and ship samples all over the country during the past four years without which this project would not have been successful. To Drs. Scott McCall, Aurelien Perron, Emily Moore, and Patrice Turchi for the constant guidance and support your team provides regarding my learning and building experience with CALPHAD modeling and predictions. To Drs. Hunter Henderson and Michael Kesler, for consistently being available to discuss results, conclusions, and how the Tennessee Vols really are the better sports program. Finally, to all my other collaborators who have supported this work in numerous ways.

Thank you, Dr. David Keffer, for your consistent input and thoughtful guidance during this process. Also, for the exciting outings in which I was included as a part of your team.

Many thanks should also be afforded to those in the Bredesen Center. Without your acceptance of me and continued support I would not be here today. Specific thanks must be afforded to Dr. Lee Riedinger, Suresh Babu, Allie Burns, and Wanda Davis for responding to innumerable emails, providing consistent and clear guidance, and being the foundation on which the program is built.

Finally, I must thank the Critical Materials Institute for funding this research and providing me the opportunity to succeed.

Abstract

Eutectic casting alloys of aluminum and cerium are a recent discovery and early research describes an alloy with great potential to meet the growing demand for a lightweight, economical, high specific strength material for use in high-temperature or extremely corrosive environments. The broad application of aluminum alloys across industry sectors is driven by their collection of balanced properties including economical cost, high specific strength, and flexibility of their production pathways. Additionally, their high corrosion resistance makes them a good choice for structural materials. Despite this, the push to use aluminum alloys in ever more extreme environments with higher temperatures, stresses, and corrosive potential has precipitated the need to develop a next generation of aluminum alloys. Aluminum-cerium alloys which take advantage of the stable eutectic intermetallic formed between aluminum and cerium has the potential to exhibit all of the necessary material properties for recognition as a next generation aluminum alloy. In this report the early stage development of aluminum-cerium alloys designed for casting will be discussed. Work will include: the discussion of castability and mechanical properties of several binary and higher order alloys, a construction of the design paradigm for aluminum-cerium alloys, discussion of possible cerium substitutes, investigation of extended high-temperature stability of aluminum-cerium alloys, a study of the many ways cerium can impact corrosion resistance of aluminum alloys, and a discussion of the possible implications broad use of aluminum-cerium alloys will have for future supply chains and foundry infrastructure. Aluminum-cerium alloys have potential to become a major family of aluminum alloys, like Al-Si and Al-Cu, but much work remains to be completed. This report clearly details the earliest work in the burgeoning field of aluminum-cerium alloys and motivates the continued research into their use in modern engineering design.

Table of Contents

List of Tables

List of Figures

1. Introduction

1.1 Background

Aluminum alloys are desirable as structural materials due to their outstanding castability, excellent mechanical properties, and low cost. They occupy a technoeconomic position where their low density but moderate strength in the 150-250 °C temperature range makes them an economical choice over more costly titanium alloys and a good choice for light weighting parts previously produced from ferrous materials. Within the transportation sector, the high strength to weight ratio, corrosion resistance, and high thermal conductivity of aluminum alloys have long motivated their use in aircraft, but their application is expanding across the automotive and aerospace industries due to the promise of improved performance and fuel economy[1–4]. This document proposes the development and study of a new family of economically competitive aluminum alloys containing 6-16 weight percent (wt. %) cerium which should exhibit dramatically improved high-temperature mechanical properties, in addition to improved castability and thermal stability when compared to existing aluminum alloys. Furthermore, they may not require post-casting heat treatment, a step which can add significantly to the manufacturing cost in terms of energy, time, and infrastructure requirements.

Castable engineering alloys are typically strengthened through precipitation of intermetallic phases from alloying elements dissolved during the casting process or driven into solution by heat-treating[5]. These strengthening precipitates improve alloy performance by increasing stiffness and strength, while lowering thermal expansion[6,7]; however they reside in kinetically frozen high energy architectures along chemical potential gradients that lead to instabilities at elevated temperatures[8]. The high mobility of traditional alloying elements leads to coarsening through processes such as Ostwald ripening; thus, prolonged exposure to high temperatures leads to dramatic changes in the microstructure and a corresponding degradation of mechanical properties[9]. The loss of mechanical performance bounds the maximum operating temperature near the alloy aging temperature during the final step of heat treatment (155-190 °C for most Al alloys)[10]. This limitation becomes particularly significant for internal combustion engines which benefit from light-weight materials compatible with higher temperatures for both the engine and nearby components.

In the early 1980's some promising research and development efforts revealed that aluminum alloys containing 4 wt% cerium exhibit high temperature mechanical properties that exceed the

best commercial aluminum casting alloys currently in production [11]. That work did not continue due to cerium cost and supply challenges, even though these alloys had both high room and elevated temperature strengths. Since that time, cerium production has ramped-up driven by increased demand for the heavier rare earth elements found as co-deposits in the most common ore bodies[12]. The increased supply with relatively low demand makes cerium an affordable and available choice for investigation as a eutectic primary addition to aluminum alloys.

Aluminum cerium alloy components prepared via powder metallurgy processing and forging exhibited tensile strengths of 297 MPa at 232 °C [11]. This compares to typical tensile strengths of 110-180 MPa for Al-Cu and Al-Mg-Zn systems at that temperature[13]. The alloy has not been developed for casting nor have the casting characteristics been determined.

The aluminum casting industry is an integral part of a performance driven market segment that immediately responds to improved properties by early adoption of technological innovations. Successful alloy development and demonstration of enhanced high-temperature mechanical properties is expected to lead to rapid commercialization in the high-performance segment followed by wide scale adaptation by the larger less dynamic cost driven markets.

1.2 Objectives

The successful development of this alloy will have broader technological impact than simply providing for a new high temperature aluminum alloy material. High Ce level aluminum alloys could assist in stabilizing the price of the heavier rare earth elements that are most important to green energy technologies and have high sensitives to supply chain disruptions. The elements in question, heavier rare earth elements Nd and Dy, are required for continued rapid growth of the renewable energy sector and vehicle electrification[14,15].

The enhanced properties enabled by Ce additions to aluminum are expected to be attractive in the transportation sector for applications such as automotive cylinder heads, turbo charger housing and cold-side impellers. Mechanical property improvements of 20-40% at high temperatures improve the thermodynamic efficiency of end products such as internal combustion engines leading to reductions in fuel consumption while enabling more extensive use of castable lightweight materials. Additionally, the enhanced high temperature mass specific mechanical properties can be used to manufacture lighter drive trains and expand the use of lightweight materials in commercial transport vehicles such as tractor trailers.

The objective of this work is then to develop baseline understanding of several material properties which are key to the early development of a new alloy family. Among the properties of interest are the castability, corrosion, high temperature performance, and compositional effects. Each of these properties has been investigated through numerous methods. The creation of a baseline understanding of each material property outlined will provide a launching point for future work and more targeted development of Al-Ce alloys and their various possible applications.

1.3 Chapter Summaries

1.3.1 Castabilty of an Aluminum Cerium Alloys

Casting, in its many embodiments, is the most common method for producing aluminum alloy products. Understanding the castability of Al-Ce alloys will be paramount for crafting a full understanding of this new family of alloys. This chapter will focus on the investigating the ability to cast aluminum-cerium alloys using expendable sand-casting techniques. A broad range of compositions will be used to study and understand the effect of ternary and quaternary additions on the castability of aluminum-cerium binary alloys, including the following:

- Al-Ce
- Al-Ce-Mg
- Al-Ce-Cu
- Al-Ce-Ni
- Al-Ce-Ti
- Al-Ce-Fe
- Al-Ce-Si-Mg
- Al-Ce-Si-Cu-Mg

The data show that Al-Ce alloys are castable across a broad range of compositions including those containing Mg and Si, two major aluminum alloying components. Additionally, the alloys were determined to be castable without the need for any foundry best-practice modifications. This means that Al-Ce alloys could be a drag-and-drop solution for end users interested in increasing mechanical strength at elevated temperature. Data additionally shows that some compositions may be ductility limited and will require further investigation to determine viability or necessary modifications.

1.3.2 Developing an Al-Ce Material Design Paradigm

The novelty of Al-Ce alloys as a family of lightweight alloys for elevated temperature applications

means little background data exists on the mechanisms which enable high temperature mechanical properties, provide for excellent castability across broad compositional ranges, and influence the formation of numerous complex intermetallic compounds during or following solidification. As a result, new CALPHAD models are developed alongside experimental work which include neutron scattering to understand the source of the material property behavior and as a groundwork for future alloy selection.

1.3.3 Efficacy of Using Mischmetal as Primary Alloying Addition

The family of light rare-earth elements are all chemically similar - possessing the same number of valence electrons, similar electronegativities, and atomic radii that changes very little from lanthanum to neodymium[16,17]. This chemical similarity between the LREEs creates nearly identical phase spaces when they are combined with other elements. For example, all feature high-temperature Al-rich intermetallic of the composition $Al_{11}(LREE)_3$ and very similar eutectic compositions. A few distinctions can be seen however, such as the slightly higher liquidus temperature in the hypereutectic region of the heavier elements. The similarity of these phase diagrams leads to the expectation one could substitute any number of these elements or combine them with cerium to produce aluminum alloys with similar properties. This flexibility in metallic primary additions creates a more diverse supply chain and lowers the risk of using LREE materials in aluminum alloys.

Al-MM alloys have been cast from a material sourced through MP materials (a subsidiary of Mountain Pass Mine) in the US. They were cast in two geometries, a permanent mold test bar and step plate. The results show: Al-MM compositions have similar microstructure to that of cast Al-Ce alloys; the intermetallic phase formed during solidification of the Al-MM alloy is an isomorphic solid solution to that of the Al11Ce3 intermetallic formed in the binary Al-Ce alloy; and mechanical strength of Al-MM alloys is slightly greater over that of the Al-Ce alloys.

1.3.4 Resistance of Al-Ce-Mg alloys to Loss of Mechanical Strength following Extended Exposure to Elevated Temperatures

Aluminum alloys have long been used in light weighting application as they have excellent specific strength and good corrosion resistance among other desirable properties[5,13,18]. However, the high sensitivity of their strength to elevated temperature has limited their application in temperatures above 250 °C. Aluminum-cerium alloys are strengthened by combining ternary addition solid

solution mechanisms with thermally stable intermetallic compounds that are highly resistant to coarsening and evolution during exposure to elevated temperature.

This chapter will focus on the comparison of the long-term thermal stability of aluminum-cerium alloys with those of more traditional aluminum alloys. Experiments will focus on probing the behavior of Al-Ce-Mg alloys at elevated temperature and if there are regions of instability due to the complex interactions of Al, Ce, and Mg. Comparing the behaviors at application relevant temperatures (250 °C and 400 °C) will enabled direct comparison between the thermal stability of Al-Ce-Mg alloys and relative low yield strength retention of traditional aluminum alloys.

1.3.5 Resistance of Al-Ce Alloys to Aqueous Corrosion

Corrosion and the material degradation it can cause costs billions of dollars in damage to structural materials annually, and in some cases the unanticipated catastrophic failure of structural or operation critical components due to corrosion can lead to physical harm and death. Al-Ce alloys are a new family of materials which do not have a robust body of literature in place to describe their behavior following exposure to corrosive environments.

For that reason, the corrosion rates of several Al-Ce-X alloy compositions has been investigated using thee distinct but different measurement techniques. The first is natural tidal pool corrosion. The second method is the salt-fog method which studies the behavior of metal through exposure to a continuous warm saline fog. The final method is measurement of susceptibility to intergranular attack. By combining all the above tests with several Al-Ce-X alloy compositions a good understanding of how Al-Ce alloy perform in comparison to traditional alloys in corrosive environments can be developed. This fundamental understanding of Al-Ce's electrochemical properties will be key in the adoption and continued development of Al-Ce as a viable next generation alloy family.

Results show that Al-Ce alloys have great potential to be very corrosion resistant when compared to 200 and 2000 series aluminum alloys. This high performance in corrosive environments extends across the testing methods and leads to higher retained material weight and lower intergranular attack depth when compared to traditionally susceptible aluminum alloys.

1.3.6 Increase in Mechanical Properties of Al-Ce-Mg Alloys Through High Pressure Processing Routes

Despite their high strength Al-Ce-Mg alloys are shown to exhibit low ductility and significant partitioning of the Mg content in cast parts outpaces the ability to solute trap at a given cooling rate. In order to allow for elevated amounts of Mg in the alloy and thus higher amounts of solid solution strengthening an alternative treatment must be pursued. Hot isostatic pressing (HIP) has the potential to rapidly solutionize Mg without effecting the interconnected microstructure of the Al-Ce binary phase. Additionally, the combination of a heat-treat free Al-Ce-Mg alloy with HIP processing can lower the overall energy burden of alloy manufacturing and increase the foundry output with little to no modification. Results of the investigation show the ability of HIP processing to improve the mechanical strength and ductility of Al-Ce-Mg alloys in less time and with less energy input than is possible for traditional heat-treatment processing.

2. Castabilty of an Aluminum Cerium Alloys

This chapter is adapted from a slightly edited version of a published work "Cerium Based Intermetallic Strengthened Aluminum Casting Alloy: High Volume Co-Product Development" published in 2016 in the Journal of Materials a publication of TMS.

Sims, Z. C.; Weiss, D.; McCall, S. K.; McGuire, M. A.; Ott, R. T.; Geer, T.; Rios, O.; Turchi, P. A. E. Cerium-Based, Intermetallic-Strengthened Aluminum Casting Alloy: High-Volume Co-Product Development. *JOM* **2016**, *68* (7), 1940–1947. https://doi.org/10.1007/s11837-016-1943-9.

My primary contributions to this paper were: selection of alloy compositions for casting, initial modeling of binary systems using CALPHAD, SEM and XRD analysis of samples, collaboration on analysis of magnetization data, and the majority of the writing and formatting of the manuscript.

2.1 Abstract

Several rare earth elements are considered by-products to rare earth mining efforts. By using one of these by-product elements in a high-volume application such as aluminum casting alloys; the supply of more valuable rare earths can be globally stabilized. Stabilizing the global rare earth market will decrease the long-term criticality of other rare earth elements. The low demand for Ce, the most abundant rare earth, contributes to the instability of rare extraction. In this report we discuss a series of intermetallic strengthened Al alloys that exhibit the potential for new high volume use of Ce. The castability, structure, and mechanical properties of binary, ternary, and quaternary Al-Ce based alloys are discussed. We have determined Al-Ce based alloys to be highly castable across a broad range of compositions. Nano-scale intermetallics dominate the microstructure and are the theorized source of the high ductility. In addition, room-temperature physical properties appear to be competitive with existing aluminum alloys with extended high temperature stability of the nanostructured intermetallic.

2.2 Introduction

Increasing demand for Ce will indirectly impact rare earth based permanent magnets and phosphors used for efficient lighting by helping to stabilize RE production [15]. The major economic

concern with currently available high-performance permanent magnets is the availability and sensitivity to price fluctuations. Technologies that increase the demand for cerium and lanthanum can make the continued production of more high value rare earths economically viable, alleviating some of the pressure associated with modern permanent magnet manufacturing. In this contribution, we describe a potential high-volume use for Ce in the aluminum castings industry. The development of high temperature aluminum cerium alloys will provide a material solution enabling the design of higher efficiency internal combustion engines and lighter drivetrains, improving fuel economy.

The economic impact could be significant with even partial adoption of this technology. Two million metric tons of aluminum are consumed annually in transportation. For every 1% of that usage that could be a 12 wt% Ce alloy, 2400 t of cerium would be required, with global production of Ce of about 24,000 t annually. High performance aluminum is a dynamic market that quickly responds to technological innovations. The commercialization path in part will depend on the cost of cerium. At an alloy cost of under $10.00/kg there could be significant interest and adoption by the automotive industry. The high strength could result in lighter weight components and significant adoption in applications requiring good high temperature strength. At alloy costs in the $10-$20 range commercialization activities would concentrate on the military, where the alloy strength could be used advantageously for lighter weight structures. At alloy costs greater than $20/kg, commercialization activity would concentrate on the commercial, general aviation and space markets where strength and high temperature performance would be justified by the high penalty of weight. Where high temperature performance would normally be addressed by the conversion of aluminum to titanium, much higher prices may be justified. The evidence suggests that as much as 25-30% of the existing titanium market (4000 t annually) is driven by temperature performance in the 150-315 °C range, which is within the expected operating range of this alloy system [19].

In the early 1980's some promising research and development efforts focused on powder metallurgy revealed that aluminum alloys containing 4 wt% cerium exhibit high temperature mechanical properties that exceed the best commercial aluminum casting alloys currently in production. Even though these alloys had both high room and elevated temperature strengths, work did not continue due to cerium cost and supply challenges coupled with the limited applicability of power metallurgy in near net shape forming of aluminum components. Aluminum cerium alloy

components prepared via hot pressing and forging exhibited tensile strengths of 300 MPa at 230 °C [20]. This compares to typical tensile strengths of 70-180 MPa for Al Cu and Al Mg Zn systems at that temperature [21]. High Ce content Al alloys have not been developed for casting nor have the casting characteristics been determined.

The successful development of this alloy will have broad technological impact spanning the energy sector to include materials critical for modern alternative energy technologies such as Nd and Dy and into the transportation sector dominated by fossil fuels. High Ce level aluminum alloys could assist in stabilizing the price of the heavier rare earth elements that are most important to green energy. The enhanced properties enabled by Ce additions to aluminum are expected to be attractive in the transportation sector. This work may lead to the development of new high-temperature aluminum alloys suitable for applications such as automotive cylinder heads, turbo charger housing and impellers. Mechanical property improvements of 20-40% at high temperatures improve the thermodynamic efficiency of end products such as internal combustion engines leading to reductions in fuel consumption while enabling more extensive use of castable lightweight materials. Additionally, the enhanced high temperature mass specific mechanical properties can be used to manufacture lighter drive trains and expand the use of lightweight materials in commercial transport vehicles such as tractor trailers.

In this paper we report results obtained during an investigation of castability of aluminum cerium alloys and determine compositional modifications that may be required to ensure the compatibility of the alloy with near net shape casting methods such as advanced sand casting, die casting, and permanent mold squeeze casting. The aluminum casting industry is an integral part of a performance driven market segment that immediately responds to improved properties by early adaptation of technological innovations. Successful alloy development and demonstration of enhanced high temperature mechanical properties is expected to lead to rapid commercialization in the high-performance segment followed by wide scale adaptation by the larger less dynamic cost driven markets such as automobile manufacturers where there is a constant push for higher efficiency. One of the most obvious ways to improve efficiency is to reduce weight. While many powertrain components are already produced by aluminum casting, increases in specific output driven by turbocharging and new direct fuel injection concepts has led to an increase thermal and mechanical loads on engine components. Maximum temperatures can locally exceed 270°C in the flame deck for high specific output heads, diesel heads, and heads with integrated exhaust

manifolds. Conventional aluminum alloys such as 356 and 319 have lower mechanical properties at elevated temperatures [21,22]. This efficiency tradeoff is problematic when trying to increase the efficiency of an engine above a threshold value. What is needed is a lightweight aluminum alloy that maintains its mechanical properties at high temperatures.

The heaviest components of heavy-duty diesel engine are cast iron heads and blocks. Replacing these with a lightweight alternative would yield appreciable increases in efficiency thanks to the reduced weight. While there do exist some aluminum alloys which have stable mechanical properties at high temperatures; such as the Al-Sc system, they remain cost prohibitive[23,24]. It is then of great interest to design an alloy for use with existing aluminum casting practices that is both mechanically stable at high temperatures and sufficiently economical for application in modern engines. In this report we show that by increasing the cerium content to 12 wt % it is possible to create an alloy compatible with modern casting practices with the potential to meet these needs.

2.3 Casting Experimental Procedure

Al-Ce alloys were cast in binary composition of 6-16 wt% Ce. Commercially pure aluminum ingots were melted and held at approximately 785 °C. Ternary and quaternary alloys with small Si and Mg additions were also investigated. In the case of the binary and ternary alloy, cerium was added last and melt was allowed to return to temperature. The quaternary alloy was poured from the remaining heel of the alloy below. During cerium addition a highly exothermic reaction was observed with the melt temperature rising almost 25 °C in 5 minutes. This temperature increase is correlated with strong associative interactions between the Al and Ce atoms resulting in a high enthalpy of mixing that is typically associated with the formation of intermetallic compounds during solidification [25]. The total mass of each melt was approximately 25 kg and castings were poured into polymer bound sand molds at 785 °C.

The quaternary alloy was made from the already formed ternary alloy. The alloy most compatible with existing casting practices is Al-12Ce, where the number preceding the alloying element is its concentration in weight percent. We will focus on three alloys in this report: Al-12Ce; Al-12Ce-0.4Mg; and Al-12Ce-4Si-0.4Mg. After casting, test bars were heat-treated to determine the effectiveness of heat-treatment on mechanical properties. A standard T6 schedule was used; test-

bars were heated to 537 °C and held for 8 hrs. After this solutionizing step, the bars were water quenched and artificially aged at 155 °C for three hours.

2.4 Alloy Castability

The castability of an alloy is related to melt fluidity, solidification shrinkage, and mechanical properties--specifically ductility along with other thermodynamic parameters such liquidus and solidus temperatures, partitioning coefficients, and reactivity with the mold [26]. Hot tearing is a defect frequently encountered in all casting alloys and is severely detrimental to mechanical properties obtained from the cast component. The physical properties that lead to this behavior are complex; however, the most clearly identifiable feature defining castability is the propensity for hot tearing. These solidification induced defects can result in part rejection, costly evaluation of individual components and stringent control of casting parameters. The terms gate, runner, riser and casting are typically used in the description of castings and are defined in the ASM Casting Handbook [26].

In order to obtain a quantitative assessment of castability and perform an accurate comparison to commercial casting alloys, variable cooling rate tests also known as step molds were cast. A step mold, shown in Figure 2.1a is used to produce multiple cross section castings which vary the mold surface to casting volume ratio. The thin sections furthest from the riser solidify at cooling rates exceeding 500 °C/sec while the thicker sections adjacent to the rise cool at modest rates of approximately 300 °C/min. A thin section midway between the riser and the furthest section of the casting is used to provide restricted feeding of liquid metal to the furthest edge of the casting. A similarly sized thin section is attached adjacent to the riser to assure maximum feeding of the casting during solidification. Comparison of the oppositely located regions provides an assessment of castability.

Alloys were also cast into 6 arm hot-tear molds shown in Figure 2.1b that were designed to vary the length of the gating between the riser and casting at the end of each arm. The shortest arm (less than 8 cm) will easily transfer heat and molten metal from the riser to the end of the gate as opposed to the longest arm (longer than 20 cm). Evaluation of the defect density across the various length arms enables an assessment of castability and a meaningful comparison of the propensity for hot tearing between alloys cast into similar molds. Both the step plate and hot tear castings were examined with x-ray imaging shown in Figure 2.1c-e.

Figure 2.1 details the results of the castability study along with differential scanning calorimetry (DSC) of heating and cooling through the solidus and liquidus temperatures for the three casting alloys included in this report. DSC measurements were recorded using a Netzsch STA 4493F3 combination DSC and TGA. Samples were started from room temperature, heated at 20 °C/min to 750 °C then cooled at the same rate. The binary Al-12Ce exhibits exceptional castability. The hot-tear and step-plate molds fill completely with no detectable macroscopic defects (larger than 500um) present in the mold. This exceptional castability is linked to a combination of increased melt fluidity and the near isothermal solidification of the Al-12Ce alloy.

Melt fluidity is a strongly dependent on enthalpy of formation[27]. Formation of the Al-Ce intermetallic phases is strongly exothermic. The exothermic reaction observed following the addition of Ce to the melt could then be related to the increase in melt fluidity and thus high castability. We determined that the castability of the Al-12Ce base alloy met or exceeded the castability of commercial aluminum silicon casting alloys [28]. This increase in melt fluidity allows the alloy to successfully fill complex molds such as the air-cooled engine pictured in Figure 2.2a, cast from Al-12Ce alloy.

Mg is commonly used as a strengthening addition in aluminum alloys [21,28], so it was selected as a ternary additive to the Al-Ce system. As expected, castability was not impaired after an addition of only 0.4wt% Mg. Very few voids were observed in the X-Ray images of the hot-tear and step-plate molds. Additionally, no hot-tearing is present in the molds. In comparison to the binary Al-12Ce alloy, castability is improved with the end constraints and arms of the hot-tear mold, and the edges of the step-plate molds showing greater aluminum density. Looking at the DSC curve for Al-12Ce-0.4Mg and comparing it to the curve for Al-12Ce, few differences were noted. A very sharp solidification peak, only 20 °C in width, remains, and no features were discernable following solidification. However, very close inspection of the region just before solidification shows the onset of a small exothermic reaction. This feature of the DSC curve is discussed in greater detail in the microstructure analysis to follow. The similarity between the two DSC curves implies that Mg does not significantly affect the thermodynamics or phase constitution of the Al-Ce binary system, but instead strengthens the matrix phase by forming intermetallic Al-Mg precipitates and metastable clusters. Intermetallic precipitates are beneficial for increasing the strength of the ductile aluminum matrix without affecting the existing $Al_{11}Ce_3$. The high castability of the Al-

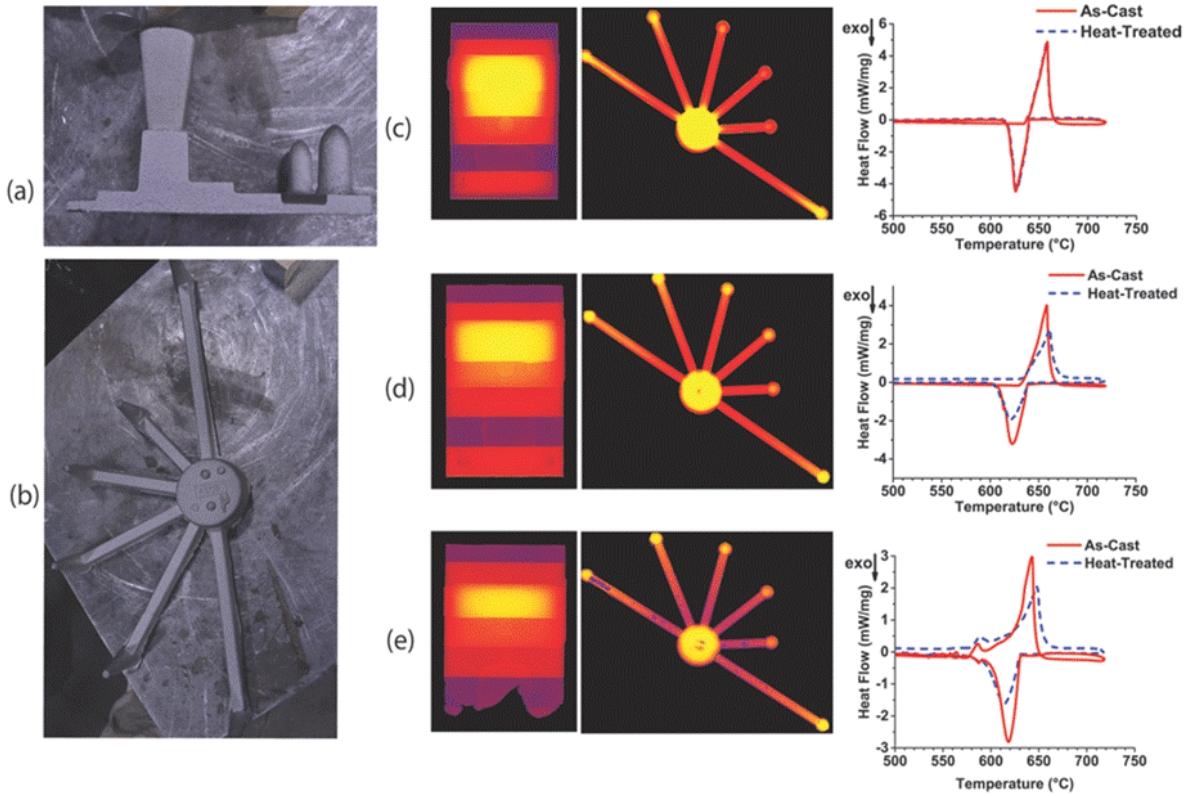

Figure 2.1: (a) Casting of step-plate used in castability assessment (b) Casting of hot-tear mold used in castability assessment. (c) Low-energy X-Ray color maps of Al-12Ce hot-tear and step-plate molds with DSC curves. (d) Low-energy X-Ray color maps of Al-12Ce-0.4Mg hot-tear and step-plate molds with DSC curves. (e) Low-energy X-Ray color maps of Al-12Ce-4Si-0.4Mg hot-tear and step-plate molds with DSC curves.

12Ce-0.4Mg enables complex geometry castings similar to those of the Al-12Ce. The smaller air-cooled cylinder head, shown in Figure 2.2b, was cast from ternary intermetallic Al-12Ce-0.4Mg and will be used to assess the applicability of Al-Ce-X alloys to engine and motor applications in the near future.

Considering the success of ternary Mg additions, investigation into quaternary additions of Si was begun. Silicon has two effects when added to conventional aluminum alloys: silicon works to increase alloy castability; and silicon, when combined with Mg normally precipitates a Mg_2Si strengthening phase [29,30]. In the casting of Al-12Ce-4Si-0.4Mg, the melt was prepared from the heel left after pouring the Al-12Ce-0.4Mg. Then additional Al was added followed by Mg, Ce, and Si. During the addition of Cerium to the molten Al-Si-Mg mixture an endothermic reaction occurred and the melt temperature dropped significantly, ~30 °C. The cause of the endothermic drop in temperature is unclear. This is in contrast to the normally exothermic reaction of the previous two alloys upon the addition of cerium. Once the melt was brought back to ~785 °C, the molten alloy was poured as before into a hot-tear and step-plate mold. Figure 2.1e shows the results of casting trials of an Al-12Ce-4Si-0.4Mg alloy. Silicon greatly inhibits the castability of the Al-Ce-X system. The step-plate mold did not completely fill but instead was stopped by a solidification front that nucleated on top of the iron chill. In the case of the hot-tear mold, a large number of voids are present, and a hot-tear is present at the base of the right-most arm. Observing the DSC curve for the quaternary alloy, it is clear that the alloy does not solidify isothermally and is not free of secondary reactions following the initial solidus peak. However, in the case Al-Ce-X alloys it would appear that high silicon content impairs the castability in contention with typical silicon aluminum results.

2.5 Microstructure

Figure 2.2c and d show binary phase diagrams for the Al-Ce and Al-Mg systems. These two diagrams aided in the decisions regarding compositions and melt temperature. Following the finalized decisions on composition test bars were cast for each alloy. Test bars are cast in a permanent steel mold. Final bars are approximately 25 cm long and weigh ~0.25kg. Discs 2 mm thick were cut from the neck of test bars prepared from each alloy. Once cut the phase fractions of each sample were measured using a Panalytical X'pert Pro powder diffractometer. Rietveld refinement was used to determine phases and phase fractions. Following X-ray diffraction, a

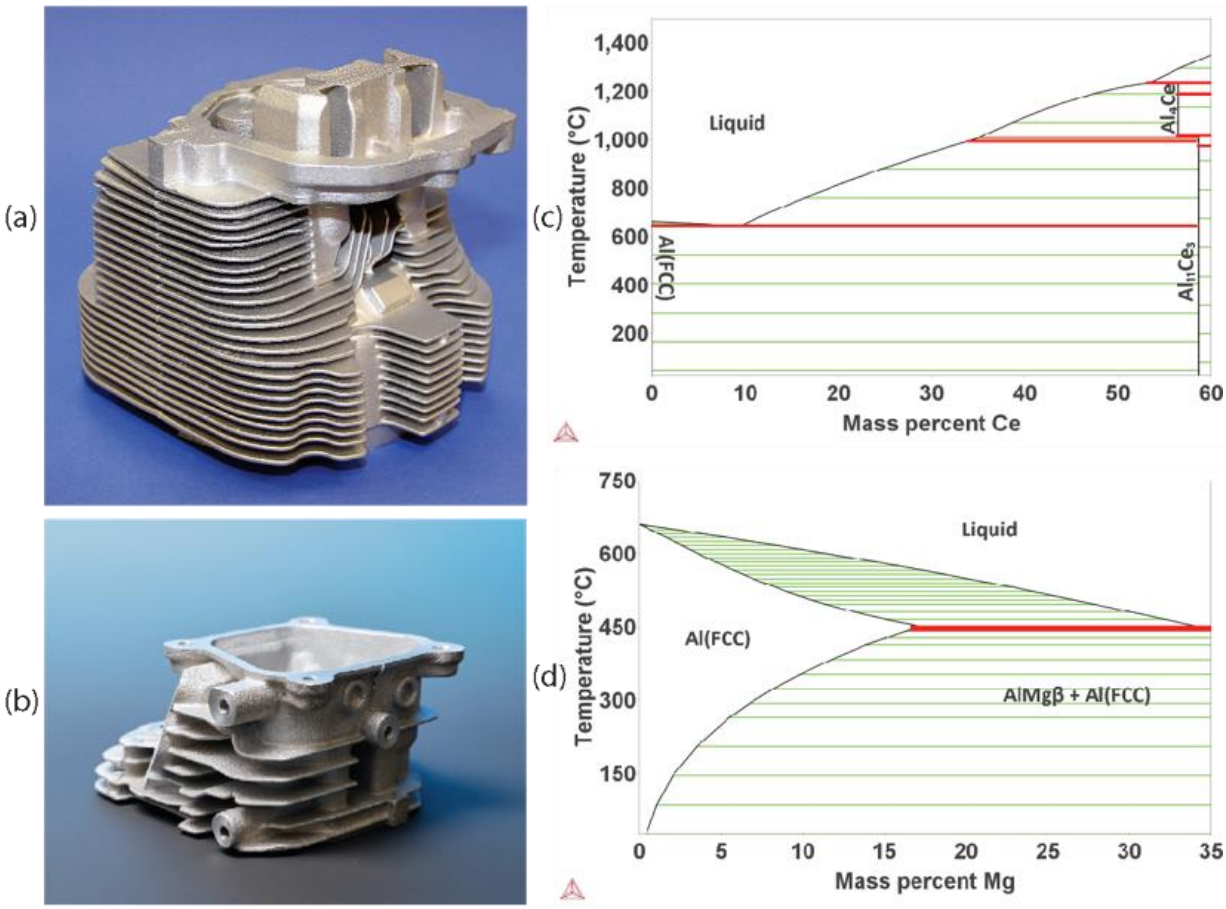

Figure 2.2: a) Air-cooled cylinder head cast from Al-12Ce (b) Air-cooled cylinder head cast form Al-12Ce-0.4Mg (c) Binary phase diagram of the Al-Ce system. (d) Binary phase diagram of the Al-Mg system

second set of discs were polished and lightly etched with Keller's reagent. Polished samples were imaged in a Hitachi S-4700 scanning electron microscope. Figure 2.3 shows the images of the as-cast samples adjacent to heat-treated samples of the same composition along with X-ray diffraction patterns for each alloy.

In the case of the binary Al-12Ce alloy (Figure 2.3a), two phases are present; aluminum metal (gray) and the binary intermetallic $Al_{11}Ce_3$ (white). The binary intermetallic, in the as-cast state, is characterized by a highly interconnected eutectic microstructure. The XRD reveals $Al_{11}Ce_3$ is orthorhombic with lattice parameters: a= 4.395, b= 10.09 and c= 13.025 Å in good agreement with literature values [31]. Since 12wt% Ce falls above the eutectic point, 10 wt% Ce, and in the primary solidification zone for the $Al_{11}Ce_3$ intermetallic, observation of primary crystallization is expected. However, no primary crystallization is observed. Al-12Ce then undercools beyond the primary zone and solidifies in a coupled eutectic growth resulting in no primary growth and high phase fraction of the eutectic intermetallic. Moving to the heat-treated binary sample, it is clear that the morphology of the microstructure has changed. The interconnected lath like structure has been replaced with a more independent particle like structure. Although the structure has changed, XRD data shows the phase fractions remain unaffected, resulting from the near zero solubility of cerium in aluminum. The stability of the microstructure phase constitution under high-temperatures offers promise toward future high-temperature mechanical properties.

The ternary Al-12Ce-0.4Mg alloy is shown in Figure 2.3b. In the as-cast state there are primary crystals of Al_3Mg_2 consisting of large cubic grains and the $Al_{11}Ce_3$ intermetallic in both the eutectic lath microstructure and primary crystals. The lattice parameter for the Al-Mg cubic phase is a = 2.82 Å [32]. These crystals are not representative of the bulk microstructure and image analysis suggests they account for roughly 1% of the areal fraction. This low fraction explains the absence of the Al_3Mg_2 from the XRD phase fraction analysis. The Al_3Mg_2 crystals remain after heat-treatment in roughly the same fraction. Mg appears to suppress the undercooling characteristics of the rapid solidification and force some small amount of primary solidification in the $Al_{11}Ce_3$ phase. The small amount of primary solidification is observable in the DSC curve just prior to the sharp onset of eutectic solidification. The eutectic microstructure is not affected by the new solidification characteristics. In the as-cast state it remains highly interconnected with very thin laths. Following heat-treatment, the same transition in the eutectic structure is observed. The finer laths have separated to form particle like independent structures. The intermetallic particles present

after heat-treatment are similarly sized to the laths present in the as-cast microstructure, and XRD shows that no phase transition has occurred with the as-cast and heat-treated spectra appearing nearly identical. The small amount of coarsening in the eutectic microstructure contrasts the ease with which Al-Si alloys coarsen after very little exposure to high-temperatures [33]The thermal stability of the phase fraction and grain size are important factors in considering whether or not Al-Ce-X alloys have the possibility to function at higher temperatures.

The quaternary Al-12-4Si-0.4Mg alloy stands out from the binary and ternary alloys in: microstructure morphology, phase constitution, and heat-treatment results. The Al-12Ce-4Si-0.4Mg alloy exists in the as-cast state as three phases. The smallest is AlSiMg accounting for under 2 wt%. The main two phases present are the aluminum (FCC) phase and the intermetallic $Al_{11}Ce_3$, both reflected in Figure 2.3c. $Al_{11}Ce_3$ shows both primary and eutectic solidification in the as-cast state. The silicon not accounted for in AlSiMg is dissolved in the aluminum matrix. Following the T6 heat-treatment, a new phase precipitates. The new phase is a ternary intermetallic, AlCeSi. This phase is tetragonal with lattice parameters a = 4.24 c= 14.538Å consistent with published values [34]. During heat-treatment the new ternary phase consumes the eutectic growth and transforms the present primary crystals to AlCeSi.

2.6 Magnetism

Since cerium often contains a partially filled 4f electron shell, it may impart a magnetic response to its alloys and compounds. As a result, the magnetic properties can help characterize the Al-Ce alloys studied here. Here the magnetization of three binary specimens (Al-xCe, x = 6, 12, and 16) was measured.

The magnetic moment per gram at 300K for the three alloys is shown in Figure 2.4a. The data are plotted as a function of the $Al_{11}Ce_3$ content determined from the x-ray diffraction refinements. The measured data closely follow the linear trend between the end members Al and $Al_{11}Ce_3$, consistent with a simple mixture of the two paramagnetic phases. The red line on Figure 2.4a is a linear fit of five data points extrapolated to the abscissa. The magnetic susceptibility exhibits Curie behavior (M/H ~ C/T, where C is the Curie constant) typical of local magnetic moments. Below about 10 K the susceptibility increases sharply (Figure 2.4b). Measurements at lower temperatures reveal ferromagnetic ordering (Curie temperature) near 7 K in Al-16Ce. A downturn below about 3.5 K suggests a transition away from a simple ferromagnetic state at lower temperatures. The observed

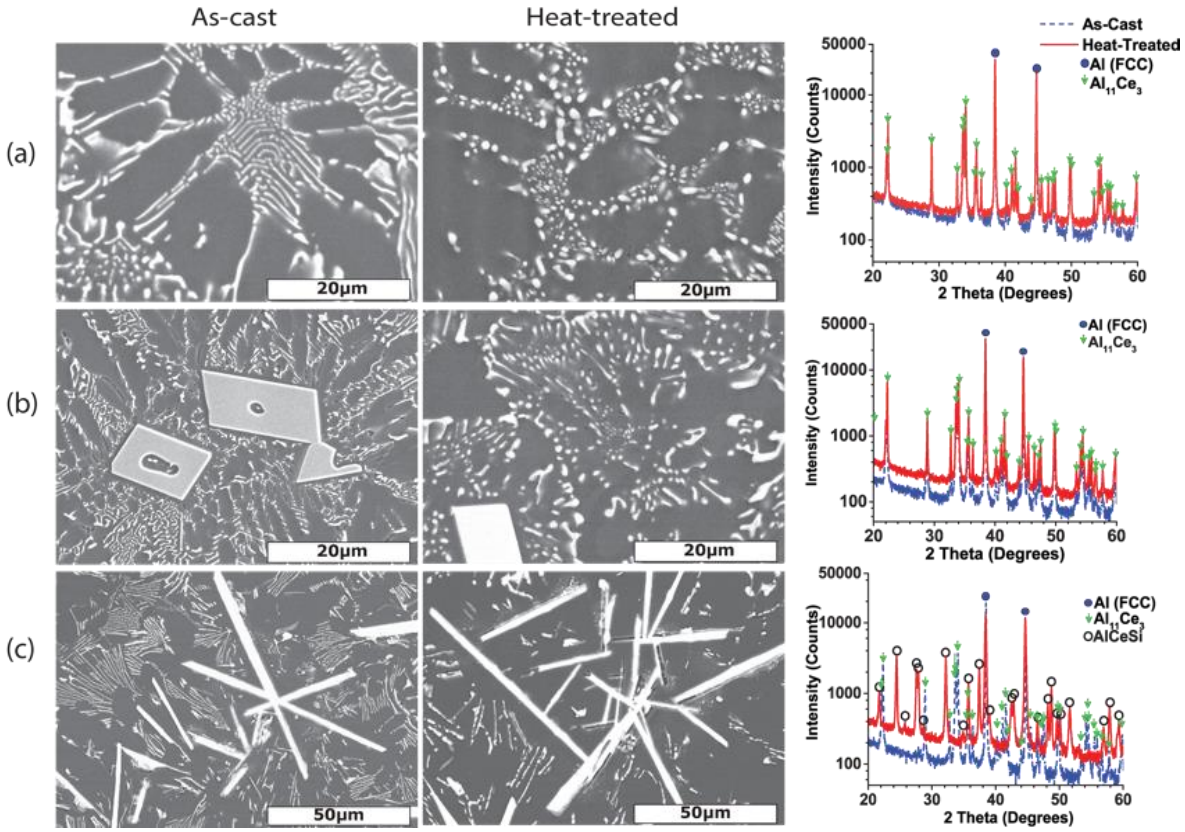

Figure 2.3: (a) As-Cast and Heat-treated SEM images of Al-12Ce with accompanying XRD spectra and phase information. (b) As-Cast and Heat-treated SEM images of Al-12Ce-0.4Mg with accompanying XRD spectra and phase information. (c) As-Cast and Heat-treated SEM images of Al-12Ce-4Si-0.4Mg with accompanying XRD spectra and phase information.

temperature dependence is consistent with literature reports for Ce_3Al_{11}, which is known to have a ferromagnetic transition at 6.3 K and a ferromagnetic to antiferromagnetic transition at 3.2 K [35].The magnetic moment per gram measured at 2K in an applied field of 5 T is 0.0030 Am^2/g (3.0 emu/g). The reported average moment for $Al_{11}Ce_3$ at this temperature and field is 0.0108 Am^2/g (10.8 emu/g). This indicates a concentration of 28 wt. % $Al_{11}Ce_3$ in the Al-16Ce alloy, similar to the XRD result (24 wt. %).

The measured values of the moment at 2 K and the susceptibility at 300 K support the presence of $Al_{11}Ce_3$ as the primary Ce containing phase in the tested Al-Ce alloys and the temperature dependence and transition temperatures indicates this phase is present in well-ordered grains which behave very similarly to bulk single crystal $Al_{11}Ce_3$.

2.7 Mechanical Properties

Results of room temperature mechanical property measurements are shown in Table 2.1, commercially pure aluminum is included for reference[13]. In the binary Al-12Ce sample ductility remains high in spite of the large intermetallic phase fraction present in the alloy. It is not certain what mechanism enables the ductility to remain high, but this phenomenon could prove useful in applications requiring alloys to be optimized for resistance to creep failure [36].Tensile and yield strengths are improved over commercially pure aluminum (CPA). Cerium does not appear to provide dispersion strengthening in the as-cast state once heat-treated though the break-down of the intermetallic into more particle like structures that are on the micrometer scale into less coherent particles negatively effects the maximum tensile and yield strengths. The lower tensile and yield strengths are accompanied by a ~100% increase in ductility. This is due to a small amount of coarsening observed in the microstructure during heat-treatment. Though the coarsening is minimal because there is no diffusion into the aluminum, the bulk mechanical properties of the alloy become more similar to those of pure aluminum, with lower tensile strength and high ductility. Optimization of heat-treatment is required for the binary alloy system in order to limit microstructural coarsening and increase mechanical properties. The ternary Al-12Ce-0.4Mg system shows a marked increase in tensile strength over the binary alloy, likely due to AlMg particles dispersed throughout the aluminum matrix causing localized dislocations. However, yield strength remains relatively low. Heat-treatment again causes a decrease in yield strength and an

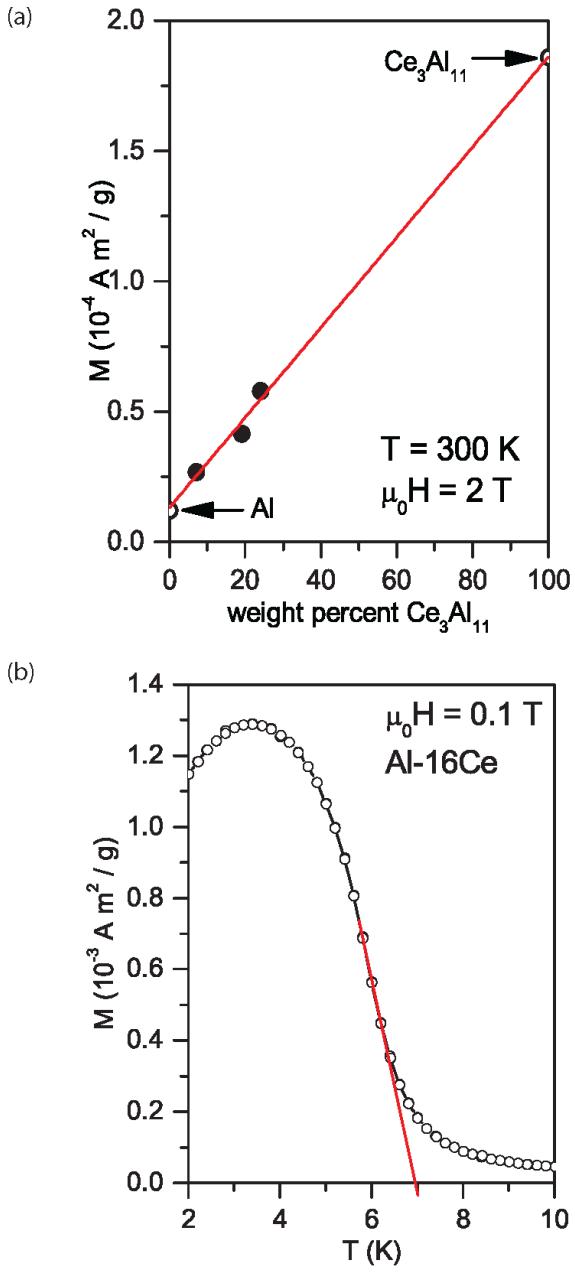

Figure 2.4: (a) Magnetic moment per gram of Al, $Al_{11}Ce_3$, and three alloys at 300K in an applied field of 2T, with a linear fit. (b) Low temperature magnetization of Al-16Ce showing the onset of ferromagnetism in the $Al_{11}Ce_3$ component near 7K as estimated by the red line, and a second magnetic transition at lower temperatures.

Table 2.1: Mechanical Properties of select Al-Ce alloys compared to commercially pure aluminum

	As-Cast				T6 Heat-Treated		
Alloy	UTS (MPa)	Yield (MPa)	Yield (4 point flexural testing)	Elongation (%)	UTS (MPa)	Yield (MPa)	Elongation (%)
CPA	90	34	--	45	--	--	--
Al-12Ce	161.3	57.2	82.0	13.5	131.7	47.6	26.5
Al-12Ce-0.4Mg	200.6	78.6	106.2	6.0	224.1	62.1	8.5
Al-12Ce-4Si-0.4Mg	141.3	75.2	155.1	2.0	252.3	128.2	8.5

increase in ductility. This is expected considering the similar microstructural transitions occurring in the alloys. The lower ductility results from the presence of large primary crystals, which act as nucleation sites for brittle fracture, and thereby decrease the overall ductility of the alloy. In contrast to the binary sample, the tensile strength is largely unaffected by heat-treatment. Though there is some difference between the heat-treated and the as-cast values, small variations between test bars could account for this change. It is then possible that the UTS is unaffected by heat-treatment. Quaternary Al-12Ce-4Si-0.4Mg has a much more traditional response to a T6 heat-treatment than did the binary or ternary alloy. Tensile and yield strengths increased while ductility decreased. The phase transition which occurs during heat-treatment appears to be the carrier for the mechanical property increase.

2.8 Conclusion

Al-Ce alloys have the possibility of replacing heavier steel and cast-irons for use in high-temperature applications. Al-Ce alloys castable along a broad range of cerium content, and are compatible with modern casting practices, requiring no changes to present foundry infrastructure. Mechanical properties are as high as 252 MPa for tensile and 128 MPa for yield strength. Though high temperature mechanical properties are not represented here, the combination of thermodynamic properties and stability following heat-treatment suggest that Al-Ce-X alloys hold great promise for high-temperature mechanical properties.

Compositional variation is possible with the Al-Ce-X alloy family; Mg and Si both have the possibility to be alloyed with Al-Ce to create a highly tailorable microstructure and mechanical properties. The impediment of silicon on castability is a negative, but it is theorized that by decreasing the silicon content good castability can be returned while maintaining the room-temperature strength of the Al-Ce-Si-Mg alloy.

2.9 Acknowledgements

This research was sponsored by the Critical Materials Institute, an Energy Innovation Hub funded by U.S. Department of Energy, Office of Energy Efficiency and Renewable Energy, Advanced Manufacturing Office. This work was performed under the auspices of the U.S. Department of Energy with Lawrence Livermore National Laboratory under Contract DE-AC52-07NA27344 and with Oak Ridge National Laboratory under U.S. Department of Energy

contract DE-AC05-00OR22725. Work at the Molecular Foundry was supported by the Office of Science, Office of Basic Energy Sciences, of the U.S. Department of Energy under Contract No. DE-AC02-05CH11231.

3. Developing and Al-Ce Alloy Design Paradigm

This chapter is adapted from a slightly edited version of a published work "High performance aluminum–cerium alloys for high-temperature applications" first published in 2017 in Materials Horizons

Sims, Z. C.; Rios, O. R.; Weiss, D.; Turchi, P. E.; Perron, A.; Lee, J. R.; Li, T. T.; Hammons, J. A.; Bagge-Hansen, M.; Willey, T. M. High Performance Aluminum–Cerium Alloys for High-Temperature Applications. *Materials Horizons* **2017**, *4* (6), 1070–1078.

My primary contributions to this paper were: selection of alloy compositions for casting, initial modeling of binary and ternary systems using CALPHAD, Room temperature mechanical testing, SEM and XRD analysis of samples, collaborative analysis of neutron scattering data, and the majority of the writing and formatting of the manuscript.

Reconstructed with permission from the Royal Society of Chemistry

3.1 Abstract

Light-weight high-temperature alloys are important to the transportation industry where weight, cost, and operating temperature are major factors in design of energy efficient vehicles. Aluminum alloys fill this gap economically but lack high-temperature mechanical performance. Alloying aluminum with cerium creates a highly castable alloy, compatible with traditional aluminum alloy additions, that exhibits dramatically improved high-temperature performance. These compositions display room temperature ultimate tensile strength of 400 MPa and yield strength of 320 MPa, with 80% mechanical property retention at 240°C. A mechanism is identified that addresses the mechanical property stability of the Al-alloys to at least 300°C and their microstructural stability to above 500°C. Finally, neutron diffraction under load provides insight into the unusual mechanisms driving the mechanical strength.

3.2 Introduction

Aluminum alloys are desirable as structural materials due to their outstanding castability, excellent mechanical properties, and low cost. They occupy the gap between inexpensive but dense iron alloys and costly, high-performance titanium alloys. Within the transportation sector, the high strength to weight ratio, corrosion resistance, and high thermal conductivity of aluminum alloys have long been important for the automotive and aerospace industries and demand continues to expand due to the promise of improved performance and fuel economy. This paper describes a

new family of economically competitive aluminum alloys containing 6-16 weight percent (wt. %) cerium which exhibits dramatically improved high-temperature mechanical properties, in addition to improved castability and thermal stability when compared to existing aluminum alloys. Furthermore, the Al-Ce alloys may not require post-casting heat treatment, which adds significantly to the manufacturing cost in terms of energy, time, and infrastructure requirements.

Castable engineering alloys are typically strengthened through precipitation of intermetallic phases from alloying elements dissolved during the casting process or driven into solution by heat-treating[1]. These strengthening precipitates improve alloy performance by increasing stiffness and strength, while lowering thermal expansion[2, 3]; however they reside in kinetically frozen high energy architectures along chemical potential gradients that lead to instabilities at elevated temperatures[4]. The high mobility of traditional alloying elements leads to coarsening through processes such as Ostwald ripening; thus, prolonged exposure to high temperatures leads to dramatic changes in the microstructure and a corresponding degradation of mechanical properties. The loss of mechanical performance bounds the maximum operating temperature near the alloy aging temperature during the final step of heat treatment (155-190 °C for most Al alloys). This limitation becomes particularly significant for internal combustion engines, which benefit from light-weight materials compatible with higher temperatures for both the engine and nearby components.

Research developing aluminum alloys with improved high temperature performance has principally focused on systems such as Al-Sc, Al-Zr, and Al-V which form stable L_{12} precipitates[5-7]. The alloy strengthening Al_3X (X = Sc, Zr, V) precipitates are stabilized on the basis of lattice coherence with the FCC aluminum, creating interfacial strain which increases thermodynamic stability and acts as a creep-diffusion barrier[8]. This coherence breaks down above the conversion temperature, e.g. about 300 °C for Al-Sc[9], resulting in the loss of high-temperature performance.

In contrast, Al-Ce based alloys remain thermodynamically stable, independent of their mode of preparation (e.g. extruded, wrought, cast). For example, thermo-mechanical processing via extrusion of the binary alloy results in 400 MPa ultimate tensile strength (UTS) and 340 MPa yield strength, while hot isostatic pressing (HIP), equivalent to fully dense casting, leads to 280 MPa UTS and 220 MPa yield. The mechanical properties of Al-Ce alloys using an extrusion ratio of 3:1 are competitive with leading high temperature wrought alloys such as A2618 (440 MPa UTS)

and A4032 (380 MPa UTS) which typically require extrusion ratios exceeding 10:1. The applications space for wrought materials is limited by the energy intensive processing associated with producing engineered metastable structures. In contrast, highly castable Al-Ce alloys form structures in thermodynamic equilibrium and remain so until near their melting point. This study focuses on alloys formed by casting rather than alternative processing methods due to the application versatility arising from their ability to adopt a greater range and complexity of structures.

3.3 Experimental Techniques

3.3.4 3.3.1 CALPHAD Thermodynamics

The phase diagrams presented herein have been thermodynamically assessed[15-17, 19] within the CALPHAD methodology, and the commercially available software Thermo-Calc has been used to calculate the equilibrium phase diagrams based on a user-defined thermodynamic database[29]. In this approach, the Gibbs energy of individual phases is modeled, and the model parameters are collected in a thermodynamic database. Models for the Gibbs energy are based on the crystal structures of the phases and interaction parameters are assessed to reproduce both the diagrammatic and thermodynamic data available for binary and ternary systems.

3.3.1 Casting and sample characterization

Alloys were cast using industrial practices. Industrial grade ~30lb aluminum ingots were brought to a molten state in a tilt pour resistive furnace. Once the metal was molten and temperature stabilized at 750 °C, alloying elements were added one at a time, with cerium being the final addition. If multiple compositions were being cast during a single trial, additional melts were prepared from the heel of the previous melt. Metal was poured into a ceramic lined permanent mold heated to 400 °C; each mold comprised two dog bone style test-bars 25 cm in length. Selections of bars at each composition were heat-treated with either a T6 (10 hrs at 540 °C, warm water quenched and then artificially aged for 3 hrs at 150 °C) or T4 heat-treatment (10 hrs at 540 °C, warm water quenched). As-cast and heat-treated test-bars were mechanically tested in tension using a United Calibration and Testing Universal Testing machine. For high-temperature measurements test-bar grips were threaded and bars were held at temperature for no less than thirty minutes, after which they were strained under tension until failure.

Gauge lengths of fractured bars were sectioned into 2mm disks then polished and etched using Keller's reagent. Imaging was performed on a Hitachi S-4700 Cold field emission Scanning Electron Microscope. Phase analysis was completed via X-Ray diffraction using the Panalytical X'Pert Pro system combined with Rietveld analysis through use of the High-Score plus software suite.

3.3.2 TEM measurements

For sample preparation, 3mm disks were cut from fractured bars and mechanically polished to ~150 μm thick and then further electro-polished at -15° C using an 80% methanol/15% perchloric acid /5% HF electrolyte until electron transparent. Measurements were performed using the TitanX Scanning Transmission Electron Microscope at the National Center for Electron Microscopy at the Molecular Foundry located at Lawrence Berkeley National Laboratory. The TitanX was operated at 200 kV for the STEM EDS measurements.

SAXS /USAXS: The USAXS data were collected on a combined Bonse-Hart/Pinhole SAXS/WAXS instrument at 9-IDC at the Advanced Photon Source located at Argonne National Laboratory[30]. All samples were prepared with uniform thicknesses and exposed to a monochromatic 24 keV X-ray beam for two minutes during data collection. With the sample thicknesses known, all USAXS data are calibrated and on an absolute scale[31].

3.3.3 *Neutron diffraction under load*

The neutron diffraction experiment was conducted at the Vulcan diffractometer[32] at the Spallation Neutron Source (SNS), Oak Ridge National Laboratory. The cylindrical specimen of 10x20mm was mounted horizontally in the loadframe with the axial direction parallel to the loading direction. An extensometer was attached to the specimen for measuring the engineering strain. Compressive loads were applied at a rate of -10 MPa/min (negative denotes compression) with a 15-min dwell at -25 and -50MPa in the elastic region. To avoid stress relaxation during stepwise loading during plastic deformation[25, 33, 34], the specimen was then continuously compressed at a strain rate of -0.01 h^{-1} until the strain reached -0.1. The specimen was subsequently unloaded at a stress rate of 0.8 MPa/min. The incident neutron beam, 45° to the loading direction, was focused at the center of the specimen, which remained stationary due to uniform displacement from both sides. The gauge volume was defined to about 5×5×5 mm^3 by the incident slits and radial collimators. During the mechanical test, the two detectors, located at -90° and +90° to the incident beam, continuously

recorded the diffracted neutrons with the scattering vector parallel to the longitudinal and transverse directions, respectively. The diffraction data were averaged in a 15-min interval using the VDRIVE software. The lattice parameters were extracted from Rietveld refinement of entire scattering pattern using GSAS and EXPGUI software.

The lattice strain ε of individual phases was calculated by $\varepsilon_x = (L_x - L_{x,0}) / L_{x,0}$ along a principal (i.e. crystallographic) axis, where the reference $L_{x,0}$ under zero stress was estimated using the result before loading[35]. The corresponding microstress (σ_x) of a phase along the particular axis was obtained by $\sigma_x = E_x \bullet \varepsilon_x$, where E_x is the elastic diffraction constant. E_x was estimated from the linear unloading behaviors which is assumed as an elastic process, by using $E_x = \Delta\sigma_x / \Delta\varepsilon_x$, where $\Delta\sigma_x$ and $\Delta\varepsilon_x$ are the changes of stress and strain, respectively, during the elastic unloading along the particular direction. For the Al matrix phase, the lattice strain and microstress were measured against changes in the fcc lattice parameter "a". For $Al_{11}Ce_3$ intermetallic phase, the behavior along the b-axis was selected to represent the behavior of the phase.

3.4 High Temperature Mechanical Performance

Characterization and correlation of the composition, microstructure, and mechanical behavior of cast Al-Ce-based alloys was conducted to understand the origin and mechanisms of their highly desirable performance reported previously at room temperature[10] and, as demonstrated here, at elevated temperatures, with the implicit understanding that thermo-mechanical processing should further enhance the mechanical properties.

These behaviors are driven by the exceptional change in Ce solubility between the liquid and solid phases of aluminum near the eutectic point, which leads to a high stable intermetallic precipitating into a nano-scale architecture during initial solidification. The superior elongation of cast Al-Ce alloys compared to many commercial Al-alloys is illustrated in Figure 3.1a. The intermetallic secondary phases are far more brittle than the surrounding aluminum matrix, and as a result, elongation to failure is driven down as intermetallic content increases[3, 11]. The retention of mechanical properties at elevated temperatures is demonstrated in Figure 3.1b where the ratio of the 300° C to room temperature yield strength is compared against the ratio of the 300° C to room temperature UTS. The Ce alloys retain over 60% of their room-temperature yield and more than 40% of their UTS at 300° C. This compares favorably to the traditional aluminum alloys which at the highest retention values do no exceed 45% yield and 50% UTS retention values at 300 °C.

Incorporating traditional Al alloying elements such as Si and/or Mg into the Al-Ce parent alloy retains thermomechanical properties (Figure 3.1b inset) at elevated temperature compared to traditional alloys. It is important to note here Al-Ce alloys differ from most tested aluminum alloy in that; while the UTS retention of Al-Ce alloys at high temperature is comparable to some of the most high performance aluminum alloys, Al-Ce alloys maintain a far more significant amount of yield strength at elevated temperature. The deformation mechanism responsible for the high-temperature yield retention will be presented during the analysis of the neutron scattering study to follow.

This superior mechanical property retention in the Al-Ce alloys can be understood in terms of the behavior of their constituent phases at elevated temperatures, specifically the solubility and diffusion of Ce. Several atomic percent of common aluminum alloying additions, such as Cu, Si, and Mg can dissolve into the aluminum matrix during a heat treatment as their solubility increases with temperature (see supplementary material)[11]. These are the primary additions in the A206, A356, and A535 alloys, respectively. Quenching retains the solute atoms in a supersaturated solution and enables finely dispersed precipitate formation via age hardening, which may be accelerated by soaking at 100-200°C[12]. Nonetheless, this same solubility limits the high-temperature stability of the alloy due to precipitate dissolution and the resulting changes to the microstructure. In contrast to the common Al-alloying elements, the solubility of Ce in solid aluminum is very low. Near the eutectic temperature (642° C), the upper limit of solubility is ~0.05 wt.% Ce in Al with the solubility falling below 0.02 wt.% by 600° C[13, 14] as compared to Cu, which has a solubility exceeding 5% by 600° C[11]. Even Sc, which leads to the most competitive high-temperature alloys has a solubility of 0.2 wt.% at 600° C, exceeding the solid solubility of Ce by an order of magnitude[14]. The Ce values are consistent with the CALPHAD thermodynamic assessment of the Al-Ce binary phase diagram (Figure 3.1c-d) which predicts a similarly low solubility for Ce in the Al matrix[15], and renders the strengthening intermetallic, $Al_{11}Ce_3$, far more stable against dissolution in solid Al than the intermetallics of standard commercial alloys. Dissolution of strengthening phases into the aluminum matrix is illustrated in property diagrams (Figure 3.1e) where the fraction of intermetallic precipitates retained decreases with increasing temperature. It is evident that the phase fraction of intermetallic, in this case $Al_{11}Ce_3$, retained at elevated temperatures far exceeds any of the other alloying elements. Electron microscopy data

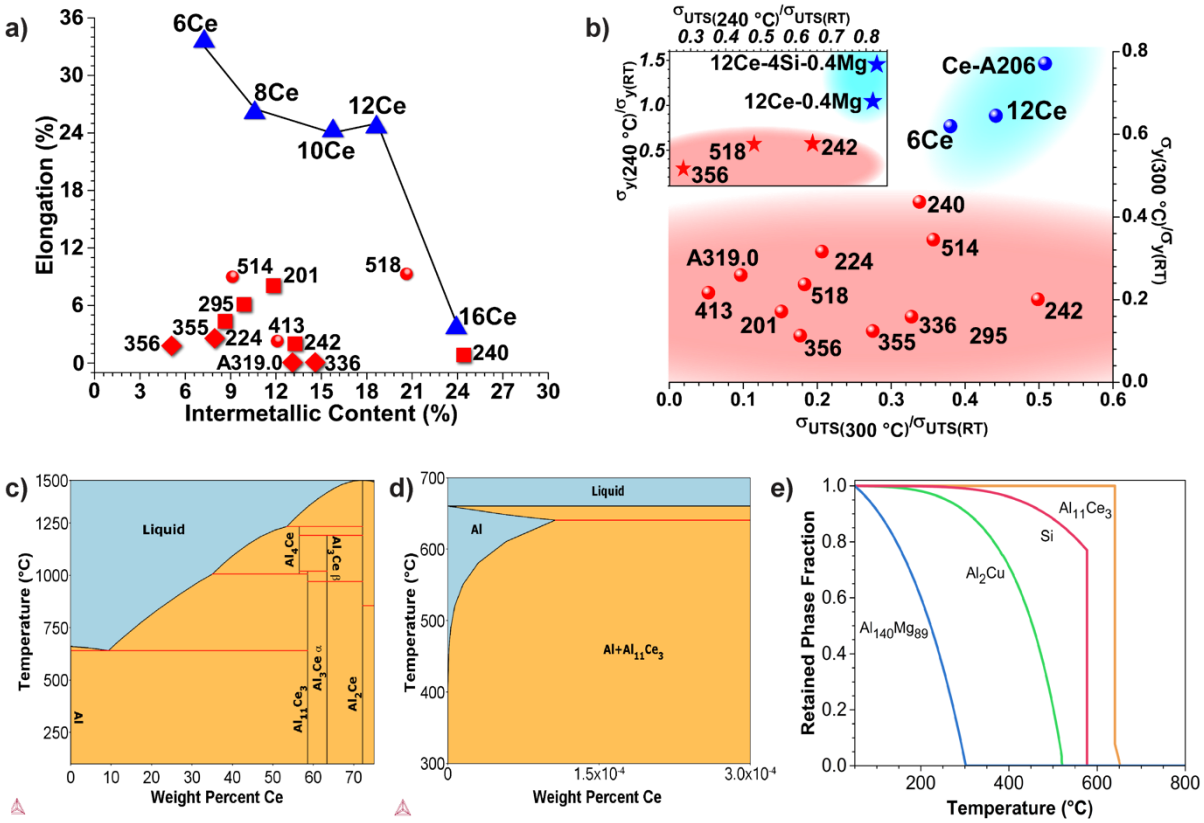

Figure 3.1: Al-Ce alloy properties. (a) Elongation vs. intermetallic content for Al-Ce (wt.%) alloys (blue triangles) with a line to guide the eye compared to traditional aluminum alloys (red). (b) Ratio of 300° C to room temperature yield strength vs ratio of ultimate tensile strength at 300° C to room temperature, demonstrating superior thermomechanical stability for Al-Ce alloys. Ce-A206 is A206 alloy with 8 wt.% Ce. The inset shows Al-Ce based alloys at 240 °C against standard alloys at 200 °C. Al-Ce-Si-Mg alloys show increased yield at elevated temperature and Al-Ce-Mg shows no decrease relative to room temperature. (c, d) Al-rich region of the Al-Ce phase diagram based on a where the Al matrix exhibits almost no Ce solubility. (e) Phase stability of major precipitate phase fraction relative to room temperature in aluminum alloys highlighting the thermal stability of $Al_{11}Ce_3$. Color code: 500-series (blue), 200 series (green), 300 series (red), and the new Al-10Ce (wt.%) alloy (orange).

(Figure 3.2) reinforce the assignment of near-zero solubility of Ce in Al and intermetallic stability of $Al_{11}Ce_3$ at elevated temperatures. Figure 3.2c contains an Energy Dispersive X-Ray Spectroscopy (EDS) map of a 10 wt.% cerium alloy inset in the high angle annular dark-field transmission electron microscopy (HAADF TEM) image (see Supplementary Material. for additional images). The EDS map reveals a distinct dividing line between the Al rich phase and the Ce rich intermetallic, while detailed TEM studies show a coherent phase boundary. The lack of Ce dispersion at the phase boundary reflects the thermodynamic stability of $Al_{11}Ce_3$ (ΔHf = -42.7 kJ/mol at room temperature relative to Al and Ce) which drives the Ce toward intermetallic formation[15].

In addition to their low solubility, the large size of the Ce atoms results in a reduced diffusion coefficient when compared to other alloying elements. As an illustration, the diffusion coefficient for Ce at 500 ° C is 5.7x10-14 cm2/s, which is about 10,000 times smaller than for Cu, 6.0x10-10 cm2/s or Mg, 1.4x10-9 cm2/s , at comparable temperatures[1, 16]. Strong vacancy binding to Ce atoms[17] further decreases degradation of the $Al_{11}Ce_3$ intermetallics as it impedes and, therefore, reduces vacancy diffusion—the dominant transport mechanism for solute atoms within the matrix[18].

3.5 Microstructural Analysis

Experimental evidence supporting the low solubility and diffusion of the Ce within the Al-Ce systems is provided by the scanning electron microscopy (SEM) back-scatter images of as-cast and heat-treated 12 wt.% Ce alloys respectively in Figure 3.2(a-b). The as-cast alloys show a very fine interconnected eutectic microstructure (white) and the pure aluminum phase (gray). The scale of the laths, as small as 100 nm, along with their uniform distribution, and interdendritic spacing all aid in improving the alloy mechanical properties[11]. Exposing the same alloy to a 20-hour soak at 520°C results in a eutectic microstructure that has undergone only minor morphological changes. Instead of thin and interconnected laths, they have rounded in many places and become less interconnected. This represents a localized minimization of the microconstituent surface energy at the eutectic through interdiffusion within the intermetallic and accompanying spheroidization, rather than bulk diffusion through the matrix. The overall scale of the intermetallic phase has not changed: laths and rods remain at widths near 100 nm, and the phase fractions are consistent across samples thereby demonstrating the conversion temperature is above 520°C.

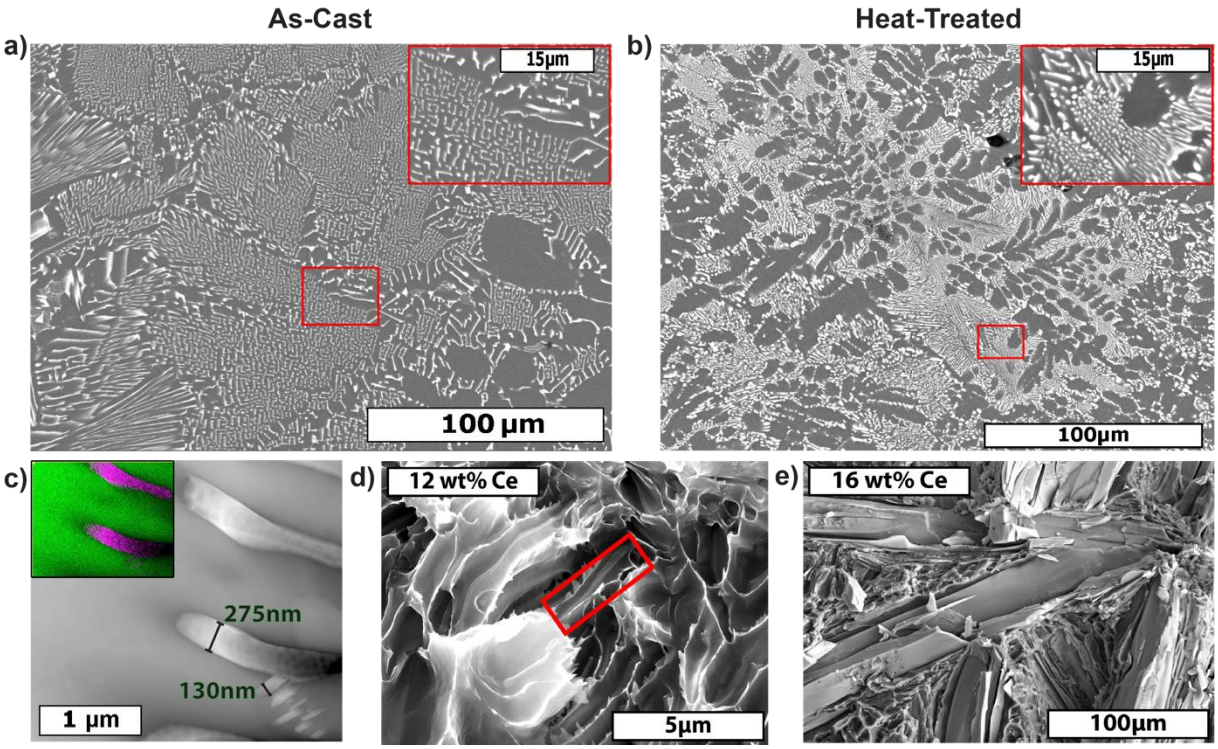

Figure 3.2: Micrographs of Al-12Ce (wt.%) alloy (a) as-cast, and (b) after T6 heat treatment showing mild spheroidization but no change of the larger features. (c) TEM HAADF image of Al-10Ce (wt.%) where the $Al_{11}Ce_3$ laths are 100-200 nm wide. The false color inset shows the $Al_{11}Ce_3$ regions (purple in the EDS map). (d, e) Fracture surfaces of Al-12Ce and Al-16Ce (wt.%), respectively, illustrating ductile fracture in the former and a mix of ductile and brittle fracture in the latter. Red area in (d) shows fracture along a eutectic intermetallic lath with ductile fracture surrounding. Ductile fracture can be observed in the eutectic zone surrounding the brittle primary crystals in (e). These eutectic zones lead to the elevated ductility of this alloy over alloys with similar intermetallic content. Note the different scale bars between (d) and (e).

The fcc phase regions remain relatively small and well distributed throughout the sample after heat-treatment. Thus, a combination of low Ce solubility in the Al matrix and low Ce diffusion coefficients avoids coarsening mechanisms through Ostwald ripening, while the high thermodynamic stability of the $Al_{11}Ce_3$ intermetallic resists substantial microstructural evolution in the Al-Ce alloys and, by extension, degraded mechanical properties.

The fracture surfaces for Al-12Ce and Al-16Ce (wt.%) are shown in Figure 3.2d-e, respectively. Significant dimpling, a characteristic of ductile fracture, dominates the fracture surface of Al-12Ce (wt.%). Primary $Al_{11}Ce_3$ solidification begins around 10 wt.% Ce addition, just beyond the Ce-Al eutectic point (Figure 3.1c). The cooling rates of the experimental castings were sufficiently fast to undercool the 12 wt.% alloy into the eutectic region, while at 16 wt.% Ce, large primary crystals of $Al_{11}Ce_3$ precipitate surrounded by eutectic laths. The large crystals promote brittle fracture, yet some ductility remains due to the surrounding matrix-eutectic ductile fracture mechanism.

The dominant brittle fracture along the crystal faces leads to the drastic drop in ductility between the 12 wt.% and 16 wt.% Ce alloys shown in Figure 3.1a. Even then, ductility values remain comparable to that of many commercial aluminum alloys with equivalent intermetallic content.

The alloy mechanical properties are significantly improved with small quantities of ternary and quaternary additions. Representative castings of Al-12Ce-4Si (wt.%) and Al-12Ce-4Si-0.4Mg (wt.%) illustrate these properties. Cerium reacts favorably with many traditional solutionizing elements, including Mg and Si, to form thermally stable intermetallics without microstructural coarsening in the solid state. Small additions of Si lead to the tetragonal intermetallic $Ce(Si_{1-x}Al_x)_2$, with x = 0.1 – 0.9, identified in Figure 3.3a as the τ_1 phase (I_{41}/amd space group) which extends across the central portion of the phase diagram and exhibits a high range of temperature stability in the aluminum matrix once formed[15, 19-21], similar to that of $Al_{11}Ce_3$ in the binary. The low solubility of Ce in Al and Si[22] along with the tight bonding of vacancies to Ce[17] and the formation enthalpy of the τ_1 phase, which reaches a minimum of -67 kJ/mol near x=0.5, all contribute to the stability of this phase. The solubility of Si in the Al matrix phase is 1.5 wt.% at high temperatures and it is possible to quench a supersaturated solids solution to 11 wt.%, whereas the low mobility and reactivity of Ce leads to immediate intermetallic formation. Thus, the structure of the as-cast Al-Ce-Si comprises $Al_{11}Ce_3$ intermetallic laths formed through an invariant reaction in an Al matrix that seed precipitation of Si from the supersaturated solution as the matrix solidifies. After

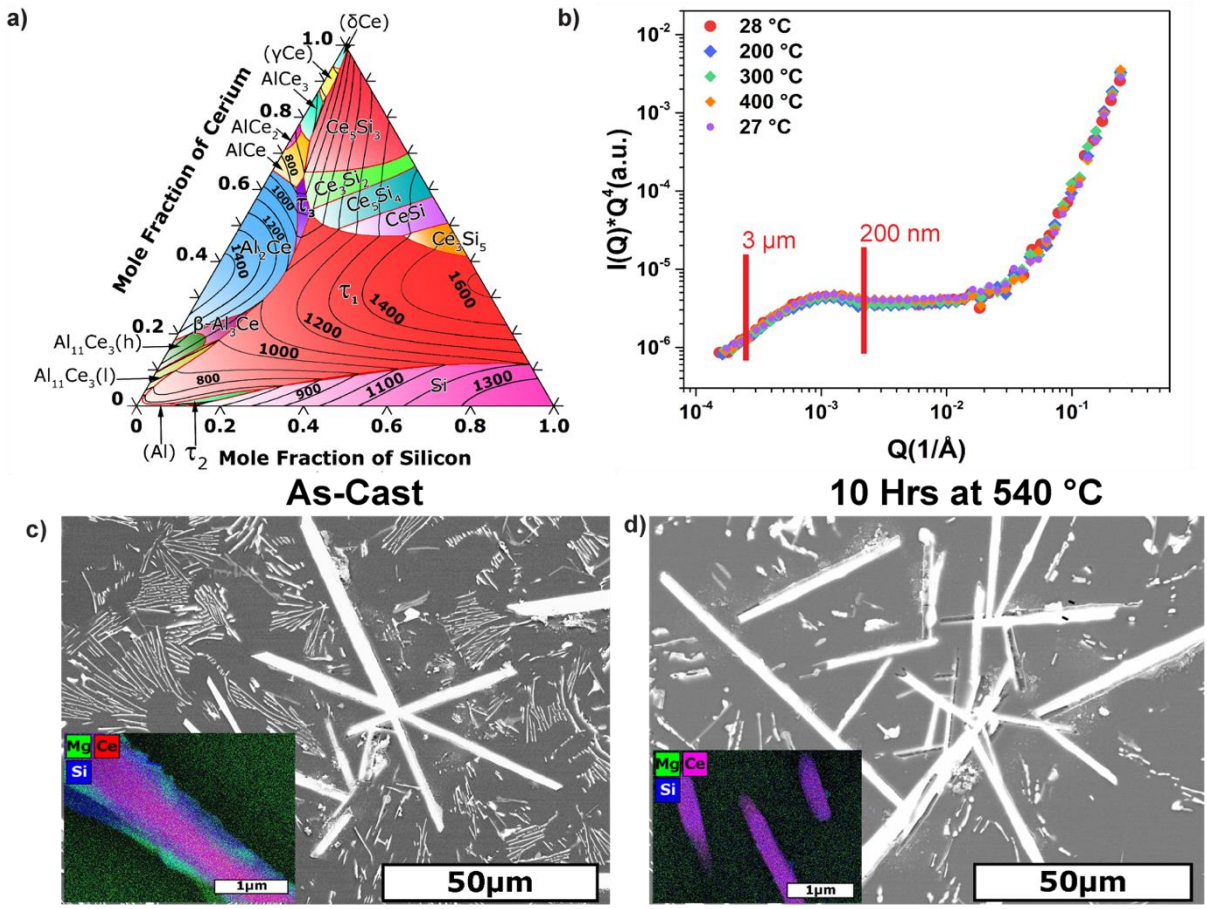

Figure 3.3: Thermal stability of the alloy. (a) Al-Ce-Si ternary liquidus projection based on a CALPHAD assessment (see text). (b) USAXS/SAXS for Al-12Ce-4Si-0.4Mg (wt.%) illustrating heating has negligible effect on particle size (or shape: see Supplement S3-4). (c, d) SEM micrograph of Al-12Ce-4Si-0.4Mg (wt.%) as-cast and after T6 heat treatment. Insets show EDS of intermetallic precipitates of same composition (Al contribution removed for clarity) illustrating internal changes in microstructure.

a T6 heat-treatment the morphology persists, with the precipitates serving as templates for the ternary $Ce(Si_{1-x}Al_x)_2$. The associated mechanical properties improve from a yield and UTS of 83 MPa and 150 MPa, respectively to 128 MPa and 255 MPa after a T6 heat treatment. Similarly, the elongation improves from 2% to 8.5% before fracture.

3.6 X-Ray Scattering Study of Microstructural Stability

The stability of these multicomponent phases at elevated temperatures was explored through a series of volume averaged ultra-small and small angle x-ray scattering (USAXS/SAXS) measurements. Analysis of the scattering data provides insight into the size, shape, number density, and size dispersion of structural inhomogeneities (i.e. intermetallics in the alloys) and, as such, these methods are ideally suited for investigating the structure and structural evolution of these alloys. A T6 heat treated Al-12Ce-4Si-0.4Mg (wt.%) specimen was heated in 100 °C increments between which the sample was cooled to room temperature, with measurements performed at both the elevated and base temperature (Figure 3.3b). Should any microstructural changes result, deflections would be observed in the scattering vector. That there is no deviation between individual spectra in successive measurements indicate no changes in the underlying microstructure in either size or shape to at least 400° C (see S.I. for a detailed analysis)[23, 24]. SEM images before and after heat-treatment of the Al-12Ce-4Si-0.4Mg (wt.%) alloy (Figure 3.3c-d) further illustrate the high-temperature stability of the system. In the as-cast state, primary crystals of Ce-rich intermetallics are surrounded by thin laths of Al-Si and Al-Si-Mg intermetallics. After 10 hrs at 540 °C the Mg diffuses uniformly throughout the aluminum matrix while the primary crystals transition to $Ce(Si_{1-x}Al_x)_2$, as illustrated in the TEM false-color images (insets to Figure 3.3c-d). The surrounding eutectic displays similar morphological changes to those seen in the binaries with more isolated and less interconnected intermetallic structures forming from surface energy minimization. Thermodynamic stability is important to retaining the high temperature mechanical strength, but identification of the underlying strengthening mechanisms requires further investigation.

3.7 Neutron Diffraction Investigation of Mechanical Deformation Behavior

Neutron diffraction measurements enabled investigation of the mechanical behavior as a function of compressive loading. These experiments focused on the simplest alloys, whose behavior is reflective of this family of materials: the Al-12Ce (wt.%) binary and the structurally equivalent

Al-12Ce-0.4Mg (wt.%) ternary. These specimens provide distinct peaks for both the Al matrix and intermetallic $Al_{11}Ce_3$, as shown in Figure 3.4a for the binary alloy. Analysis of these diffraction peaks as a function of loading enables assignment of the lattice strain within each phase, and by extension, identification of load partitioning in the system. Emphasis is placed upon analysis of the diffraction data from the Al matrix because it has a simple cubic unit cell; since the Al-Ce alloys are two component systems, the properties of the complex anisotropic $Al_{11}Ce_3$ intermetallics can then be inferred from the behavior of the Al matrix. Figure 3.4b details the true strain behavior of the Al matrix in both the binary and ternary alloys, revealing a three-stage behavior with anomalous lattice strains instead of the linear stress-strain behavior expected in a conventional Al alloy[25, 26]. Figure 3.4c-d details how the load is partitioned or shared between the two phases present in the alloy. During the initial loading (Stage I), the Al matrix and intermetallic deform elastically under low stress (i.e. below 50 MPa). After early yielding, there is a transition to Stage II, denoted by red arrows in Figure 3.4b, where additional stress leads to the Al matrix showing a decelerated lattice strain response while applied stress increases. During this stage, the intermetallic phase carries an increasing share of the applied load. The increasing deformation observed at stage III is triggered (black arrows) once the dislocations reach a critical density and the intermetallic yields. Here, the Al matrix starts to take on more stress, indicated by the increase in slope, and the load partition rebalances between the two phases leading to destructive plastic deformation in the aluminum matrix. The transitive load behavior of Al-Ce and Al-Ce-Mg alloys is similar to the load partitioning characteristics of dispersion strengthened metal matrix composite alloys[27], which have been shown to exhibit high-strength and good thermal stability[28]. The reverse exchange behavior between phase II and III is attributed to elastic saturation in the fine intermetallic phase leading to subsequent plastic flow in the ductile matrix accompanied by cracking in the intermetallic. This cracking leads to isolated nanoparticles with coherent interfaces which strengthen the alloy. The two-stage complex yield behavior prior to total plastic deformation described above is a potent mechanism for yield retention at elevated temperature; and as detailed previous, Al-Ce alloys show markedly better retention levels in their yield strengths at elevated temperature. In the initial fully linear elastic region and transitional yield region (i.e. 2% offset) the exceptional thermal stability of the Al-Ce intermetallic phase at high temperature ensures little change to the micro-mechanical interactions between matrix phase and the nearby the intermetallic crystals. Furthermore, intermetallic crystals continue to act as powerful sites for dislocation

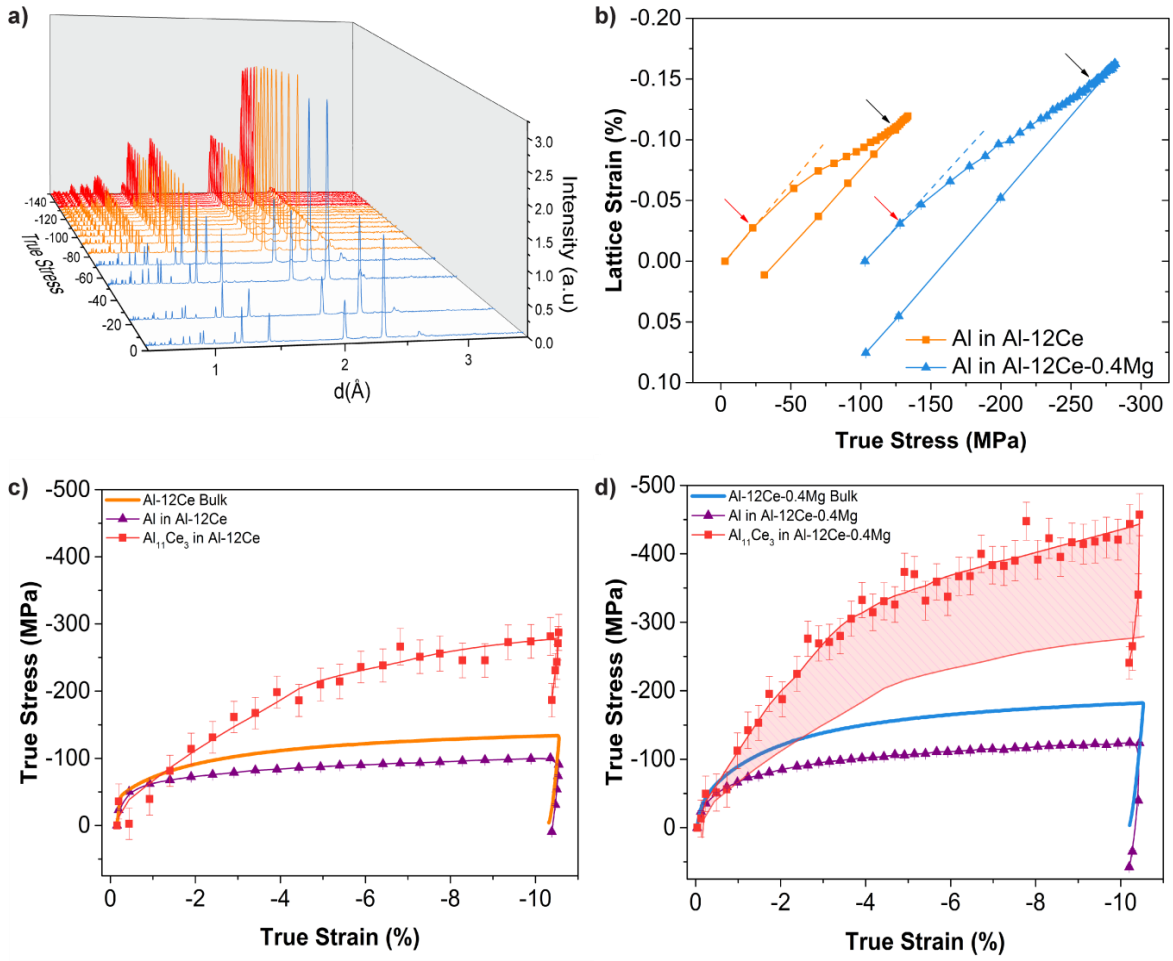

Figure 3.4: a) Neutron Spectrums showing change in scattering intensity as applied compressive strain increases. b) Strain measurements of Al-12Ce and Al-12Ce-0.4Mg (wt.%) performed under compressive load (the latter is offset by 100 MPa for visibility). Here the arrows denote onset of phases II (red), and III (black) described in the text. c) phase load-sharing for Al-12Ce under compressive load. d) phase load-sharing for Al-12Ce-0.4Mg under compressive load. Shaded region denote difference between binary and ternary alloy composition's mechanical response.

pinning until the matrix phase yields. Once initial plastic deformation has begun in the matrix phase, the intermetallic phase having been unchanged by exposure to elevated temperatures begins to take on elastic load. The reduction in yield at high-temperature is then a result of the softer aluminum matrix which yields earlier, but the retention occurs through the stable intermetallic phase carrying very similar amounts of elastic strain to room temperature values. The conclusion can then be made that the semi-coherency of the interface combined with high-temperature intermetallic phase stability leads the Al-Ce alloys to maintain a much higher portion of their yield strength at elevated temperatures when compared to traditional aluminum alloys, which are strengthened by metastable phases tending to breakdown at high-temperature. A significant residual compressive strain exists in the hard $Al_{11}Ce_3$ phase while a slight tensile load resides in the soft Al matrix, which is expected behavior after unloading given the two-phase coexistence and complex load sharing. Comparing Figure 3.4c-d reveals that the strengthening mechanism of the Al-Ce alloy does not change following the addition of Mg. Instead, Mg increases the magnitude of the load which can be carried by the intermetallic phase before dislocation saturation and subsequent redistribution of load to the aluminum matrix. The difference is depicted by the shaded region in Figure 3.4d.

The room temperature strength of the Al-Ce alloy family derives from the extremely fine distribution of dendritic intermetallic phases uniformly across the alloy which form during casting. The very low solubility of Ce in the solid Al matrix favors retention of this structure to very high temperatures compared to traditional casting Al alloys, and this is reflected in the superior retention of mechanical properties to above 300°C. These features lead to complex load-sharing in the binary Al-Ce alloy, where slight Mg addition markedly improves the material strength and offers a guide to further improvements in this new class of Al alloys.

3.8 Conclusion

Cerium strengthened aluminum alloys exhibit highly desirable behavior for many applications: high ductility, robust room-temperature mechanical properties, exceptional high-temperature mechanical property retention, high tolerance to casting defects, and excellent castability across a broad range of compositions. In fact, the cast materials approach the mechanical properties of traditional wrought alloys. The microstructure remains stable to above 500oC, corresponding to a

homologous temperature (T/TMelt) greater than 0.84, which rivals the stability observed in heat tolerant materials such as superalloys.

Given the high availability and low cost of cerium metal, these alloys are economically viable for large volume industries such as the transportation sector, where their properties make them ideally suited for vehicle light weighting. Elimination or reduction of heat-treatment amplifies the economic and environmental benefits of light weighting in the transportation sectors. Adoption of these alloys by industry will not only impact current technologies but will provide the basis with which to develop the next generation of high temperature aluminum alloys. Finally, by creating demand for Ce, which is overproduced, the economics of rare-earth mining improve. In a typical deposit, one-third to one-half of the rare-earth content by weight is cerium, so converting a by-product into a co-product will help stabilize global production and encourage diversification of the rare-earth supply chain.

3.9 Acknowledgements

This research was sponsored by the Critical Materials Institute, an Energy Innovation Hub funded by U.S. Department of Energy (DOE), Office of Energy Efficiency and Renewable Energy, Advanced Manufacturing Office and Eck Industries. This work was performed under the auspices of the U.S. DOE with ORNL under contract DE-AC05-00OR22725 and with LLNL under Contract DE-AC52-07NA27344. Work at the Molecular Foundry was supported by the Office of Basic Energy Sciences, of the U.S. DOE under Contract No. DE-AC02-05CH11231. Use of the Advanced Photon Source, an Office of Science User Facility operated by Argonne National Laboratory, was supported by the U.S. DOE under Contract No. DE-AC02-06CH11357. The authors thank Dr. Jan Ilavsky for support on 9-ID-C of the APS and Dr. Melissa Santala for preliminary TEM support.

4. Efficacy of Using Mischmetal as a Primary Alloying Addition

This chapter is adapted from a slightly edited version of a published work "The Efficacy of Replacing Metallic Cerium in Aluminum–Cerium Alloys with LREE Mischmetal" first published in the 2020 edition of Light Metals a conference proceeding publication of TMS.

Sims, Z. C.; Weiss, D.; Rios, O.; Henderson, H. B.; Kesler, M. S.; McCall, S. K.; Thompson, M. J.; Perron, A.; Moore, E. E. The Efficacy of Replacing Metallic Cerium in Aluminum–Cerium Alloys with LREE Mischmetal. In *Light Metals 2020*; Tomsett, A., Ed.; The Minerals, Metals & Materials Series; Springer International Publishing: Cham, 2020; pp 216–221. https://doi.org/10.1007/978-3-030-36408-3_30.

My primary contributions to this paper were: selection of alloy compositions for casting, modeling of binary CALPHAD systems, SEM and XRD analysis of samples, and the entirety of the writing and formatting of the manuscript.

4.1 Abstract

The ongoing development of aluminum-cerium alloys has produced materials exhibiting elevated temperature mechanical property retention, long term microstructural stability, and flexible processability compared to traditional aluminum alloys, accommodating the growing demand for high temperature aluminum alloys not requiring the use of high-cost elements like scandium. To date, reported Al-Ce alloy compositions contain large amounts of elemental cerium. Mischmetal (MM), a mixture of lanthanum, cerium, and other light rare earth elements (LREE) is less expensive and more available than pure cerium. The chemical similarity of the LREEs means there is possibility to use MM as the primary alloy addition, lowering alloy cost. This talk will report the effect of using MM instead of cerium in a 12 wt% binary alloy on mechanical properties, phase constituency, thermal stability, and load sharing. Results will show that MM can be substituted completely for cerium with a mostly positive impact on alloy performance.

4.2 Introduction

Aluminum alloys have long been the center of interest for light weighting of numerous end-product systems due largely to their elevated specific strength compared to ferrous materials, low cost relative to other light weight material, ease of processing, and good corrosion resistance, but they are limited in their use for high temperature applications creating a techno-economic gap [37,38]. The

limited application at high temperature is a result of the most often used strengthening mechanism which relies on soluble precipitates of a certain scale which when exposed to elevated temperature grow beyond their optimal size for material strengthening[18,39,40]. However, it remains attractive to close the techno-economic gap by developing an aluminum alloy that can be used at elevated temperature, but also possesses traditional characteristics of aluminum alloys: affordability, fabricability, and availability [18,41,42].

For that purpose, aluminum-cerium alloys are being developed. These alloys make use of a strengthening mechanism which is not sensitive to elevated temperature excursions which can in some case be achieved without heat-treatment[43–45]. The mechanism for high temperature strength relies on the solidification of stable intermetallic compounds composed of insoluble light rare-earth elements in combination with aluminum and other additions directly from the molten material whose structure can be controlled through higher order additions, melt modification, and solidification pathways[44].

Cerium, a light rare-earth element (LREE), is outside the traditional family of primary alloy additions for aluminum alloys, creating a new supply stream input. Cerium, though known as a rare earth, has a relatively high crustal abundance, being nearly as common as copper[46]. However, cerium metal and other rare earth metal supply lines are nearly single source. This is concerning for many industrial activities, as interruptions in supply of cerium from single source Chinese processing facilities would mean a shortfall in product delivery[41,47].

Though single source, the family of light rare-earth elements are all chemically similar - possessing the same number of valence electrons, similar electronegativities, and atomic radii that changes very little from lanthanum to neodymium[16,17]. This chemical similarity between the LREEs creates nearly identical phase spaces when they are combined with other elements. For example, Figure 4.1 1 shows the binary phase diagrams of the first four rare-earth lanthanides with aluminum produced from a custom CALPHAD database developed at Lawrence Livermore National Laboratory. This collection of diagrams helps to detail the high level of chemical and thermodynamic similarity of the first four LREE lanthanide metals. For example, all feature first line compound intermetallics of the composition $Al_{11}(LREE)_3$ and very similar eutectic compositions. A few distinctions can be seen however, such as the slightly higher liquidus temperature in the hypereutectic region of the heavier elements. The similarity of these phase

diagrams leads to the expectation one could substitute any number of these elements or combine them with cerium to produce aluminum alloys with similar properties. This flexibility in metallic primary additions creates a more diverse supply chain and lowers the risk of using LREE materials in aluminum alloys.

For investigating the possibility of diversifying the supply chain of LREE elements for use a primary addition in aluminum alloys, a mixed metal compound known as mischmetal (a combination of La, Ce, Pr, Nd with other small elemental components) was used as the primary alloying addition and compared against an alloy using the same weight percent addition of pure cerium. Mischmetal is often produced as a mine byproduct because separation of the LREEs is economically intensive with little advantage, making the material abundant and affordable[12,48,49]. If it is determined mischmetal can be used in place of pure metallic cerium, this will limit the impact of price and supply volatility on aluminum-LREE alloys, thus increasing the likelihood of adoption as well as providing feedstock supply diversity.

In this study Al-12 wt% (Ce or MM) alloys were produced using permanent mold casting, characterized, and compared (all values will be in weight percent). The cast alloys were characterized using x-ray diffraction (XRD), scanning electron microscopy, energy dispersive x-ray spectroscopy (EDS), and mechanical test methods

4.3 Experimental Techniques

4.3.1 Casting and Mechanical Testing

Casting of mechanical test bars was performed using a resistive 20kg furnace with a ceramic coated ferrous crucible and a coated ferrous permanent mold. The alloy component used to produce test bars were commodity grade products commonly used throughout industrial firms. Aluminum and metallic cerium ingots of >99% purity were used for the 12% Ce samples. The standard industrial MM alloy was composed of 51.9% Ce, 26.15% La, 5.35% Pr, and 16.60% Nd. For both alloys the aluminum charge metal was melted under an argon cover gas. Once a temperature of 750 °C was reached and the aluminum was entirely molten, cerium or MM materials were added in small increments to ensure full incorporation between additions. After full incorporation, the melt was fluxed with a fluorinated salt compound to remove contaminants.

Test bars were cast into 400 °C preheated permanent molds and removed once fully solid. Bars

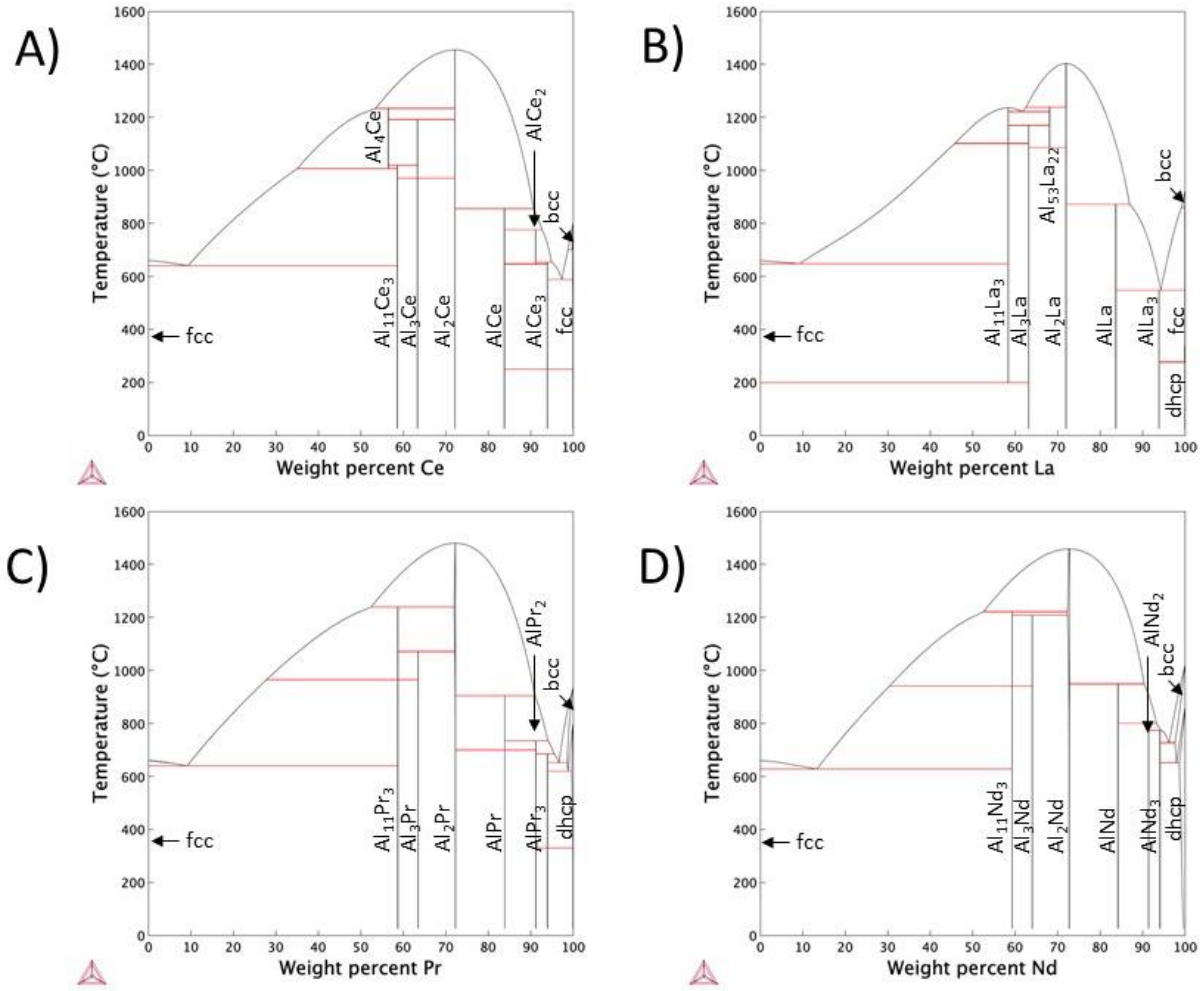

Figure 4.1: Binary phase diagram of LREE elements with marked phases: A) Al-Ce, B) Al-La, C) Al-Pr, D) Al-Nd

were left in the as-cast state for this study as heat-treatment has little effect on these binary alloy systems. Mechanical testing was carried out on a United Test Systems (Fullerton, CA) universal mechanical tester with wedge grips designed to work in conjunction with the test-bar geometry.

4.3.2 Bulk Phase Composition Analysis

Bulk phase compositions were measured using XRD techniques. The XRD system used was a Panalytical X'Pert Pro equipped with a copper source and a Kα monochromator. Samples were loaded onto a spinner sample plate to reduce the effect of any texturing present.

4.3.3 Microstructure and Secondary Phase Analysis

Samples were prepared for SEM imaging using standard metallographic techniques without etching. Imaging was performed using a Hitachi S-4700 SEM in backscatter mode to detect Z contrast between the phases present. EDS analysis was performed in the same system using an Oxford Instruments EDS system.

4.4 Results

4.4.4 Microstructural Analysis

The Al-LREE phase diagrams in Figure 4.1 illustrate that any combination of 12%LREE combined with aluminum is expected to produce a largely eutectic solidification structure with some areas of primary Al. Figure 4.2 is a collection of SEM images taken from the Al-12Ce (a,b) and Al-12MM(c, d) alloys. Al-12Ce material exhibits a eutectic solidification structure with distinct colonies of coupled eutectic growth composed of aluminum and the intermetallic $Al_{11}Ce_3$.

In contrast the microstructures of the 12MM alloy show a small fraction of large, high aspect ratio primary crystals of the $Al_{11}(LREE)_3$ intermetallic. Though the Al-12MM alloys shows some primary solidification of the $Al_{11}(LREE)_3$ intermetallic, the eutectic colonies of both samples show similar feature size, spacing, and shape. Lath thickness in both samples is approximately 250 nm. The alloy matrix shows a lower Z value (as measured through phase contrast in back-scatter imaging)-as expected with the extremely low solubility of all the LREE metals in the bulk aluminum metal. SEM imaging of localized contamination show small amounts of third and sometimes fourth phases which likely result from the extra contaminate metals found in the cerium, MM compound, and industrial grade aluminum.

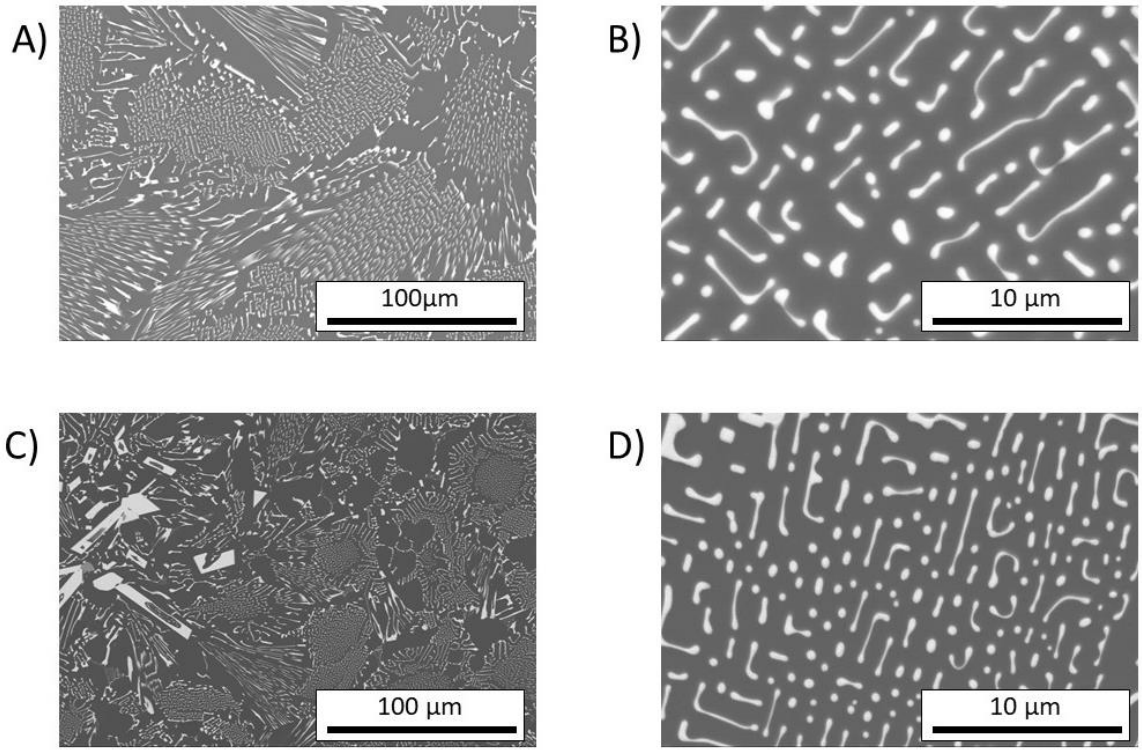

Figure 4.2: SEM backscatter micrographs of A) Low magnification as-cast Al-12Ce, B) High magnification as-cast Al-12Ce, C) Low magnification Al-12MM, D) High magnification Al-12MM

4.4.5 Phase Composition

Following backscatter imaging, EDS analysis was carried out on a large single-phase primary crystal of the majority intermetallic phase present in the Al-12MM sample. Figure 4.3 shows the location and size of the EDS analysis area. The area was significantly larger than the interaction volume of the beam and thus elemental quantification can be considered representative of the local composition.

Table 4.1 lists the elemental composition of the area analyzed in the 12MM sample. The analyzed area represents a substitutional intermetallic compound with a composition is very close to that of $Al_{11}(Ce,La,Nd)_3$. A number of other spectrums were analyzed, and all showed a nearly identical composition within the measurement error of the EDS system. Heavier LREE elements appear to be in lower concentration in the primary laths than is expected from the composition of the MM compound. This could result from the convolution of the weaker Nd and Pr peaks with the peaks of La and Ce in the EDS spectra. Contaminant phases mentioned above were smaller than could be measured effectively with EDS, but their lower Z-contrast in the backscatter mode indicates they are rich in aluminum and lighter transition metals with very little LREE metal.

4.4.6 Mechanical Strength

Both the Al-12Ce and Al-12MM alloys were cast into cylindrical test bars and tested in tension to failure. Figure 4.5 shows the measured strength values. Al-12MM samples showed higher yield strength but lower ultimate tensile (UTS) strength compared to the same alloy produced from pure metallic cerium. In addition to lower ultimate tensile strength the samples of Al-12MM show reduced ductility compared to its pure cerium alloyed counterpart.

4.5 Discussion

The reported results indicate that mischmetal may be a good candidate for use in place of or to supplement Ce in aluminum alloys as a primary addition. However, some differences between the two metallic additions are evident. For example, in observing the microstructures of the Al-MM and Al-Ce alloys, there are notable amounts of large primary crystals in the 12MM sample that are not equally present in the Al-12Ce sample. Considering the alloys were cast in the same mold using the same melt superheat, this appears to be an effect of the mixed metal system of the 12MM alloy. The higher liquidus temperature in the hypereutectic on the phase diagrams in Figure 4.1

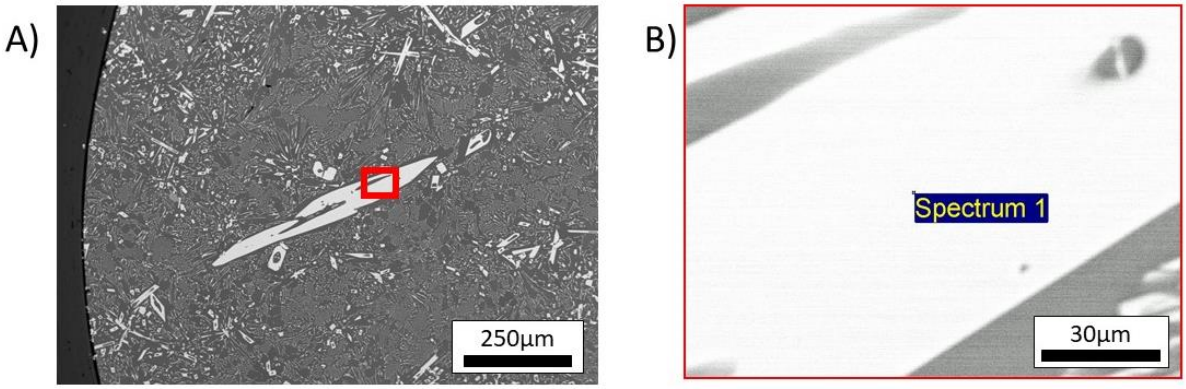

Figure 4.3: A) SEM micrograph showing position of EDS analysis area highlighted in a red box. B) High magnification of analysis area marked as Spectrum 1

Table 4.1: Elemental Composition of EDS spot analysis from Figure 4.3

Element	wt.%	at.%
Al-K	43.5	80.01
La-L	17.1	6.11
Ce-L	31.99	11.33
Nd-L	7.41	2.55

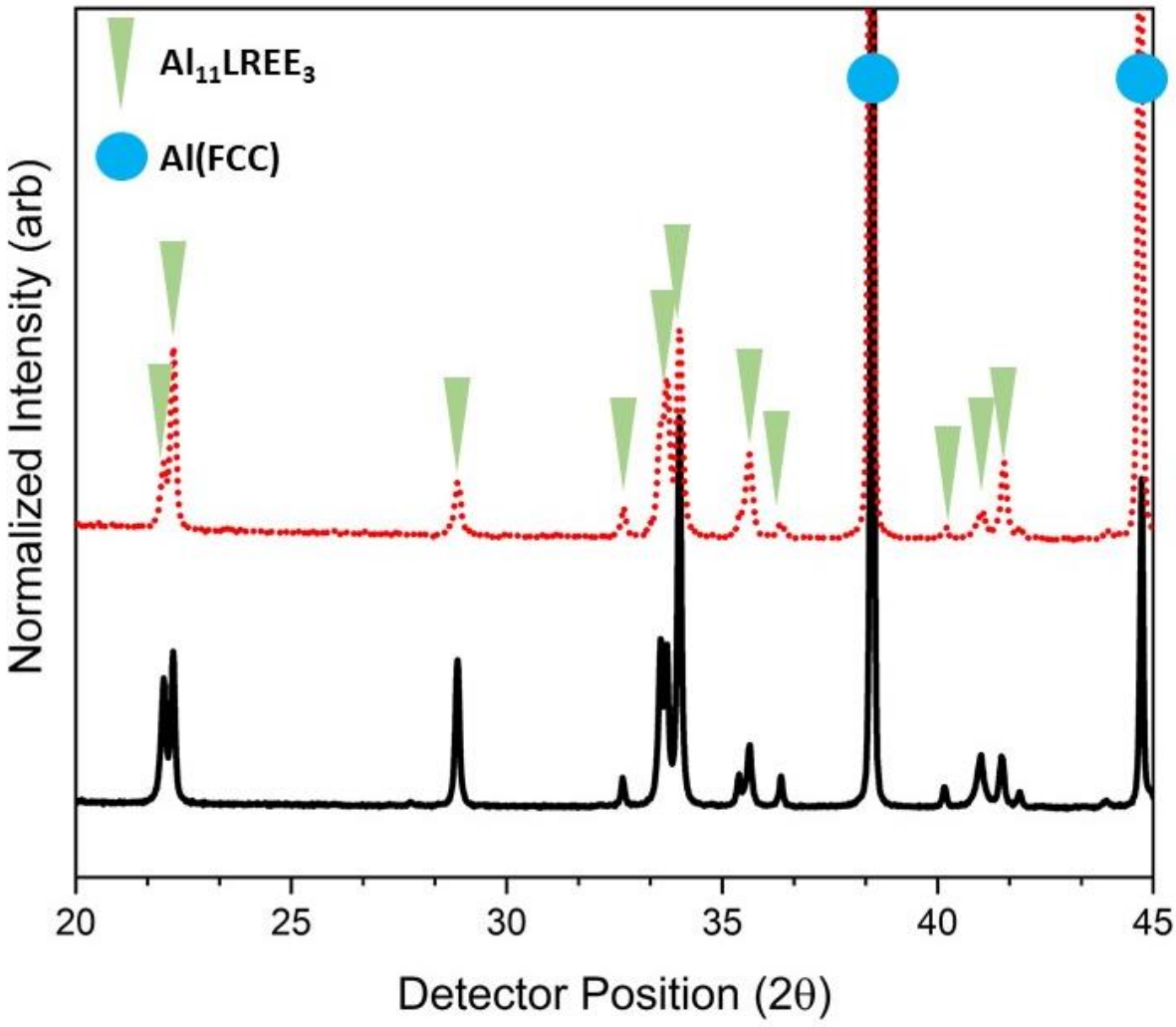

Figure 4.4: Stacked XRD spectra of Al-12MM (solid black) and Al-12Ce (red dashed)

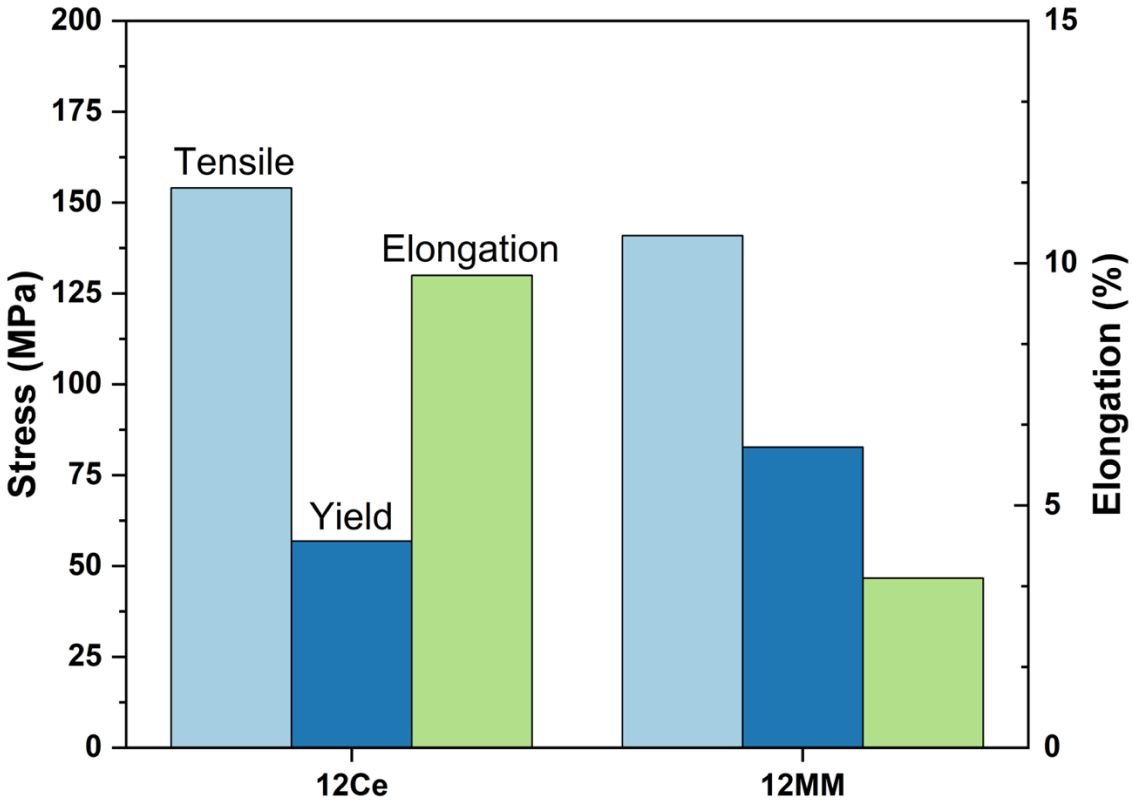

Figure 4.5: Ultimate tensile strength, Yield strength, and Elongation % of both Al-12MM and Al-12Ce alloys

is noted for the 12MM alloy. The moderate undercooling occurring in the permanent mold castings may not have been enough to overcome primary solidification mechanisms in the Al-12MM alloy sample. This could be overcome by lowering the mold preheat or increasing the melt superheat to provide for more undercooling and transitioning the sample to a more uniform eutectic structure.

The lower ductility of the 12MM sample likely can be attributed to the large primary crystals which act as crack nucleation sites and cleavage fracture. The increased strength of the MM alloy is not yet explained and may require more advanced techniques such as transmission electron microscopy or load sharing studies to characterize the difference and increase understanding.

Based on the low solubility of all the LREE elements in MM and the near-identical eutectic microstructure to the 12Ce sample, it is expected that the high temperature stability and mechanical strength retention in the Al-Ce alloy system would remain a characteristic of the Al-MM alloy system.

4.6 Conclusion

Despite the differences between the Al-12Ce and Al-12MM alloys it is expected that by combining aluminum with MM instead of cerium would result in a very similar alloy family and could be a route to reducing supply risk and cost. Aluminum alloy producers may be able to diversify their supply chain by leveraging the similarities between cerium and the other light rare earth elements to provide a flexible sourcing of LREE compounds for producing high temperature aluminum-LREE alloys.

4.7 Acknowledgements

This research was sponsored by the Critical Materials Institute, an Energy Innovation Hub funded by the U.S. Department of Energy (DOE), Office of Energy Efficiency and Renewable Energy, Advanced Manufacturing Office, and Eck Industries. This research was supported in part by an appointment to the Oak Ridge National Laboratory HERE and SULI program. This work was performed under the auspices of the U.S. DOE with ORNL under contract DE-AC05-00OR22725 and with LLNL under Contract DE-AC52-07NA27344.

5. Resistance of Al-Ce-Mg alloys to Loss of Mechanical Strength following Extended Exposure to Elevated Temperatures

This chapter is adapted from a soon to be submitted version of a manuscript with a provisional title “Long Term Thermal Stability of Al-Ce-Mg alloys”

My primary contributions to this paper were: selection of alloy compositions for casting, modeling of CALPHAD systems, SEM and XRD analysis of samples, and the entirety of the writing and formatting of the manuscript.

5.1 Abstract

Expanded use of aluminum alloy materials in elevated temperature environment is driving interest in development of new alloy families capable of surviving long term exposure at elevated temperatures while maintaining significant portions of their original material strength. Al-Ce alloys possess the necessary properties: high thermal stability, coarsening resistant microstructures, broad manufacturing compatibility, and relative low cost. However, their mechanical stability after extended thermal exposure has not been studied. This report will investigate the effect of long-term thermal exposure on Al-Ce alloys and compare them against those of current commercial alloys. Data on mechanical strength and microstructural transformations combined with CALPHAD modeling will show Al-Ce alloys to be extraordinarily stable when compared to current commercial products.

5.2 Introduction

The low density and relative low cost of aluminum (Al) alloys make them a prime candidate for many applications where light weighting is key to achieving increased system performance[50]. For example, internal combustion engines (ICE) are becoming more efficient and smaller in part thanks to effective low density material selection and engineering design to replace ferrous metals with lightweight nonferrous where possible[51,52]. However, the current library of aluminum alloys in commercial use are nearing the limit of engineering design for elevated temperature application. It is necessary, then, to design new aluminum alloys for extended use at elevated temperatures between the range of 200-350 °C.

Development in aluminum-LREE alloys have shown great promise for attaining a cost-effective high temperature material which can attain the properties necessary for the next generation of aluminum based elevated temperature alloys[44,53,54]. These materials are stabilized through a microstructure which resists coarsening at elevated temperatures due to extremely low rates of

diffusion combined with near-zero solubility in the majority aluminum matrix[44]. The microstructures of Al-LREE alloys is composed of at least one equilibrium Al-LREE rich intermetallic which has a melting temperature well above that of the bulk material[55,56]. Furthermore, the relative economic burden of LREE materials like cerium and lanthanum is comparable to other common aluminum alloying elements like Si and Cu because it is produced as an undesirable by-product to rare-earth mining[12].

An equilibrium intermetallic majority secondary phase and relatively low cost of aluminum-LREE alloys contrasts against other well researched high temperature aluminum alloys such as those strengthened by coherent L12 cubic precipitates[38]. Alloys such as Al-Sc, Al-Zr, and Al-V for example are well known to exhibit high temperature material properties but have several short falls[37]. For example, alloys of Al-Zr and Al-V require long complex heat-treatments to precipitate the metastable L12 phase in an appropriate size[38]. Additionally, the coherent L12 phase is likely to transform into an incoherent brittle fracture inducing D022 phase should material temperature ever exceed tight operational windows during normal use[37]. Additionally, the highest strength alloy system among the L12 strengthened alloys, Al-Sc, is prohibitively expensive, restricting it to niche cost inelastic applications.

Al-LREE alloys further separate themselves from common aluminum alloying methodology by taking advantage of eutectic coupled growth to create an equilibrium interconnected eutectic microstructure directly from solidification that often does not require heat-treatment to attain maximum material strength[44,57]. This mechanism is very different from other aluminum alloys such as the Al-Cu (2xxx series) and the Al-Si (3xxx series) which both require two step solution and aging treatments to attain maximum strength[39]. The heat-treatment and precipitation method for creating strength has long been the most common means to produce economical alloys, however it by its very nature is sensitive to elevated temperature. Because the small precipitate structures that lead to the optimal material properties are developed through targeted elevated temperature aging. Over-aging, occurring during elevated temperature application, results in reduced material properties. Thus, traditional two step heat-treatment aluminum alloys have inherent compatibility issues with elevated temperature applications[58]. The development of Al-LREE alloys have created a pathway to realizing new methods for producing strong, thermally stable aluminum alloys without the same inherent sensitivity to high temperatures that have limited the use of traditional aluminum alloys in certain applications.

Within the growing research field of Al-LREE, Al-Ce alloys have been the major interest to ongoing efforts as Ce is the most readily available LREE thanks to high levels of overproduction[59]. Al-Ce alloys form the equilibrium intermetallic phase $Al_{11}Ce_3$ that can survive high temperature excursions, even those up to a homologous temperature of 0.9[53]. Additionally, Al-Ce alloys have been shown compatible with a broad range of processing technologies including casting, extrusion, additive manufacturing, and other advanced processing techniques[37,60,61]. The high level of manufacturing flexibility extends to ternary and quaternary alloys of Al-Ce with several common alloying additions such as Mg, Cu, Si, and Fe[53].

Despite the growing knowledge of Al-Ce alloy design, work has not focused on long term microstructural and mechanical stability at elevated temperature for eutectic Al-Ce alloys. Work on short term exposures to elevated temperature show exceptional stability when compared to common aluminum alloys, but efforts to develop fundamental understanding of performance under long life operating conditions remains uncertain. This report will answer the questions regarding long term stability of Al-Ce-Mg alloys through extended exposures and comparison with common commercial aluminum alloys A206 and A356. An Al-Ce-Mg alloy was chosen as the material of most interest for this study because the system has been shown to have excellent room temperature mechanical properties in the as-cast state with exceptional stability at temperatures very close to the solidus temperature[44]. Additionally, Al-Ce-Mg is strengthened through a Al-Mg solid solution which should be stable at elevated temperature as Mg is driven into solution at high temperature likely increasing material strength[62].

5.3 Experimental Method

To understand the effect of long-term elevated temperature exposure on common aluminum alloys in comparison with Al-Ce-Mg alloys the production of a large number of test bar samples was required. Test bar samples for this report were produced using a 700lb natural gas furnace and a boron nitride coated iron gravity filled ASTM B108 test bar permanent mold preheated to above 400 °C to ensure proper filling and uniform structure. A356 and A206 samples were cast from industrial commercial products, composition limits can be found in the supplementary material, following standard industrial practices concerning melt superheat, cleaning, and pouring. Compositions of A206 and A356 were confirmed using an arc spectrometer. For this trial no additional modifications were needed as the A356 and A206 were within the industrial

specification for the material. Once cast the A356 and A206 alloys where heat-treated to an optimal strength condition. A356 underwent a T6 treatment with a solutionizing temperature of 540 °C for 8hrs followed by a water quench and 155 °C aging for 4 hours. A206 was heat-treated to a T7 condition with stepped solutionizing of 515 °C for 2 hours followed by 530 °C for 8 hours. A206 samples were then warm water (80 °C) quenched and aged at 200 °C for 4 hours.

Al-Ce-Mg samples were cast from commodity grade Al, Ce, and Mg with purities all above 99 %. Ce and Mg were added to molten pure aluminum in that order in steps and allowed to incorporate before making subsequent additions. A composition of Al-8wt% Ce-10wt% Mg (all compositions will be listed in weight percent for the remainder of this report) was selected for its high castability, good mechanical strength, and solid solution strengthening potential. During the melting and holding process the furnace was maintained under an argon blanket to prevent oxidation. Once the melt was returned to and stabilized at a holding temperature of 780 °C following all additions, the melt was cleaned and degassed using a nonreactive rotary method with argon gas. Compositions of the Al-Ce-Mg alloy could not be measured via arc spectrometry as the available machine was not programmed with the appropriate standards for cerium. Instead, additions were carefully weighed and tabulated to create a nominal composition for the alloy. After the melt was prepared the Al-8Ce-10Mg alloy was cast into the same preheated permanent ASTM B108 mold used for A356 and A206 alloys. Bars were extracted from the mold and allowed to cool. No heat-treatment was carried out on Al-Ce-Mg alloys as they do not require heat-treatments to attain high mechanical strength.

Initial room temperature mechanical test established a baseline for mechanical performance of the cast material. Mechanical tests for all samples were carried out using a United model STM-100KN tensile testing machine with a constant crosshead speed of 0.5” per minute following the ASTM E8, Rev 88 standard for tensile testing of metallic materials. Elongation was measured in program and confirmed manually following failure of the test specimen.

Thermal exposure of remaining test bars was carried out in a 3-zone tube furnace. To ensure accurate temperatures and limit thermal gradients, only furnace end zones were employed for thermal exposure. The center zone was fully insulated and left unused, creating a buffer between the two zones of different temperatures. Temperatures of 250 °C and 400 °C were selected as they represent a desirable temperature for next generation aluminum alloys and an extreme upper limit

for some stationary applications. Samples were loaded with furnace at temperature and left for 500hrs and 1000hrs respectively. Once removed, samples were allowed to cool naturally and measured for mechanical strength at room temperature using the same method as above.

Test bars sections of both pre and post exposure samples were mounted in resin and polished without etching for scanning electron microscopy (SEM) microstructural imaging. SEM images of all samples were captured on a Hitachi S-4700 in backscatter mode with an accelerating voltage of 10kV to highlight Z-contrast differences.

Knowing long term thermal exposure will have a marked effect on the amount of Mg in solid solution for the Al-Ce-Mg alloy, X-ray diffraction (XRD) was performed. XRD analysis was conducted using lightly polished alloy disk sections of test bar samples. The Panalytical X'Pert Pro system was used to collect X-Ray data. The system was equipped with a Cu source and Kα monochromator. In order to limit any effects of texturing the sample was spun at a rate of 1 revolution per second. Fitting was performed using the Rietveld method and HighScore Plus software.

5.4 Results

5.4.1 Mechanical Testing

Following successful thermal exposures both common commercial aluminum alloys A356 and A206 were tested at room temperature to understand how extended elevated temperature exposure would affect material properties. Figure 5.1 details the mechanical yield strength retention of the traditional aluminum alloys vs Al-Ce-Mg alloys. For full tables of final mechanical properties, please refer to the appendix (Table A.2). Traditional aluminum alloys show a precipitous drop in mechanical properties at 500 hours with a little change between 500 and 1000 hours. Differences exists between the traditional alloys as well when temperature is considered. Al-Si alloys appear to lose the majority of their strength at 250 °C, and only seeing an additional 5% drop off in strength between 250 °C and 400 °C. This is in contrast to A206 which at 250 °C retains the majority (70%) it's as-treated yield strength. However, unlike A356, A206 shows a large reduction in material properties between 250 °C and 400 °C with overall yield retention dropping to 41 % at 500 hrs and remaining largely stable through 1000 hrs.

The performance of both traditional aluminum alloys are in great contrast to the Al-8Ce-10Mg alloy. Al-8Ce-10Mg shows very little reduction in mechanical properties at 500 hrs and 250 °C but continues to see reductions in mechanical properties out to 1000 hrs unlike the traditional alloys. Despite this Al-8Ce-10Mg retains more then 90% of this as-cast material properties; a nearly 30% improvement over A206 and a 60% improvement over A356. The performance of Al-8Ce-10Mg at 400 °C is remarkable as the material increases steadily in strength as exposure time increases. Thus, as 1000 hrs Al-8Ce-10Mg has a 20% higher yield strength than it did in the as-cast state meaning a nearly 80% and 90% improvement in yield strength retention over A206 and A356 respectively.

5.4.2 Microstructure Evolution in Traditional Alloys

For understanding why mechanical properties evolved as they did, it is instructive to investigate the microstructure of the materials being studied. SEM micrographs of A206, A356, and Al-8Ce-10Mg can be observed in Figure 5.3-4. A206-T7 in the as-treated state (Figure 5.2a) shows distinct θ'' plates with high aspect ratios and good distribution within the matrix phase grains. These coherent phases are known to produce very high mechanical strength when optimally aged and evenly distributed[63,64]. Additionally, large amounts of θ precipitates are beginning to form at the grain boundary and triple junctions creating a thin precipitate free zone between the strengthening θ'' plates and intermetallic rich grain boundary. This structure is common and desirable in A206 for material strength[65]. After being exposed to an elevated temperature of 250 °C for 500 hours much of the microstructure has undergone significant transformation. The majority of the θ'' plates have become over aged and converted into θ' plates as clear from their lowered aspect ratio and less homogenous distribution. While still effective for strengthening θ' is not the most desirable strengthening phase and this amount is considered to be over aged. Furthermore, the width of the PFZ has increased, and the interconnectedness of the θ phase at the grain boundary has also increased. These combination of a transition from θ" to θ' and the increasing amount of θ phase at the grain boundary both influence the reduction in yield strength retention following exposure. As expected from the mechanical property results little change can be observed between the 500- and 1000-hour exposure times for the 250 °C sample. θ' plates remain the majority phase within the microstructure. The PFZ of the 1000hr sample appears to be more well defined than in the 500hr sample, but this might be a local variation and not representative of the total sample microstructure

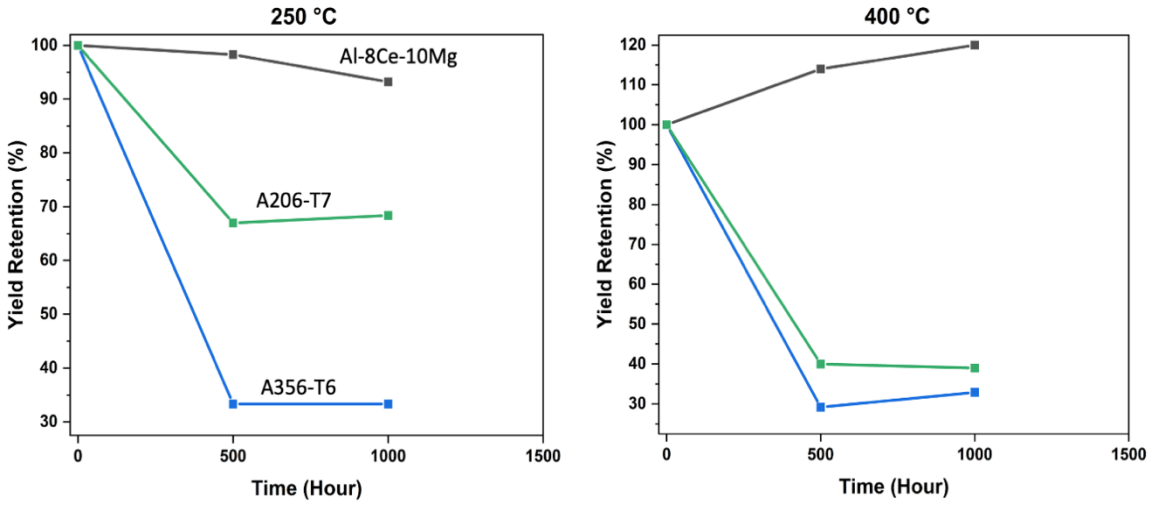

Figure 5.1: Yield strength retention of Al-Ce-Mg alloys compared against A206 and A356 showing major differences in property retention following long term thermal exposure

after 1000hrs at 400 °C. Grain boundary θ phase remains thin and interconnected with one notable large particle being observed in the sample.

Increasing the temperature to 400 °C coarsens the microstructure with further transformation of the optimal θ'' metastable phase. 400 °C additionally results in the precipitation of θ phase within the grain and thus further decreases material strength. In addition, larger amounts of Cu are able to migrate to the grain boundary where it can easily diffuse and coarsen. Thus, large θ phase particle are seen at the grain boundary with much lower interconnectedness at the higher 400 °C temperature. Similar to the samples tested at 250 °C little change can be observed in the grain's microstructure after 1000-hour exposure times. Minor changes in the number and distribution of θ phase within the grains can be observed, but this distinction may be accounted for by sample to sample variations or measurement location as the mechanical properties appear nearly identical. Similar to the interior of the grains, the intergranular region of the A206 sample exposed at 1000 hours does not exhibit a visible increase in θ particle coarsening or content. The lack of marked change between the 500- and 1000-hour samples at both temperatures eludes to the fact that 500hrs appears a sufficient time for near equilibrium conditions to be reached in the A206 alloy system. A356 being a near-eutectic Al-Si alloy exhibits a very distinct microstructure and thermal exposure response from that of A206. Microstructures of A356 in the as-treated and thermally exposed conditions can be found in Figure 5.2. Observing the as-treated state, a fine microstructure composed of eutectic silicon can be seen to have solidified before heat-treatment with subsequent minor coarsening in the interdendritic regions of the alloy occurring during heat-treatment. What is difficult to observe is any presence of Mg_2Si phase which plays a major role in strengthening particle size has coarsened to be contained much smaller colonies composed of larger individual Si particles each of sizes between 10-15 μm. Like with A206 there is little change between the 500- and 1000-hour samples to be observed. The majority of the loss in mechanical properties is explained through the coarsening of Mg2Si particles which again remain below the detection limit of the SEM micrographs in Figure 5.3. Little difference is observed between the 250 °C and 400 °C sample. This is expected since the material properties appear to not see significant additional degradation as the temperature is increased to 400 °C. It is likely that the lower properties of the 500 hr samples compared to the 1000hr are likely the result of bar to bar variation and not of a remarkable microstructural change resulting from the longer exposure time.

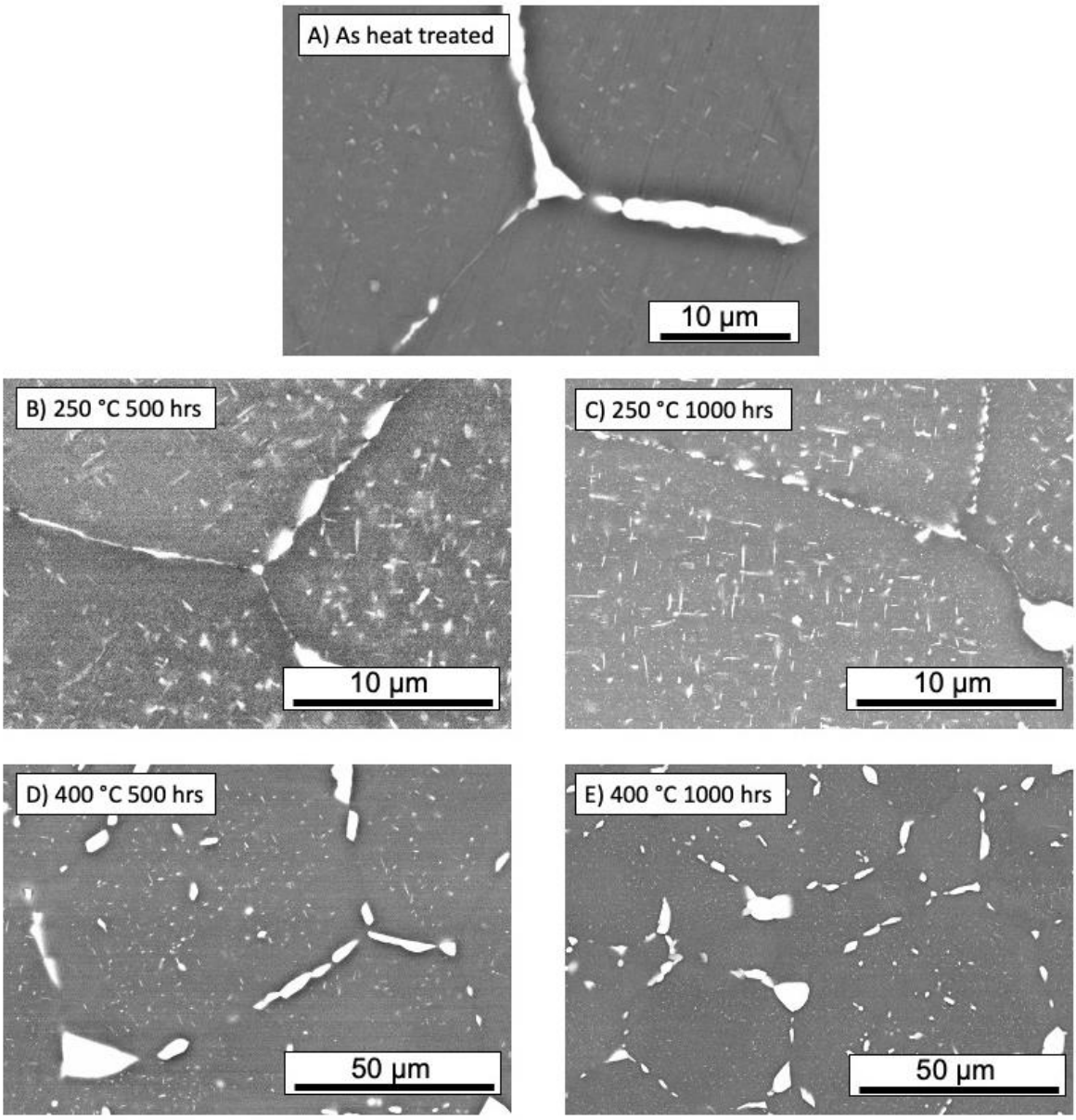

Figure 5.2 SEM micrographs representative of alloy A206 alloy at different thermal exposure levels detailing effects on phase microstructure A) As heat-treated T7 B) 250 °C 500hrs C) 250 °C 1000hrs D) 400 °C 500hrs E) 400 °C 1000hrs

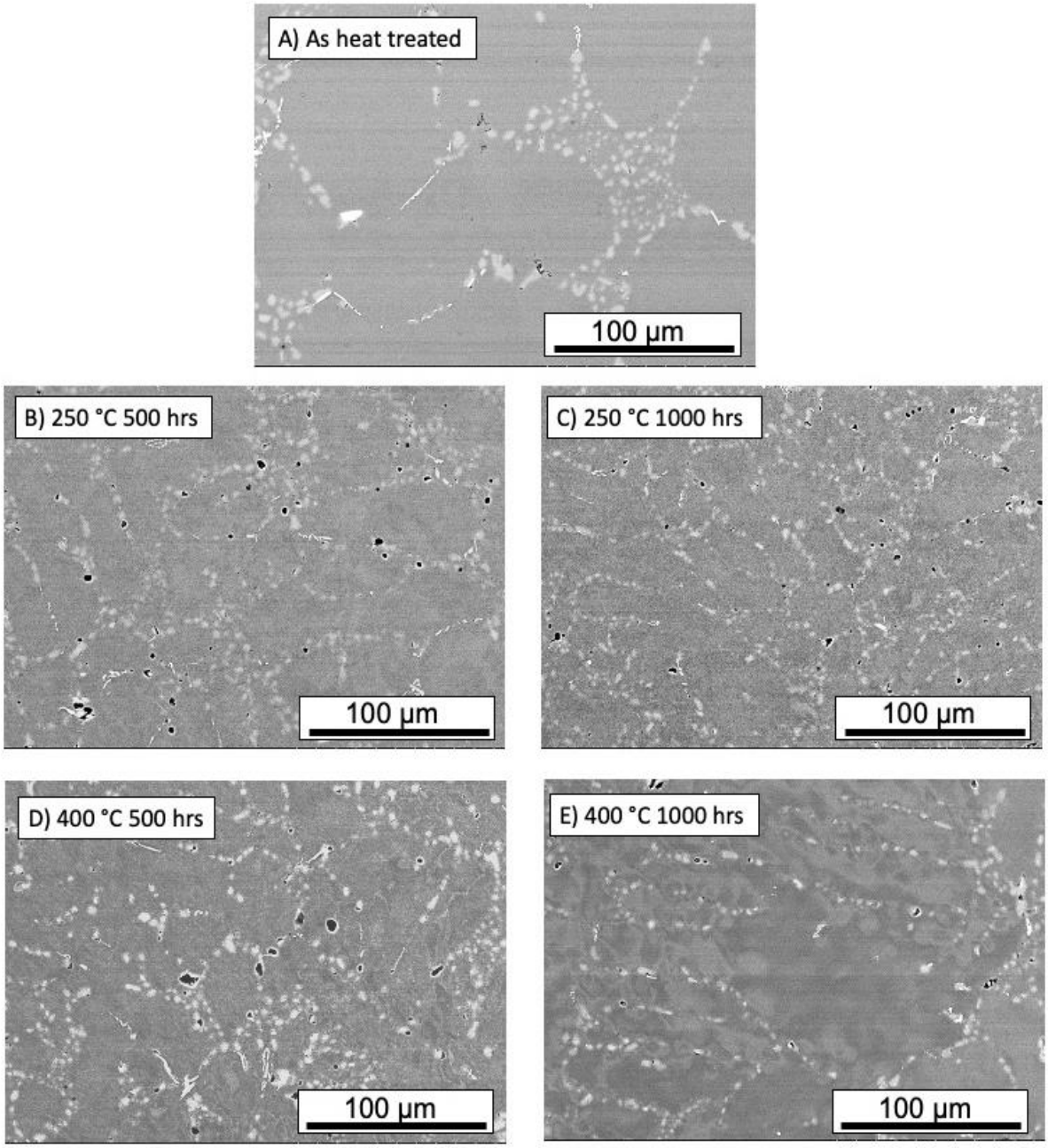

Figure 5.3: SEM micrographs representative of alloy A356 alloy at different thermal exposure levels detailing effects on phase microstructure A) As heat-treated T6 B) 250 °C 500hrs C) 250 °C 1000hrs D) 400 °C 500hrs E) 400 °C 1000hrs

5.4.3 *Microstructure Evolution in Al-Ce-Mg Alloy*

Al-8Ce-10Mg shows a unique response compared to the other two alloys which both coarsen their majority secondary phase readily at 250 and 400 °C. In observing the as-cast material in Figure 5.4a, there are 4 phases or groups of phases which can be identified. The first being the majority matrix phase (medium gray) composed of a solid solution of Al and Mg. The majority intermetallic phase is the well-studied $Al_{11}Ce_3$ phase (bright white) which is now to be stable at elevated temperatures across a wide range of compositions[53]. A second intermetallic phase can be seen forming in "pools" throughout the sample and this phase is a divorced eutectic Al-Mg β phase. Finally, as this material is cast using industrial practices, there are impurity phases present in the sample which do not greatly contribute or detract from material properties as they are scarce in number and do not agglomerate.

Furthermore, unlike the commercial alloys Al-8Ce-10Mg is the only alloy which shows an inverse phase stability behavior with overall microstructure looking less changed from as-cast at 400 °C than at 250 °C. Observing the 250 °C samples it becomes clear that the temperature appears to be detrimental to the stability of the solid solution matrix which is present in the matrix. At 250 °C large amounts of β-phase precipitated from the matrix and created a dense interconnected structure. This phase instability does not appear to have reached equilibrium by 500hrs and instead continues to precipitate more β phase out to 1000 hours with large globular colonies now being observed in some areas surrounding $Al_{11}Ce_3$ intermetallic. Despite the observable changes occurring in the matrix the structure and content of the $Al_{11}Ce_3$ remains unchanged at 250 °C at both 500 and 1000hr intervals. No observable coarsening is present in the areas of coupled eutectic growth retained from solidification.

400 °C appears to be a more stable temperature for the microstructure of the Al-8Ce-10Mg alloy as β phase content appears to have been slightly decreased from the as-cast state. Yield strength data would point to a reduction in the amount of β phase present in the alloy as strength increases with increased levels of dissolved solute Mg. Thus, the matrix of those Al-8Ce-10Mg alloys exposed to 400 °C show little change, but likely have increased Mg in solution compared to the as-cast sample. Despite the differences in the make-up of the matrix between the 250 and 400 °C samples, the $Al_{11}Ce_3$ intermetallic phase fraction appears again to be largely unaffected by the high temperature exposure. One notable change is how after 1000 hours at 400 °C the thinnest sections

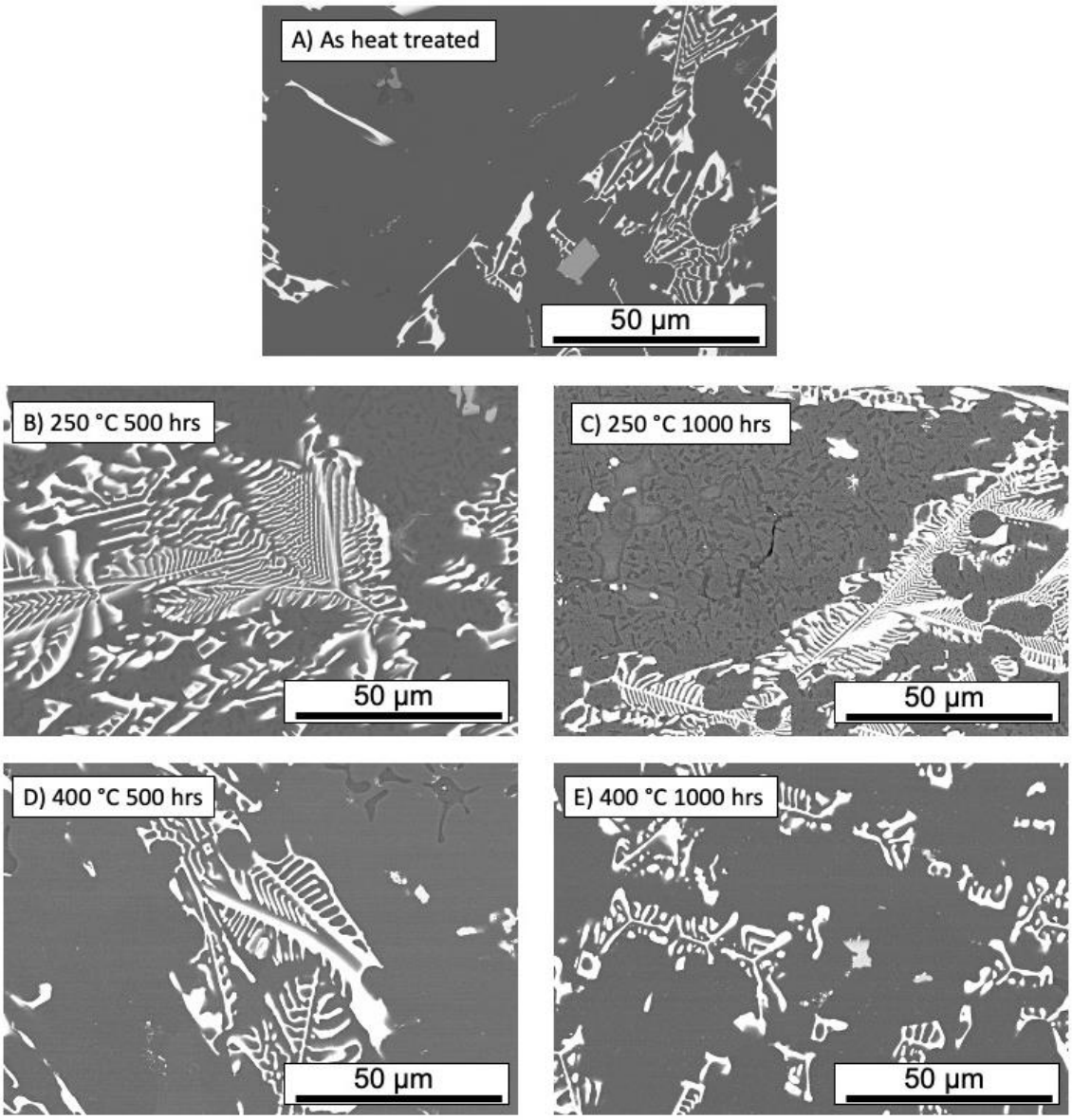

Figure 5.4: SEM micrographs representative of Al-8Ce-10Mg alloy at different thermal exposure levels detailing effects on phase microstructure A) As cast B) 250 °C 500hrs C) 250 °C 1000hrs D) 400 °C 500hrs E) 400 °C 1000hrs

of eutectic solidification appear to have self-diffused and lowered their aspect ratio. This is common in studied low mobility systems and is the result of thermodynamic driving forces which seek to limit surface energy of the system. Additionally, at 1000hrs even fewer areas of β phase can be observed with only a handful existing in the imaged cross-section.

The solid-state transformation of the Al-8Ce-10Mg alloy toward containing a β rich matrix was modeled using CALPHAD methods. The results of which can be found in Figure 5.5. Al-Ce-Mg systems behave like a pseudo-binary once solidified. The property diagram in Figure 5.5c shows that the $Al_{11}Ce_3$ intermetallic phase mass fraction remains unchanged at either test temperature. However, the matrix underdoes significant change in the temperature range between 250 °C and 400 °C. A mass fraction of nearly 0.2 β is the equilibrium phase at 250 °C, and this is reflected in the micrographs accompanying the CALPHAD models. After 1000 hours the sample has reached a near equilibrium content of β and large globular colonies exist alongside interconnected crystallites. Neither of these phase morphologies are expected to be coherent [67]and are known to limit ductility of Al-Mg alloys[68]. Increasing the temperature to 400 °C for extended periods of time was enough to dissolve the β phase present in the as-cast sample, pushing the additional Mg back into solution with the Al matrix.

To understand how the aluminum matrix is affected by the additional amount Mg in solution, XRD was used to measure the evolution of the Al-FCC phase lattice parameter. Increasing the amount of Mg in solution will in turn increase the FCC lattice parameter, due to the larger size of the substitutional Mg atom[69]. XRD spectra for three samples is shown in Figure 5.6. Spectra for the as-cast, 250 °C for 1000hr, 400 °C for 1000hr sample all show distinct properties. The as-cast sample possesses a small but measurable amount of β phase in the alloy. While the 250 °C sample is measured to possess a much larger amount of β than either of the other samples as expected. $Al_{11}Ce_3$ is present in all compositions at roughly the same phase fraction. The difference in location of the Al-FCC peaks shows a definite correlation between exposure temperature and Mg solid solution content as expected.

Measurement of the Al-FCC lattice parameter can reveal the changes in Mg content in solid solution within the alloy itself. Previous work has measured the correlation between lattice parameter and Mg content in solid solution[69]. Figure 5.7 shows the calculated lattice parameter of each alloy using the Rietveld method and its correlation to Mg content in the Al-rich matrix phase.

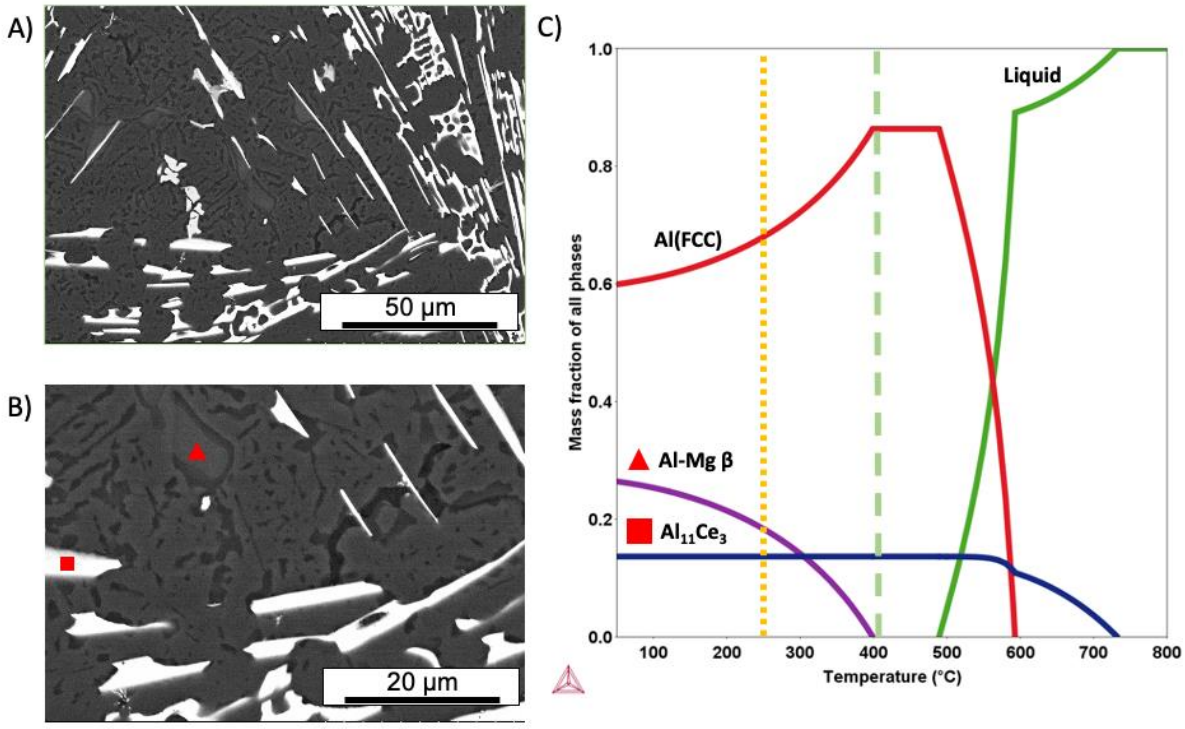

Figure 5.5: A) SEM micrograph of Al-8Ce-10Mg with presence of large amounts of precipitated β phase B) High magnification SEM micrograph of Al-8Ce-10Mg sample with phases marked, red square Al11Ce3, red triangle Al-Mg β phase. C) CALPHAD property diagram model of Al-8Ce-10Mg showing β phase dissolution at upper testing temperature.

As expected, the as-cast sample falls between that of the 250 °C and 400 °C sample. The as-cast Mg content being much closer to that of the 400 °C exposed sample than the 250 °C sample; meaning that solidification of the Al-8Ce-10Mg sample in the test bar permanent mold is sufficient to capture the majority of the Mg in solution. A property that reflects the knowledge of Al-Ce-Mg alloys being able to find application without the need for heat-treatment.

In addition, Al-8Ce-10Mg alloys exposed at 400 ° C show concentrations of Mg in solution very near the theoretical limit of 12.8%[70]. Meaning this sample has reached as near an equilibrium composition as is likely. The above 10% concentration results from the reduced amount of aluminum in the matrix relative to nominal composition due to the high content of $Al_{11}Ce_3$. For this reason, there can still be β phase observed in the 400 °C throughout the matrix in a much lower amount likely below the detection limit of XRD methods.

5.5 Discussion

Behaviors of the traditional aluminum alloys following exposure to elevated temperatures is as expected. The process of precipitation strengthening aluminum alloys by nature produces thermally unstable intermetallic phases which at room temperature can remain at an optimal size for the lifetime of the alloy in application. However, when temperature is increased the ease of diffusion and shift in alloy equilibrium condition towards a solid solution and away from nanoscale intermetallics creates a driving force for mobility and coarsening of the precipitates[63,71]. Both A206 and A356 appear to have reached a plateau in their mechanical degradation by 500 hours with little change occurring following. This would mean that for these alloys, the standard lifetime of many components which is 1000s of hours would result in the alloy reaching a minimum material strength after only a fraction of the parts lifespan. Thus, engineers need design for the expected material strength after it has overaged and reached and minimum performance point well before the part is expected to fail or be replaced. This process requires significant design compromises and often results in higher part costs and weight due to the need for greater reinforcement and complexity. In some more extreme cases it is impossible to design a part from lightweight aluminum alloys as they do not retain enough material strength following short exposures. It is also instructive to consider the effect of further elevating temperatures beyond standard operating ranges for aluminum alloys. 400 °C can be thought to represent the material response in the case of extended operation outside engineered ranges. For A356 little negative effect is observed

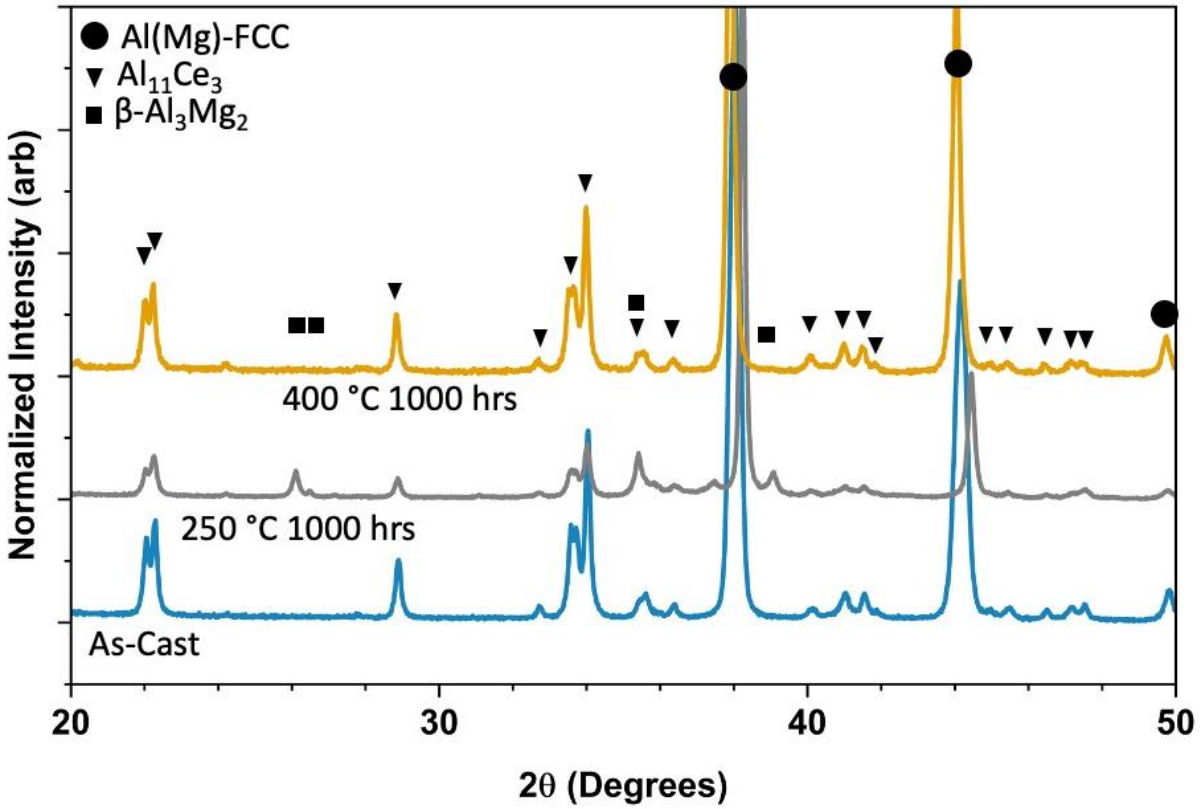

Figure 5.6: XRD spectra of Al-8Ce-10Mg alloys in the as-cast and thermally exposed conditions showing the distinct shift in lattice parameter of the FCC phase and precipitation of β phase with thermal exposure

meaning it would be possible parts or materials designed from A356 might survive temporary excursions to operating temperatures well above designed limits. A206 on the other hand, sees a large drop off in material properties when exposure temperature is increased from 250 to 400 °C. The sharp reduction in properties means A206 alloys are not well suited to applications where operating temperatures are prone to fluctuate outside design limits for extended periods of time.

Al-8Ce-10Mg shows a vastly different response from either of the traditional aluminum alloys by being almost completely mechanically unaffected at temperatures of 250 °C. The improvement in material property retention of Al-Ce-Mg based alloys makes possible new design methodology in next generation materials as they can reduce the need to design for long-term property degradation. Not having to design for forecast property loss over time means that parts could be made even thinner and lighter depending on the application. These design changes could decrease the amount of material needed, increase efficiency for some applications, and change the elected manufacturing technique increasing design flexibility.

Furthermore, Al-8Ce-10Mg increases in strength after high temperature 400 °C exposure. This is in comparison to A206 which shows a large drop off in properties when exposed to the further elevated temperature of 400 °C. The precipitous reduction comes about as a result of the increased coarsening of θ'' and θ' precipitates into the incoherent θ particles and their migration to the grain boundary[65]. This process is made more rapid at high temperature as the solubility of Cu in the Al-rich matrix increases[64]. This property of A206 alloys means that for many applications where extreme temperatures may be encountered it would be necessary or prudent to completely replace parts following an excursion to above designed operating temperatures for any length of time. Al-Ce-Mg alloys on the other hand show a measurable increase in properties once returned to room temperature from 400 °C. The increase as discussed is a result of the solid solution strengthening of the high Mg content of the Al-8Ce-10Mg alloy which increases at elevated temperature exposure. The increase in properties means that not only could a part produced from Al-Ce-Mg alloys continue to be used as is without the need to be replaced following extended over temperature excursion, but also that parts designed using Al-Ce-Mg could be returned to full operating strength and ductility by maintained excursions at temperatures above designed operational ranges. This potential opens the door for designing lightweight aluminum parts with extended lifetimes over those produced from traditional alloys.

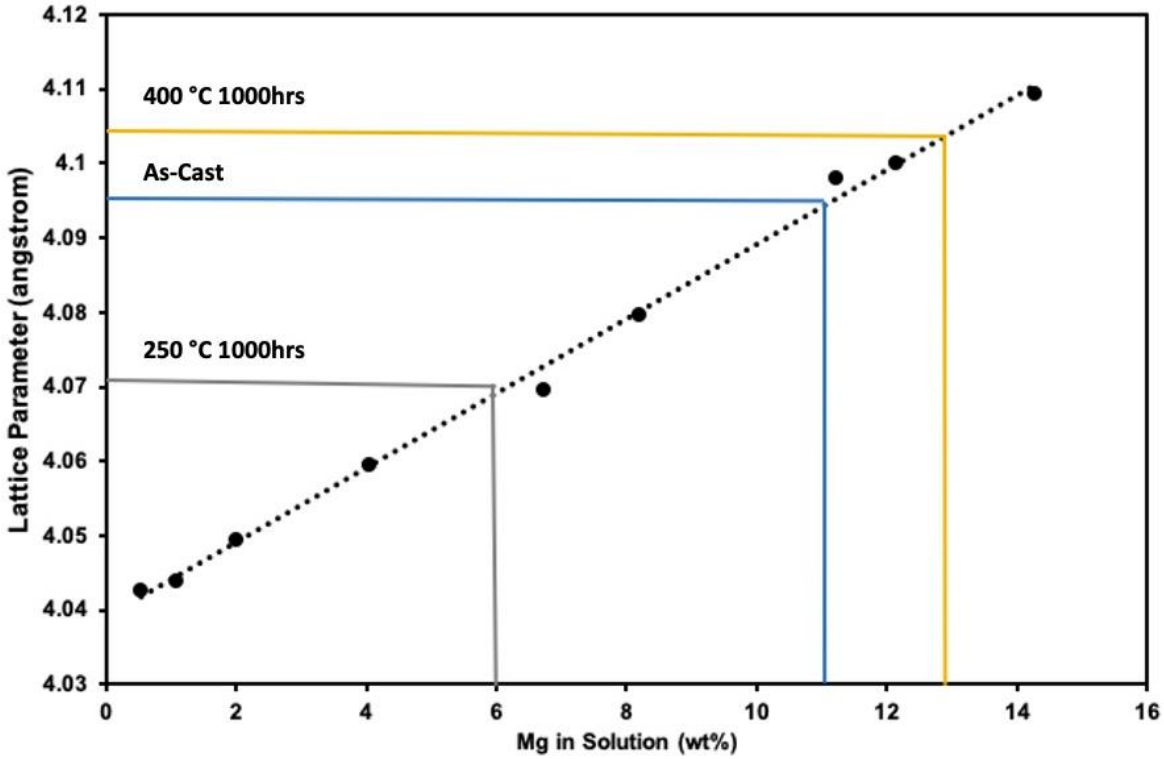

Figure 5.7: Calculation of amount of Mg in solution for each treatment condition to understand the amount of Mg rich β phase precipitated data fit to Pearson experimental data for Mg effect on lattice parameter

Despite the positive results of the Al-Ce-Mg alloys when compared to traditional alloys, there are necessary improvements which need to be made for Al-Ce-Mg alloys to become an industry standard for new generation applications. The high amount of solid solution strengthening provided by the Mg content also limits ductility, and as shown produces an unstable precipitate structure that leads to further ductility reduction when exposed for long periods at current preferred operating temperatures. This process might be controlled by targeting lower additions of Mg to limit the amount which can be dissolved in the aluminum matrix, retaining the majority of the material strength but reducing the impact on tensile ductility. The precipitation of large amounts of β might also be controlled by increasing the operating temperature in the applications which adopt Al-Ce-Mg alloys. The second options provide for opportunity in many applications such as ICE systems to further increase attainable efficiency and decrease fossil fuel use.

5.6 Conclusion

Al-Ce-Mg alloys have the potential to be a good choice for material deign where elevated temperature stability is an important factor. Al-Ce alloys offer a mechanical property stability above that of traditional commercial alloys. Al-Ce shows up a 50% improvement over Al-Si and a 30% improvement over Al-Cu alloys at 250 °C and a 90% improvement at 400 °C over both Al-Si and Al-Cu alloys. Al-Ce alloys are not without their shortfalls however, and ductility of Al-Ce-Mg alloys remains a concern. Solutions which might be possible are lowering the amount of Mg present in the alloys to limit embrittlement and balance properties.

Additionally, the proposition of an aluminum alloy which can survive temporary excursion to well above the proposed operating temperature is interesting. This property of Al-Ce alloys is in comparison to traditional options which as shown above might suffer catastrophic reductions in material properties which would create a source of part failure. Overall the results show clearly that Al-Ce alloys are a viable option for taking the place of current aluminum alloys in many stationary and dynamic elevated temperature applications thanks to their retention of high amounts of material mechanical properties when compared to their traditional counterparts.

5.7 Acknowledgements

This research was sponsored by the Critical Materials Institute, an Energy Innovation Hub funded by the U.S. Department of Energy (DOE), Office of Energy Efficiency and Renewable Energy, Advanced

Manufacturing Office, and Eck Industries. This research was supported in part by an appointment to the Oak Ridge National Laboratory HERE and SULI program. This work was performed under the auspices of the U.S. DOE with ORNL under contract DE-AC05-00OR22725 and with LLNL under Contract DE-AC52-07NA27344.

6. Resistance of Al-Ce Alloys to Aqueous Corrosion

This chapter has been adapted from a soon to be published manuscript with a provisional title "Understanding the effects of Cerium Additions on the Corrosion of Aluminum Alloys"

6.1 Abstract

Among factors effecting the viability of a new aluminum alloy for broad adoption, few are as important as corrosion resistance. The impact of corrosion on modern materials in engineering applications is widespread, costly, and in some cases deadly. Al-Ce alloys are a new family of aluminum alloys with attractive properties for high temperature application. Despite this, no study of the corrosion properties of Al-Ce alloys and the effect of Ce as an alloying addition to inhibit corrosion has been undertaken. This report will seek to close those gaps in knowledge by investigating the effect cerium as on corrosion properties of aluminum as a: main alloying addition, a minor addition to current commercial alloys, and as a scavenger of impurity elements. Studies will be carried out using several corrosion characterization techniques including salt-spray, intergranular attack, and tidal exposure. Reported data will show that Ce is highly corrosion resistant and can be used effectively as a main addition or to augment alloy corrosion resistance.

6.2 Introduction

For structural materials one the most important properties is resistance to corrosive attack. Failures, both anticipated and catastrophic, due to corrosion leads to billions of dollars in damage every year and may lead to injury or death if not properly managed[72–75]. Among modern materials, aluminum (Al) is highly desired for its mechanical strength, ease of manufacturing, relative low cost when compared to other lightweight materials[18,76,77]. Additionally, Al and its alloys exhibit a natural resistance to corrosion as Al immediately forms a protective passivation layer upon exposure to oxygen[78]. Despite this natural resistance many applications require additional corrosion resistance and for those there are several methods for improving the corrosion resistance of Al alloys[78–80]. Coatings are one of the most common methods preventing corrosion in Al alloys. These can include paint or dip coating, but the most used are method which rely on growth of artificially thick oxide layers[80,81]. Anodization, a process of electrochemically promoting oxide growth on an alloy substrate is common and offers great corrosion resistance improvement. Conversion coatings, another common but more niche method, require additional processing steps and cost, making them cumbersome and suited mostly for applications which will be exposed to harsh environments for extended times. Additionally, the most effective family of conversion coatings,

chromium-based coatings, have been largely outlawed except for some mission critical applications due to their extreme health risk and environmental impact[82]. For this reason new coating technologies and additional techniques for preventing Al material corrosion are of great interest[82–84].

One possible option which has been researched over the past two decades is the use of light rare-earth elements (LREE) in conversion coatings to prevent corrosion of Al alloys[79,83]. Of most interest is the use of Ce and La halide compounds in submersion baths to promote the formation of very stable mixed oxide conversion coatings[79,85,86]. The results of these studies make it clear that LREE-based methods have the potential to have nearly the same level of corrosion resistance as chromium-based methods[83]. Direct additions of LREEs to aluminum and its alloys as main alloying component, inhibitors, and impurity scavengers is underexplored, but some work has shown promise. Previous studies has shown that additions of numerous rare-earth elements (REE) can have positive impacts on the corrosion potential and passivation behavior of certain Al alloys, with heavier REEs being most effective[87]. Also, research focused on the impact of small additions, <2%, of La and Ce on microstructural refinement in common Al alloys shows that many REEs can be effective refining agents without being affecting corrosion performance[88,89], but there is still limited understanding of how LREEs impact corrosion of Al alloys as both primary and minor additions. The report will close some of the gaps in the knowledge of direct additions of LREE by studying several different methods for additions of cerium (Ce) to Al alloys.

Ce is a practical choice of REE to study for improving Al corrosion resistance because of its significant crustal abundance, similar to that of copper, and its low-cost relative to other REEs. During the mining of REE, more than 50% of the material remaining after the ore is concentrated is Ce and supply is greatly outpacing demand. The excess of supply results in a suppressed price which drives the cost of the heavier more critical REEs upwards. Currently, Ce is largely a by-product of REE mining and only finds application in low value, low demand technologies like lighter flints, NiCd batteries, and CFL bulb phosphors[90,91]. The low demand for Ce and La hurt mine economics which are forced instead to rely on less abundant elements like Nd and Dy that have high demand in emerging technologies to remain profitable. Thus, increasing the demand for Ce and La is a viable pathway to stabilizing REE supply chains and prices. Increasing demand for Ce metal will improve overall REE mine economics and help to stabilize a supply chain that remains largely out of balance[12].

Among the LREEs, there are emerging applications for Ce which may help create significant, stable, long-term demand. Al-Ce alloys have been a focus of recent research with promise as lightweight alloys for elevated temperature application[43,44,54]. These alloys exhibit properties sought after for new Al alloys including reduced cost over current high-temperature Al alloys, excellent manufacturability, and good mechanical properties at room and elevated temperature. Despite this collection of properties, corrosion performance of Al-Ce alloys remains unstudied. The electrochemical properties of any new alloy are important for its successful adoption. It is then important to understand how these new alloys perform in corrosive environments when compared to existing commercial alloy systems.

Three focus areas for addition of Ce will be presented: (1) Addition of Ce as a main alloying element with Al, (2) Modification of common Al alloys with Ce to reducing corrosion susceptibility, and (3) Addition of Ce to scrap streams to scavenging impurity elements and improve corrosion resistance of certain Al alloys, improving Al recycling generally.

6.3 Methods

6.3.1 Metal Casting

All casting of metal alloy test bars for this report was performed in a 25kg electric resistance melting furnace operated with an argon cover gas. Commercial high purity aluminum and cerium ingot with a purity above 99.9% were used to attain desired composition. Cu was introduced to melt when necessary in the form of 99.9% copper shot. Metals were added aluminum first, followed by cerium, and finally any additional metals were added to reach target nominal composition. In the case of Ce+Cu modified 356 alloys, a high purity A356 alloy whose composition can be found in Appendix 1 was used for the parent alloy.

All compositions, once melted, were held at a pouring temperature of 760 °C under an argon blanket. Prior to casting the melt was cleaned with an alkaline flux containing halides to assist in the removal of any present impurities and oxides. Following cleaning test bars were poured using an ASTM B108 test bar permanent mold. Bars were allowed to solidify and then mechanically removed.

Industrial components including those introduced to tidal pool corrosion were produced in a 400 kg gas fired crucible furnace. For mixing the final composition of Al-12Ce-0.4Mg a master alloy of 535.2 (composition of which can be found in Appendix 1) was diluted with 99.9% pure cerium and aluminum ingots until target nominal composition was reached. Once a sufficient pouring temperature has been attained, the melt was cleaned using a rotary degasser and non-reactive argon. Then castings were poured using a manual tilt pour method and single use sand molds.

6.3.2 Tidal Exposure Testing

Samples were prepared for exposure to a tidal environment where they would undergo cyclic exposure much like parts would under real world operational environments. For preparing the sample, a hole was drilled in two places which allowed the part to hang horizontally minimizing the difference in exposure across the sample due to tidal motion. Once holes were drilled a rope was threaded through the sample which was then attached to the dock. After being attached to the dock, it was lowered and secured at a height adequate to ensure complete coverage with water during high tide environments and similarly complete atmospheric exposure during low tide.

Periodically the sample was raised to capture images of corrosion progress. During these times, the sample was disturbed as little as possible to limit the impact of the imaging on corrosion results. Sample exposure totaled 88 weeks. After which, the blade was removed and sectioned for quantitative study.

6.3.3 Salt Fog

For salt fog test performed on alloys with cerium as a main addition and those contained within the same comparison, small sections of relevant alloys were cut from cast test bars or extruded bar stock and lightly polished with 600 grit sandpaper. Once lightly polished samples were cleaned and mounted in a salt fog cabinet configured to operate under the constraints of the ASTM B117 standard. The samples were exposed for 1000 hours; after which time they were removed and lightly cleaned with water and an ultrasonic bath. Following cleaning the samples were weighed to determine final corrosion results and likely method of corrosive attack.

Those bars prepared for the impurity scavenging experiment were first sectioned and then loaded into a separate salt fog cabinet also configured to operate under ASTM B117 standards. The

samples remained in the cabinet for 1000 hours after which time they were removed and cleaned. Cleaned samples were mechanically tested and results reported against uncorroded counterparts.

6.3.4 Intergranular

For intergranular corrosion studies small samples were prepared from extruded bar stock and B108 test bars for wrought and cast alloys respectively. Sectioned samples were mounted in clear resin and polished. Following a complete polishing, samples were subjected to an ASTM G110-92 test. This test is used to measure intergranular attack and takes advantage of a dilute sodium chloride + hydrogen peroxide solution to create a rapid corrosion environment. Hydrogen peroxide acts as a potent oxidizer, increasing the rate of intergranular attack and focusing corrosion on the grain boundary through oxygen introduction[92,93]. Corrosion depth was measured as a maximum observed depth as taken from the point on the surface at which intergranular attack initiated.

6.3.5 Scanning Electron Microscopy

Scanning electron microscope (SEM) images of all samples were captured on a Hitachi S-4700 in backscatter mode with an accelerating voltage of 10kV to highlight Z-contrast differences between the elements composing the samples.

6.4 Cerium as a Main Addition

Al-Ce alloys offer promise as a principal family of alloys alongside others like Al-Si and Al-Cu. Recent research has shown them to be a viable option for elevated temperature applications such as engine blocks and turbocharger impellers and housings[57]. A distinguishing feature of these alloys is a high phase fraction of a strengthening intermetallic more stable at elevated temperatures than intermetallic phases seen in other Al alloys [43,44]. This is due to the insolubility and low diffusivity of Ce in the Al matrix preventing the coarsening of secondary phase precipitates and subsequent reduction in mechanical strength[43]. For comparison, the solubility of Ce in the Al matrix at 500°C is $4x10^{-4}$ while the solubility of copper is ~4wt% at 500 °C [94,95]. Further contributing to the high stability is the high vacancy binding energy of Ce and which prevents easy motion of Ce through the Al matrix. These mechanisms restrict coarsening of Al-Ce-based intermetallic phases, such that they remain small to strengthen the material and restrict grain boundary motion and grain growth.

Despite the benefit of a highly stable intermetallic, there is no opportunity for solid solution strengthening by Ce because of the near zero solubility. Additional alloying elements must be added to Al-Ce alloys to attain relevant mechanical properties at normal cooling rates. Magnesium (Mg) is a potent solid solution strengthening element that can be retained in solution under conventional casting cooling rates[5,96], making it a useful addition in attaining a heat-treat free Al-Ce alloy family. Al-Ce-Mg alloys possess excellent room and elevated temperature mechanical properties, are compatible with many casting techniques, and have been used in application without the need for heat-treatment[57,61,97].

As our understanding of Al-Ce alloys continues to grow it is imperative that corrosion of the materials be studied to ensure material longevity and soundness in a broad range of applications. To understand how Al-Ce material performed when exposed for long periods of time to corrosive environments, a tidal exposure experiment (Figure 6.1a) was performed. A tidal exposure experiment helps to develop knowledge of material behavior when left in an area which experiences cyclic exposure due to tidal variations.

Figure 6.1c-d shows the results of the 48-week exposure wherein the sample developed a darkened, yellow patina likely due to mild growth of a cerium rich oxide layer, Ce(IV) oxide has a pale yellow color, with no major corrosion attack present. There is however a small amount of localized corrosion attack on the sharp side of the blade resulting in a minor amount of corrosion product build up. Comparatively the sample exposed to an 88-week submersion shows measurably more corrosion with colonies of corrosion product appearing across the surface. However, corrosion product buildup still covers less than half of the material surface. In addition, no areas of scaling or pitting can be found on the surface. The highest concentration of corrosion can be found again at the sharp side of the blade where a delineation between more active and slower corrosion zones are noticeable. This delineation shows a distinct color change in the outer oxide passivating layer. Where it transitions from that of a pale yellow to a more transparent white color. It can be expected that a measurable amount of the oxide in the slower corroding region is of the Ce(IV) type present on the entire sample after 48 weeks. The white oxides of both Al and magnesium are likely the main constituents of the more active corrosion areas near the blade's edge. The clear distinction between the areas may then suggest that the corrosive environment selectively leaches the Ce rich oxides that are slowing the corrosion across the surface of the alloy. Once the area has been leached of its Ce content it appears to form larger more densely packed colonies of corrosion product

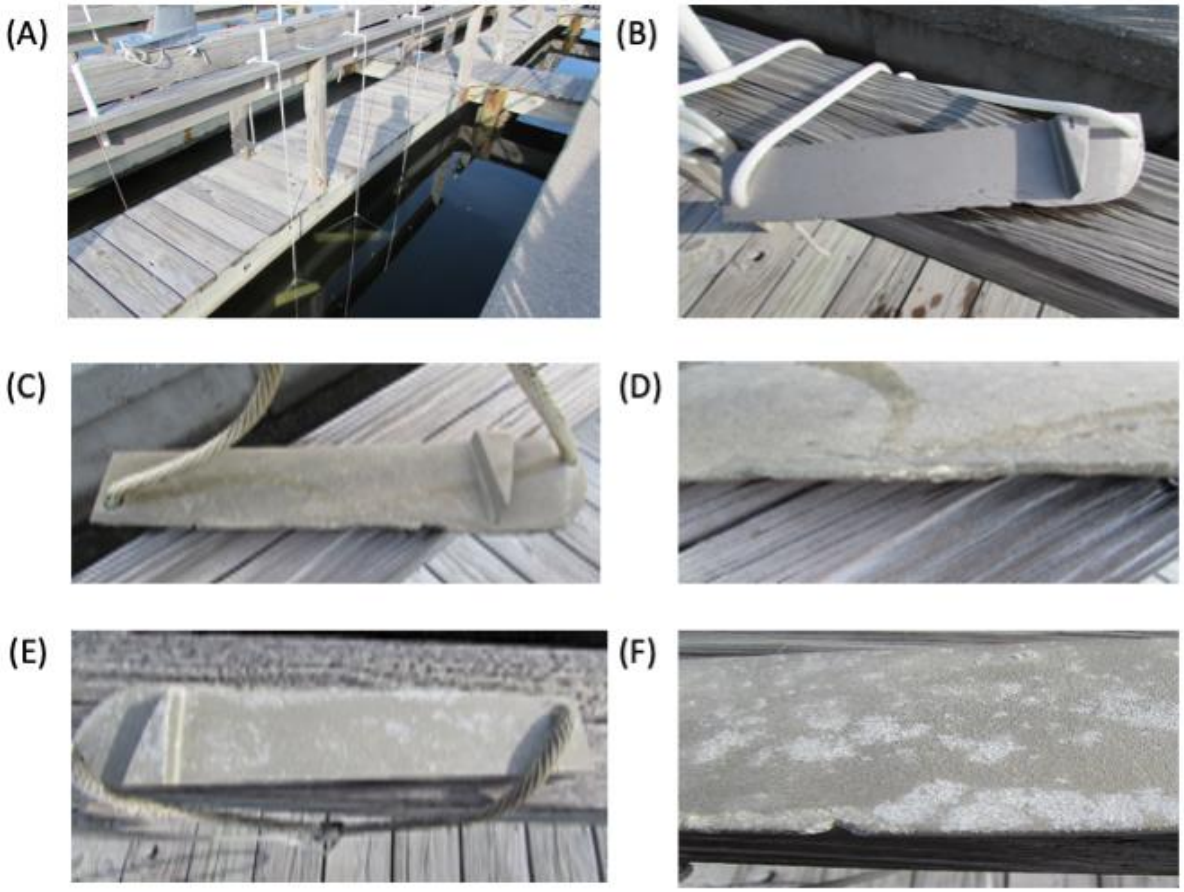

Figure 6.1: A) Tidal pool submersion dock where test pieces are submerged to study evolution of parts when exposed to highly corrosive tidal pool conditions. B) Portion of hydrokinetic turbine prior to being exposed to tidal pool conditions c) Hydrokinetic turbine blade following 48 week exposure to tidal pool. D) Close up of 48 week exposed sample showing areas most active corrosion. E) Hydrokinetic turbine after 88 weeks of exposure to tidal pool corrosion. F) Close up of 88 week exposed sample showing areas of high and low corrosion delineated by changes in surface coloration.

resulting in accelerated surface degradation.

The results of the tidal pool experiment show the propensity for Al-Ce alloys to resist corrosive attack for extended periods of time. The longer exposure, though resulting in higher levels of corrosion and what from qualitative inspection appears to be selective Ce leaching, is still very much below the typical amount of corrosion seen after such a long exposure to a tidal pool environment. The high corrosion resistance likely stems from the combined surface oxide forming in the Al-Ce-Mg system which does appear to show degradation over time but remains slow even when the Ce rich oxide has been leached away during corrosion. Further inspection and analysis of the effects of tidal pool corrosion on Al-Ce alloys will follow in a future publication.

Additional measurements were conducted on several Al-Ce alloys and compared with samples of industrial Al alloys using the salt fog method. Salt fog tests are instructive as they are most similar to natural sea environment but provide a controlled flow of corrosive media permitting quantitative analysis and easy data comparison across different bodies of work.

Figure 6.2 shows weight loss measurements of several Al-Ce-based and conventional alloys tested by salt fog. Appendix 2 includes photos of the samples post exposure, rinsing, and cleaning. The results show clearly that Al-Ce and Al-Ce-X alloys exhibit similar behavior to that of other highly corrosion resistant Al alloys like A356 and A535, which increase in mass through absorption of oxygen to form a thick passivating layer which prevents further corrosion. This is in contrast to the performance of corrosion-sensitive Al alloys like the Al-Cu and Al-Li family of alloys (Figure 6.2). The copper rich alloys A206, 2618, and 2055, show significant weight loss, which can be attributed to the significant amount of intergranular corrosion and subsequent grain fall out during rising and cleaning.

Intergranular tests were also carried out on a number of Al-Ce alloys and compared against the performance of current industrial Al alloys. Figure 6.3 contains micrographs of selected alloys from these tests. Consistent with the salt spray test, Al-Ce alloys show little corrosion with corrosive attack selectively targeting the anodic Ce-rich intermetallic phases. It should be noted that in several areas within the sample of Al-8Ce-10Mg “pools” of Mg-rich β phase can be seen at and below the surface. These are common features in Al-Ce-Mg alloys and are not the result of corrosion. Maximum depth of the corrosive attack is less than 50μm compared against the more

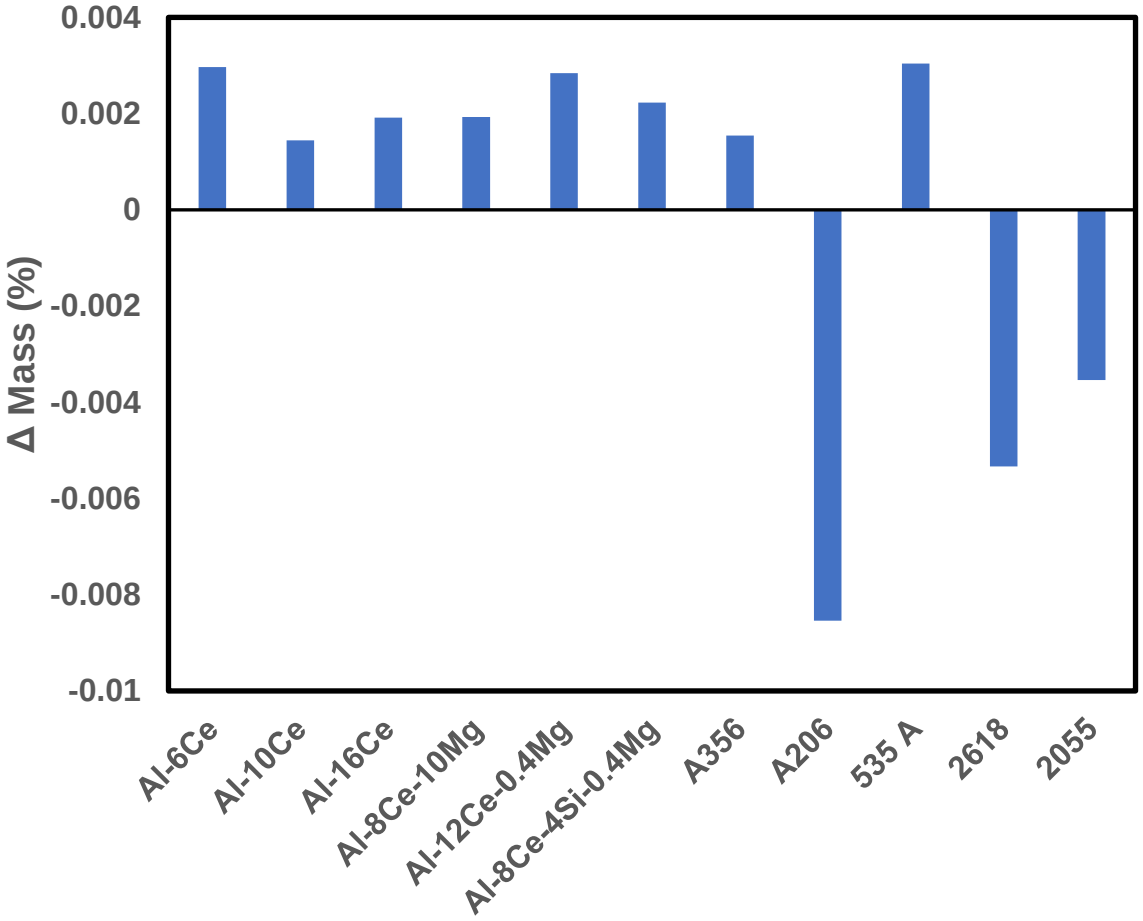

Figure 6.2: Mass change measurements of several Al-Ce alloys compared to common Al alloys showing excellent corrosion performance of Al-Ce alloys

sensitive 2055 and 2618 alloys which have intergranular attack maximum depths of up to 500 μm. The higher resistance of Al-Ce alloys to corrosion is closer to that of A356, a benchmark for Al corrosion resistance of high-performance alloys[87,98].

The combined results from the study of large parts exposed to highly corrosive tidal pool environments, targeted salt spray, and intergranular corrosion attack support that Al-Ce alloys present a viable option for producing an Al alloy which is both mechanically stable at elevated temperature and resistant to corrosive attack, opening new application spaces for Al alloys.

6.5 Cerium as an Inhibitor

Rare earth elements have a long history of being used as microalloying additions to Al alloys. Several studies have shown that small additions of LREE elements to Al alloys have the potential to greatly refine eutectic microstructures and prevent particle coarsening [88,89,98]. The effect of Ce on coarsening and microstructure evolution as a microalloying addition results from its potency as a diffusion blocker caused by its high vacancy binding power[88,99]. More recent studies have focused on using Ce as an inhibitor to increase corrosion resistance of Al alloys in service[79,100]. These studies have mostly used Ce compounds as additions to the coating processes to create more strongly passivating layers on several Al alloys; the most common compound used is $CeCl_3$[101]. Other research has investigated adding La directly to AZ91 (a Mg alloy) and Al-3%Mg alloys to aid in corrosion resistance, the results of which showed a positive impact on both material mechanical properties and corrosion performance[102,103]. Here, a study of small Ce additions (0-1 wt%) of prototypical commercial Al was conducted to further understand the impact of Ce on corrosion performance.

Test bars of common Al alloys from the major families: A206 (Al-Cu), A356 (Al-Si), A535 (Al-Mg) alloys were cast into permanent mold test bars with increasing amounts of Ce. Additions of 0, 0.5, and 1 wt% Ce were selected for this study.

Figure 6.4 displays SEM micrographs taken following sample exposure to intergranular attack. A206 shows the highest amount of intergranular attack of any of the tested alloys with or without Ce. This is expected as Al-Cu alloy are susceptible to intergranular attack due to the micro galvanic coupling which occurs between cathodic Cu rich precipitates at the grain boundary and surrounding anodic Cu depleted matrix (precipitate free zone or PFZ) resulting in rapid corrosion[104].

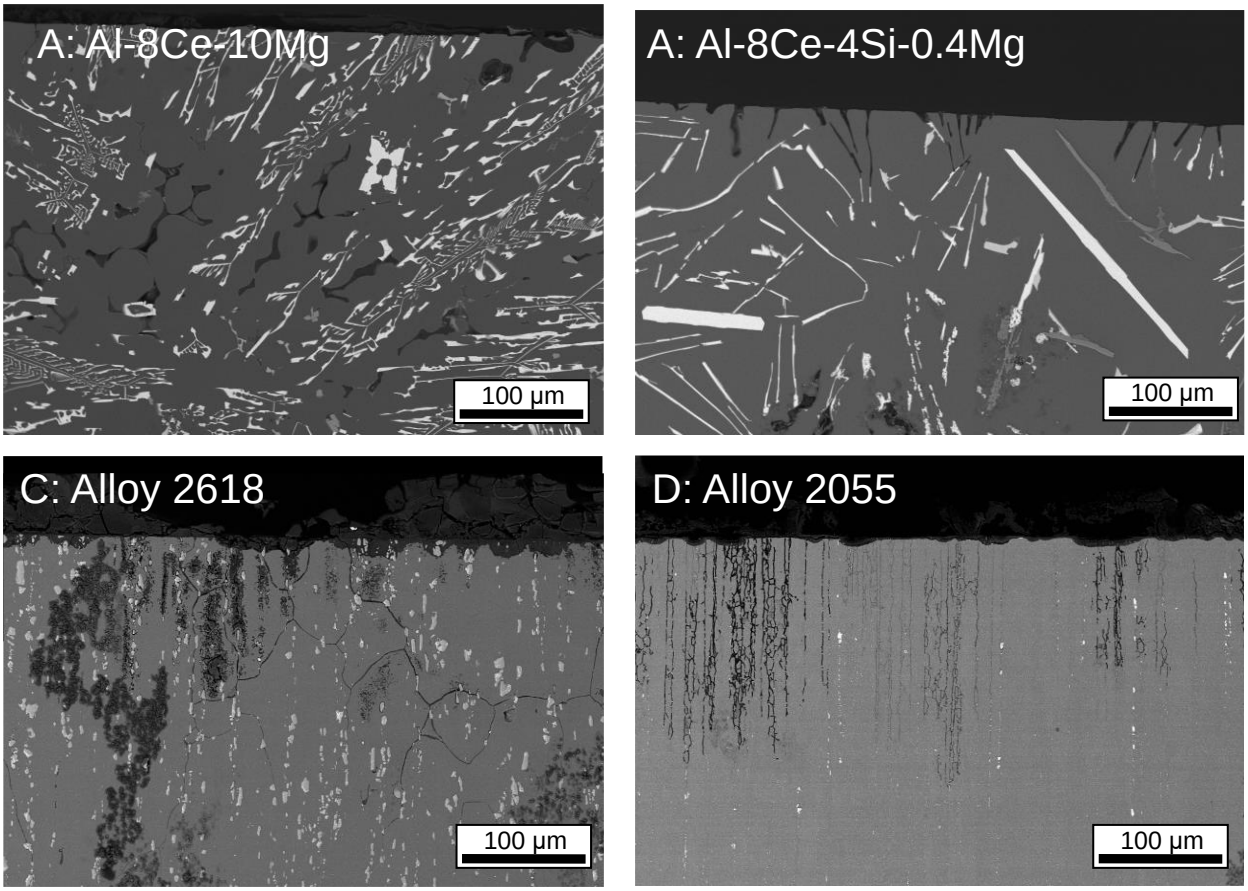

Figure 6.3: SEM Micrographs of the cross-sectional surface of several different alloys measured for sensitivity to intergranular corrosion showing improved performance of Al-Ce alloys over common high performance commercial alloys A) Al-8Ce-10Mg B) Al-8Ce-4Si-0.4Mg C) 2618 D) 2055

The addition of Ce effects both the morphology of the alloy and kinetic and thermodynamic nature of the corrosion process. Firstly, it can be seen form the Figure 6.4b that A206-1%Ce shows a reduction in average grain size over that of the unmodified sample. The reason for this grain size refinement is not the focus of this report but could result from several factors including more efficient pinning by secondary phases which form during solidification and reduced grain growth during solutionizing and aging or higher number of heterogenous nucleation sites from increased oxide impurities of the Ce modified sample. Regardless, the finer grain structure of the Ce rich Al-Cu sample increases the grain boundary volume near the surface providing for more corrosion pathways increasing the possibility of corrosion. However, many phases form at the grain boundaries beyond that of the Al_2Cu phase which change the nature of the corrosion potentials at the boundary. It is known that Ce-rich phases are typically anodic to the Al matrix and thus will likely be anodic to any Al_2Cu phases which form at the boundary leading to corrosion. Additionally, $Al_{11}Ce_3$ phases are anodic to the other areas of the A206 alloy such as the PFZ, grain interior, and etc., and will be selectively corroded first providing for complete cathodic protection of the A206 alloy. However, these phases are also very stable and much slower to corrode than the copper depleted zone in unmodified Al-Cu alloys. Therefore, the corrosion rate of A206 is greatly reduced by the presence of Ce in the alloy at both 0.5 and 1% concentrations (Figure 6.5).

A535.2 (A535 for the remainder of this report) is an Al-Mg alloy used without heat-treatment that is commonly referred to as Almag .As a result of A535's high magnesium content it has good room temperature strength and low density thus it finds use in many applications designed around high specific strength and/or dimensional stability[105]. In addition, it is considered to have good corrosion resistance, especially in saltwater environments. However, sensitization is a major concern with A535 like for many other Al-Mg alloys. This process occurs when, during operation even at room or slightly elevated temperatures, magnesium from the super saturated solution of Al(Mg) FCC begins to migrate toward the grain boundary forming interconnected networks of anodic β phase precipitates leading to rapid intergranular corrosion and eventual part failure[106–108]. Work during this experiment was conducted immediately following casting and so cannot provide a complete understanding of the effect Ce may have on sensitization of Al-Mg, but the work completed as part of this study may provide insight into whether Ce could play a role in reducing the amount of sensitization experienced by Al-Mg alloys.

The sample of A535 cast during this trial had unusual amounts of β phase near the surface which

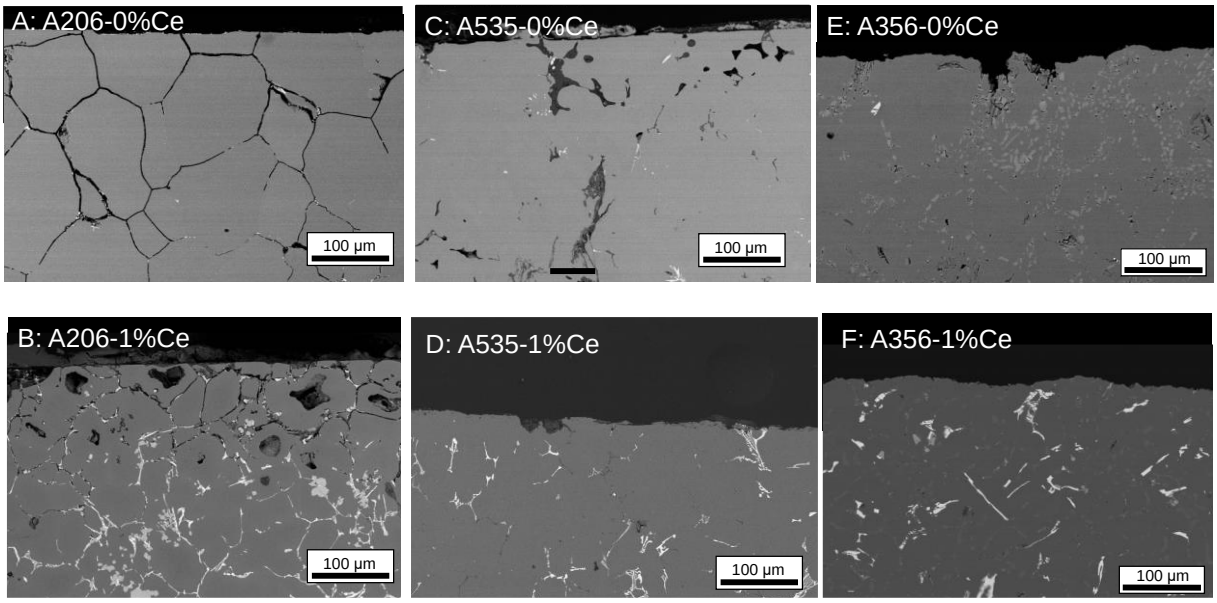

Figure 6.4: SEM micrographs of unmodified and Ce-modified Al alloys showing the positive effect of Ce additions on intergranular corrosion A) A206-0% Ce B) A206-1%Ce C) A535-0%Ce D) A535-1%Ce E) A356-0%Ce F) A356-1%Ce

lead to a large amount of measured corrosive attack depth, and it is expected that, were the samples to have a more uniform distribution of Mg throughout the sample corrosion, performance would have improved. β phase is known to be anodic to the matrix and in other Mg alloys increased amounts can cause pitting to become a problem[109]. As Ce is added up to 1wt%, intergranular corrosion is reduced and the morphology of the alloy changes. Ce presence reduces the amount of large β colonies near the surface of the alloy reducing the likelihood of high susceptibility to corrosive attack prior to the sensitization process. The reduction of beta phase is paired with formation of the more anodic Ce-rich $Al_{11}Ce_3$ phase (white phase) at the grain boundaries of the Al(Mg) matrix phase. Similar to the effect these phases had on A206, their anodic potential to the matrix and β paired with their relatively slow dissolution and current density under corrosive environment further slows the penetration of corrosion into the sample along the grain boundaries under the current test conditions.

To understand how the presence of Ce rich phases at the grain boundary might affect alloys sensitization it is important to mention the factors which can impact the amount of sensitization. Recent research shows that sensitization at the grain boundary is largely dependent on β phase continuity, with more connected and continuous β colonies having elevated susceptibility to grain boundary sensitization [107,108]. It is possible to control β colony continuity through grain orientation tailoring, but this process is complex and unlikely to result in industrially viable manufacturing methods. The presence of additional phases at the grain boundary, directly following casting, may provide a secondary pathway to limiting β phase continuity. The anodic $Al_{11}Ce_3$ phases residing in the grain boundary following casting should act to limit the ability of β phases which precipitate from the matrix during elevated temperature operation to form connected networks and provide cathodic protection, lowering the overall alloy sensitization. This process will be more closely investigated further in a follow up report on the subject of Ce's effect on Al-Mg alloy sensitization.

The final alloy studied for the effect of small Ce additions on intergranular corrosion attack is the Al-Si alloy A356. This alloy is commonly used in Al casting technologies and accounts for a large portion of the Al engine component market[52,51]. Al-Si alloys are known to be highly corrosion resistant without the addition of further inhibitor[98,110]. Despite this it was important to understand the impact Ce would have on the corrosion properties of an already highly resistant alloy. The SEM micrographs in Figure 6.4 show that A356 exhibits near-zero intergranular attack in the

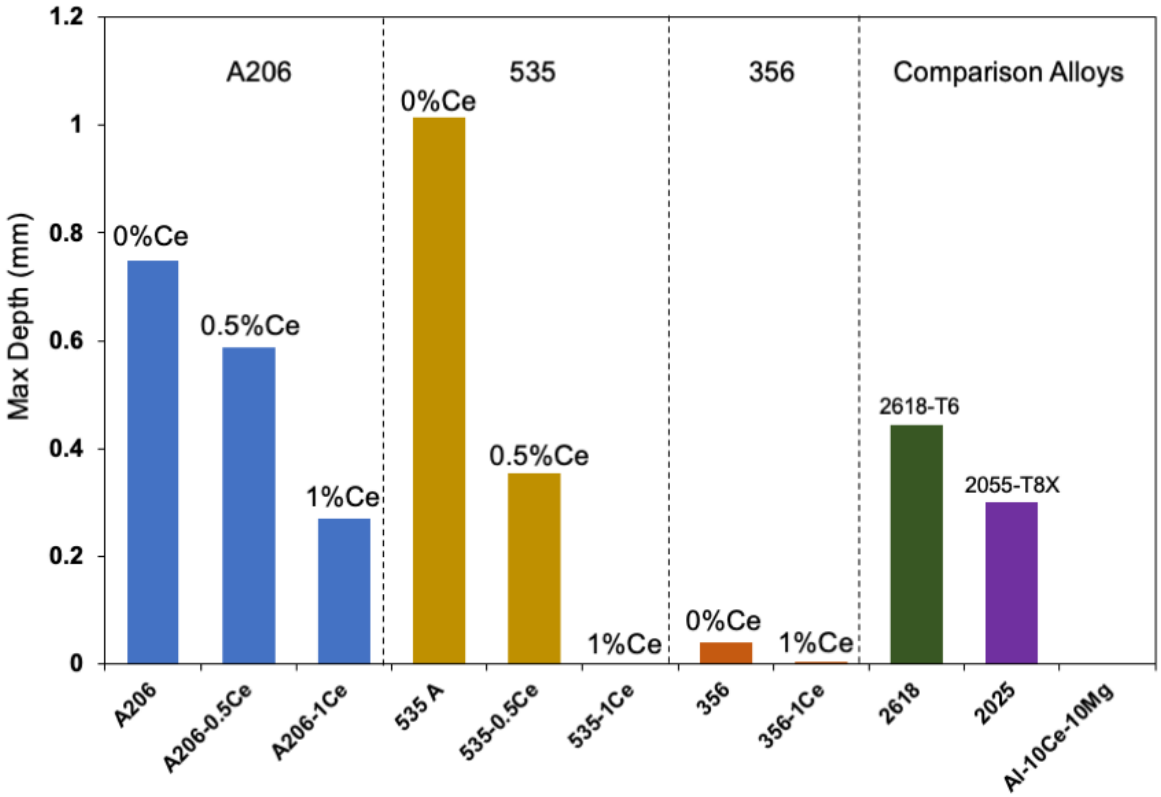

Figure 6.5: Measured impact of Ce additions on common Al alloys showing consistent reduction in depth of intergranular attack with increased addition of Ce

unmodified state only showing minor corrosion of certain eutectic silicon colonies at or near the surface of the alloy. The addition of Ce does appear to improve the corrosion of the alloy in a similar fashion to modifying effect Ce had in the Al-Mg alloys. Ce captures a portion of the Si into complex, stable ternary phases reducing the amount of free silicon which can form near the surface of the alloy. Additionally, these ternary phases form during alloy solidification and persist through heat-treatment. The capture of some amount of silicon in a stable phase leads to more even, less connected distribution of Si on the grain boundary following heat-treatment, which results in a small reduction in intergranular corrosion.

The above show the value of Ce as a minor addition to Al alloys for the goal of inhibiting corrosive attack. The mechanism for Ce in preventing intergranular corrosion appears to be suppression of grain boundary secondary phase network formation and cathodic protection where the anodic nature but low current density of Ce-based phases protects the matrix from corrosion and slows the progress of corrosion down the grain boundary.

6.6 Cerium as a Scavenging Agent for Impurities

Recycled or secondary Al relies heavily on mixed scrap streams which can result in elevated levels of impurity elements present in final cast parts. These impurity elements can negatively affect material properties[111]. Often alloy maximum impurity specifications limit the amount of recycled secondary Al that can be used, increasing alloy cost and embodied energy. A prominent example in industrial application is A356, for which a maximum Cu content of 0.2 wt.% is commonly used due to unacceptable corrosion susceptibility above this value. A small amount of mis-sorted Al-Cu-base alloy in the scrap stream can easily raise the Cu content to twice that limit, after which the alloy is commonly diluted ~50% with primary Al. Primary Al is both more expensive and much more energy intensive than secondary[41,112]. Thus, improving recyclability by relaxing impurity limits is beneficial both economically and environmentally. One option for increasing the use of secondary Al material in Al production lifecycles is to develop an effective scavenging agent for Al alloys that can either remove or capture impurity elements in stable intermetallic compounds. Ce and other rare earth elements offer promise for being effective scavenging agents as they form highly stable ternary Al-REE-TM (where TM is transition metal) intermetallic phases with many of the elements known to be detrimental to Al alloy material properties[113–115].

The potential of Ce to modify the impurity tolerance for copper in 356 was investigated by controlled additions of both copper and Ce in fixed ratios to a high purity industrial A356 alloy. The ratios 2:1 and 3:1 Ce:Cu were decided based on the necessary amount to scavenge copper into documented Al-Ce-Cu ternary phases during heat-treatment[115,116]. In addition to A356 castings, a control of pure Al with identical Cu and Ce additions was cast and heat-treated identically. This was to understand the effect of possible differences between the effect Ce and copper have when isolated as compared to their combination with the major alloying element in A356, Si. A list of compositions used for this study can be found in Al-Si alloys is presented here in the main text. The complete data set can be found in the supplementary material. The amount of copper present is a 400% increase over the typical limit for copper in A356 alloys of 0.2 wt%Cu. The decided ratios of 2:1 and 3:1 resulted in additions of 1.6 and 2.4 wt% respectively. Optical micrographs were taken following a 2000-hour exposure of test bars to a salt fog environment Figure 6.6. In the Ce free samples of both the A356 and pure Al materials, a thick layer of corrosion product forms which shows a mixed nature, Figure 6.6a. For A356, as the amount of Ce increases there is a marked reduction in the thickness of the oxide layer. Portions of the alloy containing 2.4 wt%Ce have an oxide layer too thin to be measured from optical micrographs, Figure 6.6c. details the mechanical property results from the uncorroded test bars of the A356-0.8Cu-XCe alloy. The mechanical properties of the samples after corrosion show very similar trends to those measured for samples prior to corrosion. Ductility reductions of the modified pure Al samples shows almost the same slope as those of the uncorroded sample with the 2.4Ce sample having slightly higher ductility than the uncorroded sample. This consistency eludes to the minimal impact 2000-hour salt fog tests have on pure Al but remains consistent with known impacts of Ce additions on mechanical properties. Interpretation of the A356 mechanical properties is more difficult as they do not appear to show a consistent trend, with the sample having a 1.6Ce addition The additions were made using the casting process discussed in the methods section of this report. Mechanical testing was conducted on test bars in an uncorroded state and after salt fog exposure for up to 2000 hours to determine what if any effect the presence of Ce had on mechanical performance. The composition of the salt fog was 5% NaCl by volume.

The most illustrative data set on the effect Ce can have on corrosion performance of contaminated Al-Si alloys is presented here in the main text. The complete data set can be found in the supplementary material. The amount of copper present is a 400% increase over the typical limit

for copper in A356 alloys of 0.2 wt%Cu. The decided ratios of 2:1 and 3:1 resulted in additions of 1.6 and 2.4 wt% respectively. Optical micrographs were taken following a 2000-hour exposure of test bars to a salt fog environment (Figure 6.6). In the Ce free samples of both the A356 and pure Al materials, a thick layer of corrosion product forms which shows a mixed nature. For A356, as the amount of Ce increases there is a marked reduction in the thickness of the oxide layer. Portions of the alloy containing 2.4 wt%Ce have an oxide layer too thin to be measured from optical micrographs.

Figure 6.7a details the mechanical property results from the uncorroded test bars of the A356-0.8Cu-XCe alloy. The mechanical properties of the samples after corrosion show very similar trends to those measured for samples prior to corrosion. Ductility reductions of the modified pure Al samples shows almost the same slope as those of the uncorroded sample with the 2.4Ce sample having slightly higher ductility than the uncorroded sample. This consistency eludes to the minimal impact 2000-hour salt fog tests have on pure Al but remains consistent with known impacts of Ce additions on mechanical properties. Interpretation of the A356 mechanical properties is more difficult as they do not appear to show a consistent trend, with the sample having a 1.6Ce addition failing in brittle fracture before reaching plastic deformation. Thus, mechanical properties show that the presence of Ce and copper have little effect on the monotonic yield and tensile strength of A356. However, the addition of Ce does have a noticeable impact on the elongation to failure of the material, and to be an effective scavenging agent this effect must be better understood. Observing the control samples of pure Al, it is clear that the addition of Ce to the alloy has a strong impact on elongation and that copper alone is not enough to degrade alloy ductility to the extent measured. In the case of pure Al, the addition of 2.4 wt% Ce reduces ductility of the alloy by more than 60% while providing a slight increase to the yield strength. Though mechanical property data is largely inconclusive about the impact of Ce on copper scavenging, microscopy results show that Ce additions can have positive impacts on corrosion rates of Cu contaminated samples. There remains questions on how to effectively balance the reduction in ductility vs the reduction in corrosion rate which results from the addition of Ce, but overall Ce additions appear to have the chance to be used in a way that can increase the tolerance of Cu in A356, and as a result increase

Table 6.1: List of alloys used to measure the impact of Ce additions on Cu scavenging in A356

Alloy Number	Base Material	Copper Addition (wt%)	Ce Addition (wt%)
1	A356	0.8	0
2	A356	0.8	1.6
3	A356	0.8	2.4
4	Al	0.8	0
5	Al	0.8	1.6
6	Al	0.8	2.4

the compatibility of secondary Al with A356 production pathways.

6.7 Conclusions

Improving corrosion resistance and manufacturing flexibility of Al alloys is among the most important properties for continued growth in Al alloy adoption. Presented in this report is data and analysis which makes it clear that Ce has potential to improve corrosion properties of Al alloys in several ways:

- Ce used a primary addition to Al alloys created the potential for producing an alloy that combines excellent elevated temperature stability and strength with near Al-Si alloy levels of corrosion resistance.
- Minor additions of Ce below 1% can greatly improve the corrosion resistance of current Al alloys through blocking grain boundary dissolution and alloy sensitization processes.
- Measured additions of Ce and Ce containing alloys to scrap supply streams may be a pathway to easing restrictions on particular scrap metal in the production of Al alloys that are sensitive to Cu impurities deleterious to high corrosion resistance.

Overall Ce appears to be an option for reducing corrosion of Al alloys whether as a minor or main understand how Ce effects the mechanical properties of alloys to which it is added as a minor addition, specifically how additions of Ce can be made without sacrificing measurable portions of alloy ductility. Regardless of the shortfalls of Ce as a minor addition, the results included in this report show Ce alloys present a viable pathway to realizing a new family of cost effective, corrosion resistant, manufacturable, elevated temperature Al alloys should their development continue.

6.8 Acknowledgements

This work was performed under the auspices of the U.S. Department of Energy by Lawrence Livermore National Laboratory under Contract DE-AC52-07NA27344.

This research was sponsored by the Critical Materials Institute, an Energy Innovation Hub funded by the U.S. Department of Energy (DOE), Office of Energy Efficiency and Renewable Energy,

Advanced Manufacturing Office, and Eck Industries. This work was performed under the auspices of the U.S. DOE with ORNL under contract DE-AC05-00OR22725 and with LLNL under contract DE-AC52-07NA27344.

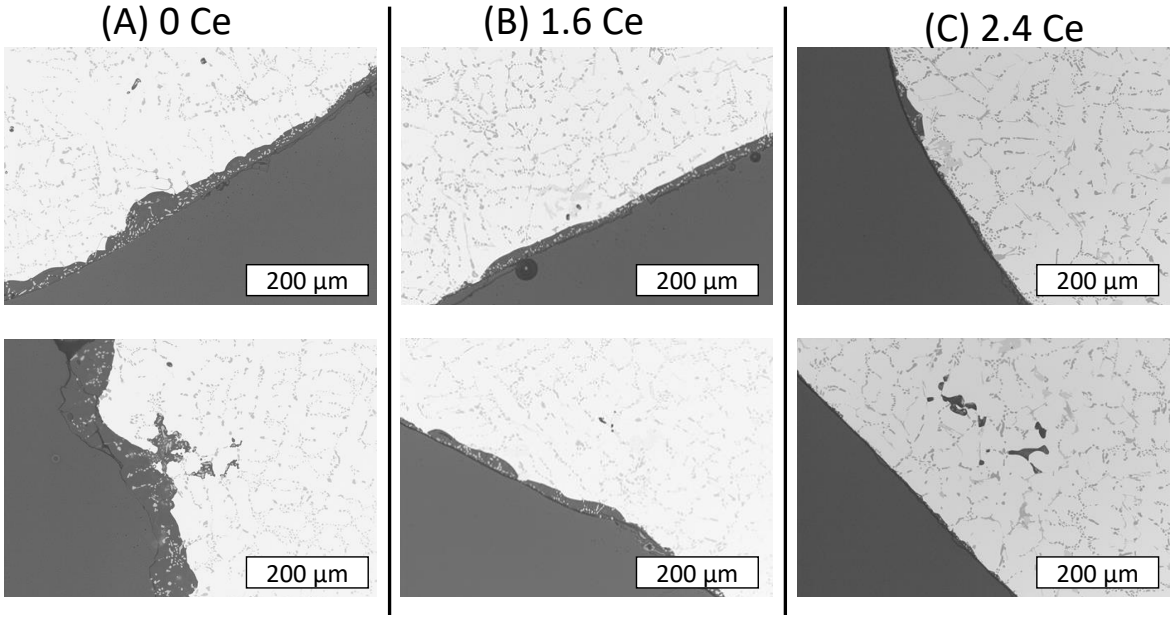

Figure 6.6: Optical micrographs taken from the cross section at the surface of A356-0.8Cu-XCe samples showing a distinct reduction the thickness of the corrosion product layer as Ce content is increased from A) 0% B) 1.6% C) 2.4%

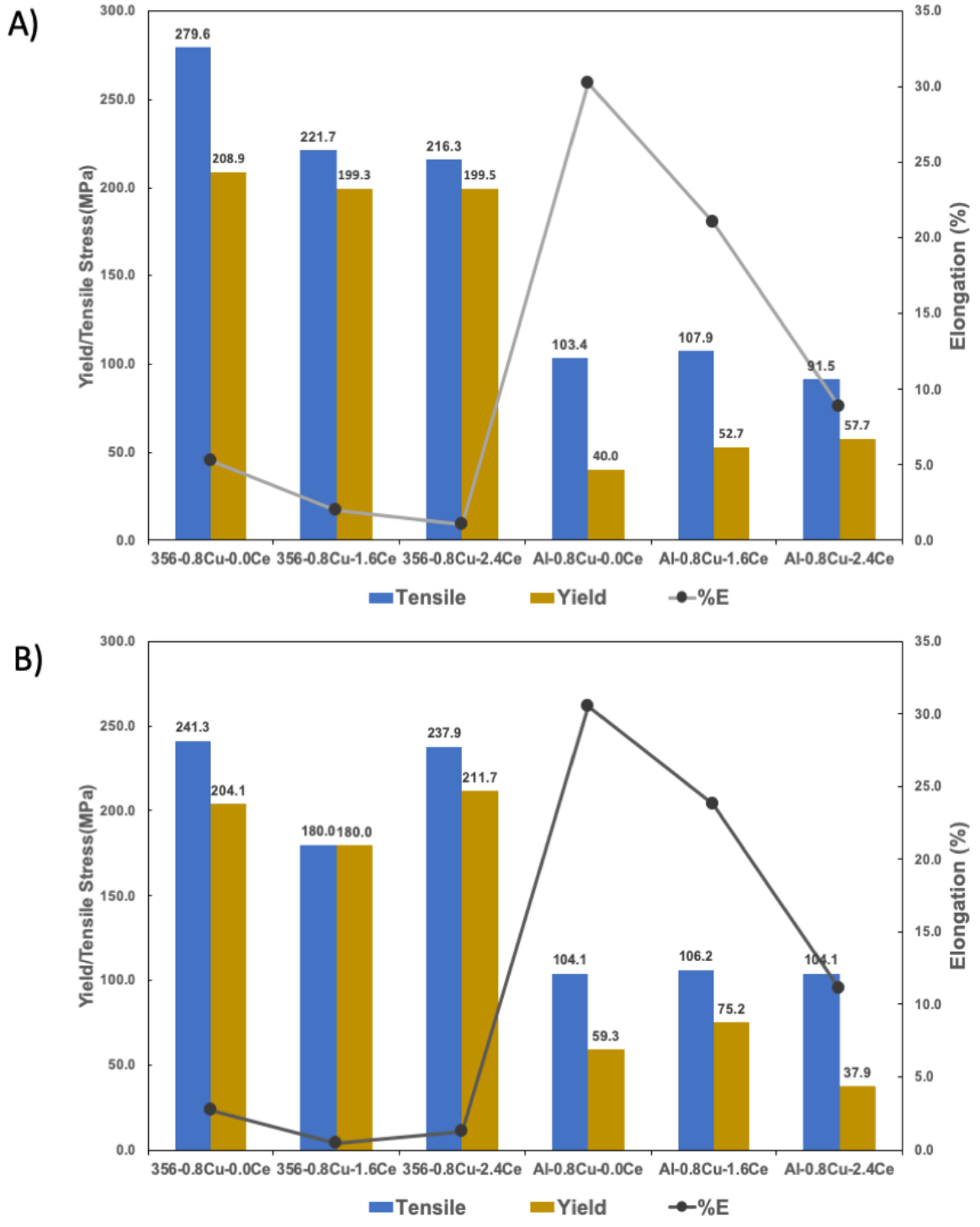

Figure 6.7: Mechanical properties of alloys used to measure the impact of Ce on copper scavenging in A356 A) uncorroded B) corroded

7. Increase in Mechanical Properties of Al-Ce-Mg Alloys Through High Pressure Processing Routes

This chapter has been adapted from a soon to be submitted manuscript with a provisional title "Propagative Benefits of Rare Earth Co-production and Heat Treat-free Al Alloys" soon to be submitted for publication to the Journal of Cleaner Production

7.1 Abstract

Rare earth elements are among the most valuable elements for catalyzing the next generation of renewable energy technologies among several other important applications. However, their supply chain is imbalanced; creating a volatile market. Ce is the most abundant but underexploited of the rare earth elements. It currently finds use in several distributed applications, all of which are very low value. Finding a more suitable high-volume application for cerium could stabilize demand. Al-Ce alloys can create this demand if when adopted on a larger scale, and thus their study and development is of great importance. Their ability to be used without heat-treatment and retain excellent properties at high-temperature make them a prime candidate for use in several desirable aluminum applications. The combined impact of these benefits to two separate marketplaces by leveraging a single underuse material is propagative and can reorganize multiple sectors with a single action. This report will cover the possible impact to the rare earth supply chain, aluminum energy use, and production timelines should a viable Al-Ce alloy be adopted. Results will show that Al-Ce alloys are a possible new space to create the needed demand for Ce and that introducing cerium to aluminum alloys offers great benefit to a growing material demand and application space.

7.2 Introduction

Growing demand for advanced technology in both developed and emerging economies places pressure on current supply chains to increase output, but changing international standards for production sustainability are forcing manufacturers to identify opportunities for exploiting upstream value through propagative benefits[117]. Propagative benefits are defined as those found in manufacturing where a single material or method creates multiple benefits at different, and sometimes seemingly disparate, steps in the production pathway. Proper leveraging of propagative benefits minimizes overall supply chain imbalance and waste. Often, upstream processes several steps removed from a final manufactured part reveal opportunity for decreasing supply chain vulnerabilities and/or energy expenses. The economization of each part in a supply chain, whether directly used or a byproduct of other steps, requires a multidisciplinary analysis and design

approach for recognizing value capture opportunity. Properly leveraging the entire supply chain will result in more robust price/demand inelasticity creating an efficient, dynamic market that can adjust to new or reduced demand at any point.

REEs have been identified as critical to the continued growth of the sustainable energy economy that relies on powerful rare earth neodymium (Nd) and dysprosium (Dy) magnets for energy conversion[118]. However, there is currently an imbalance in REE mining, wherein the economic driving force for resource exploitation (Nd and Dy) is only a small fraction, less than 20%, of the final separated mine product. The remaining material (mostly Ce and La) is primarily considered a byproduct and is either sold for low-value applications at heavily depressed prices due to limited demand[119], stockpiled, or returned to the mine at its natural abundance ratio at a cost to the mine. Should a viable, high-volume application for REE byproducts arise, the industrial demand will increase and production of technologically critical REEs will become more financially appealing.

Increased demand for products is accompanied by proportional increase in energy expenditure for their manufacturing. Among the most energy intensive modern materials are Al alloys. Much of the energy needed to produce Al alloys results from the process required to reduce a raw bauxite ore to pure Al, referred to as primary metal[112,120,121]. The use of secondary recycled Al, having up to an order of magnitude less embodied energy, is increasing rapidly thanks to international efforts[121,122]. Despite this trend, more efficient manufacturing will be required to flatten energy use in aluminum production with growing demand. Reducing or eliminating the heat-treatment step of aluminum production is a viable option for decreasing aluminum manufacturing energy use[112,123]. During heat-treatment, parts are held at elevated temperatures for hours before being quenched and often heated a second time in separate furnaces to produce desired properties[39]. The typical furnace used for this process is less than 25% efficient and occupies a large portion of the foundry infrastructure. Most commercial Al alloys require heat treatment, so a large reduction in alloy manufacturing energy use could be realized if heat-treatment was reduced or eliminated. Furthermore, a reduction in heat-treatment requirements for commercial alloys can decrease foundry footprint and production timelines, increasing output with limited capital expenditure.

Al is desirable for many applications as it strikes a balance of cost, density, and mechanical properties that other material systems, such as steel and titanium, cannot reach. Al is therefore often the material of choice for new engine designs in passenger cars. However, as the energy

intensity of modern engine design increases the operating temperature of many products has been forced to increase as well. Over the past several decades, engines have evolved from large steel, naturally aspirated products to smaller aluminum, forced induction designs[124,125]. Though as engines have become smaller, their power output has remained the same or increased through higher energy density. Smaller, more energetic engines operate at much higher temperatures than previous designs. These elevated temperatures produced a more efficient combustion cycle and improved fuel economy. However, current engine designs are nearing the limit of material properties for cost- effective lightweight metals like Al. The the upward trend of aluminum use in energy dense applications is to continue, a new alloy capable of withstanding elevated temperature applications with flexible manufacturing pathways must be developed.

Here we present a case study for capturing propagating benefits in a manufacturing supply chain. The current example investigates aluminum (Al) alloyed with a rare-earth elements (REE), cerium (Ce) and lanthanum (La), and the opportunity this technology presents for upstream and downstream benefits to supply chain stability and environmental impact. Using Ce and La as an alloying addition to Al is promising. As Al alloy production worldwide is over 90 megatonnes and is expected to increase to nearly 140 megatonnes by 2040 thanks to growing demand for lightweight materials[126]. The implications are that a small penetration of Al-REE alloys into existing market sectors, ~.1% demand capture, would result in 72 kt of realized byproduct REE demand. This level of demand could be sufficient to rebalance the light rare earth element (LREE) mining industry. Additionally, this new group of alloys can be used in many cases without the need for heat treatment or with greatly modified and shortened treatments, reducing energy expense and increasing material production rates. Thus, this alloy has the potential to positively impact both REE mining and the Al alloy market simultaneously.

7.3 Coproduction of Metals

Overproduction of industrial byproducts and waste is a pervasive issue in both mining industries and goods manufacturing. One increasingly prominent example, as mentioned above, is the imbalanced demand for REEs. Global REE extraction has been constantly growing, with production increasing from about 80 kiltonnes of rare-earth oxides in 2000 to over 130 kt in 2017[127]. The growth in rare earth production is majority driven by Nd demand for permanent magnets. Permanent magnets being necessary for the production of vehicle electric motors, wind

turbines, and hard disk drives[128]. REEs are chemically very similar being co-located within the same ore bodies and initially mined together as a single mineral, such as bastnaesite and monazite. The neodyminum content of the refined ore body concentrate is on average only 15% while Dy and samarium, two other important elements to permanent magnet industries, account for less than 1% (Figure 7.1)[129]. On the other hand, Ce and La together makeup over 70% of the REE concentrate content[130]. Despite making up the majority portion of the refined material, Ce and La have few high-value industrial demands, finding use as catalysts, polishing compounds, flint material, and in NiMH batteries. Several other REEs find application in fields outside the emerging alternative energy markets and have largely balanced supply chains with demand on track with supply. Praseodymium, for example, is about 4-6% of ore content and the majority of the produced material is used to impart yellow color to glass and ceramics[131]. Terbium, lutetium, and yttrium together consist only about 2% of ore content and are used in the production of industrial phosphors[131].

Like Ce and La, there are several elements which have no dedicated production pathways and instead are produced incidental to other materials. This process is called either byproduction or coproduction. The distinction depends on the economic value of the supplemental materials produced, with coproducts having a measurable economic value and byproducts having little or no value when compared against the main value drivers. Ce and La often do not have demand when mined and are largely considered byproducts. Unlike Ce and La, other byproducts typically account for small portions of a mine's output. Indium, for example, is exclusively produced during Zn and Cu mining. In 2013, 13,500 kt of Zn was produced globally with only 0.63 kt of In being produced as byproduct[132]. The small amount of by-product compared to majority mine economic driver means that overall mine profitability is not dependent on difficult to extract, low production volume elements. This is in contrast to REE mines which depend on Nd and Dy for profit. Thus, the overproduction and oversupply of Ce and La as a companion to Nd[133,134] creates an economic burden on producers. This can be made further evident when Nd is compared to other low crustal abundance elements critical to the energy transition. Lithium has roughly half the crustal abundance of Nd, but often trades at one third the price[135]. It's ease of separation mixed with valuable co-products like magnesium (Mg) and calcium (Ca) mean that its cost can be kept relatively low[59,136]. Nd on the other hand is very difficult to separate from its fellow elements and because the majority elements during the separations and extraction process have little inherent

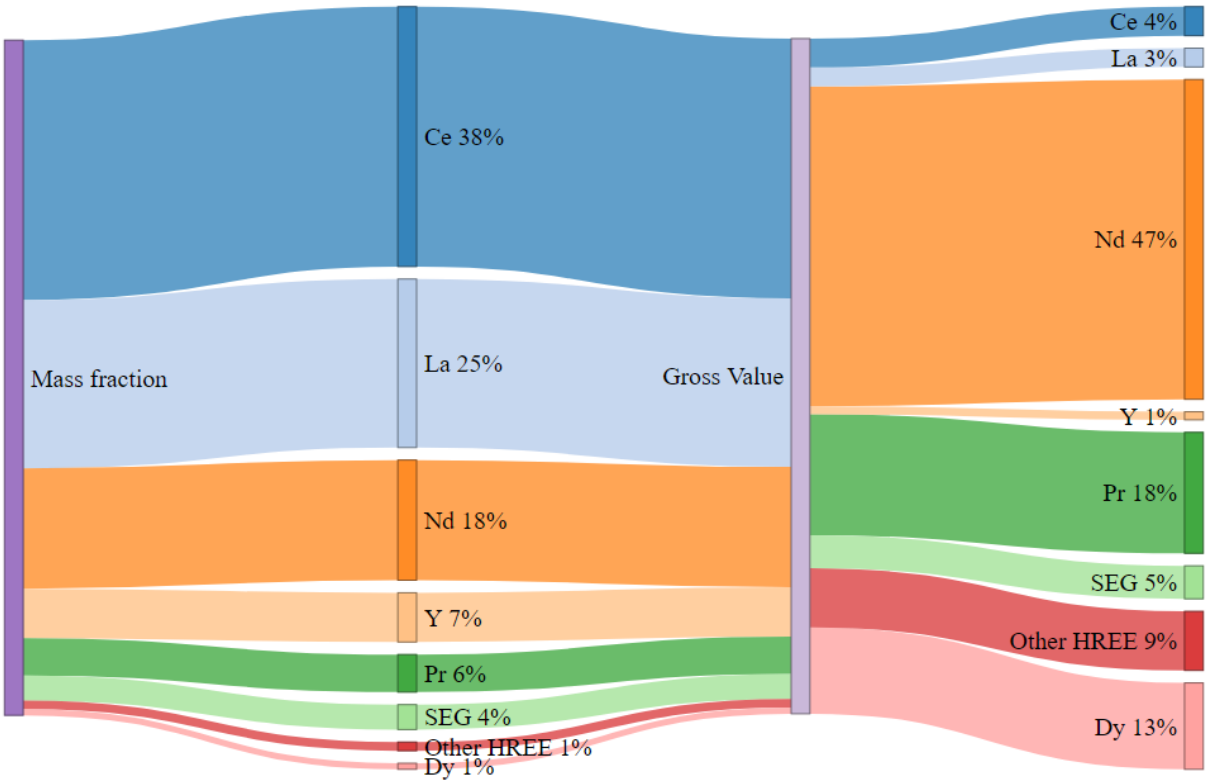

Figure 7.1: REE production and separation streams. High value REEs like Nd, Dy, and Tb make up a minority of ore concentrate, with a majority being low-value Ce and La that are mostly waste products. However, the minority elements make up for the majority of the economic value of the mined material.

value Nd is required to carry the majority of the economic cost of the mining operation. This imbalance is reflected in their prices: in 2015, Ce oxide or La oxide traded for only US$3 per kg, while Nd oxide cost US$48 per kg[130]. Various solutions to the balance problem have been proposed, including diversification of REE resources, recycling, substitution, reduced use, and new high-volume applications to create co-products from by-products[119]. These options would reduce economic imbalance of REE mining and make operations more productive. Al-LREE have the potential to become a new high volume application for Ce and La by-products thereby lowering the burden of Nd and Dy mining.

7.4 Al-LREE alloys

Modern aluminum alloy research has seen focus on developing affordable, easy to manufacture alloys suitable for use at elevated temperatures. Several options have been discovered that meet the property requirements for a high-temperature aluminum alloys but that cannot be manufactured affordably, such as Al-Sc. Recent work has shown Al-LREE alloys to be a possible option for producing an affordable elevated temperature alloy since Ce is a low-cost material to purchase. Additionally, Al-LREE alloys have been investigated for compatibility with numerous manufacturing methods[43,61]. These studies show that Al-LREE alloys can be manufactured using any number of modern techniques including sand and permanent mold casting, die-casting, extrusion, and additive manufacturing, for which Al-Ce alloys, in particular, are uniquely suited[137,138].

Al-LREE alloys are composed of a combination of Al and a single lanthanide element or multiple abundant lanthanides (La, Ce, or Mischmetal) along with traditional alloying elements. The reactions between Al, the lanthanide, and other alloying elements produce thermodynamically and morphologically stable intermetallics (a compound composed of two or more metals in an ordered structure) during solidification[55,139]. The formation of the intermetallic phases during solidification is distinct from the majority of commercial aluminum alloys by not being reliant on solid state precipitation of temperature-limited intermetallics and/or local compositional modulations produced during heat treatment[39,140]. Instead, Al-LREE alloy mechanical properties are tailored during casting through compositional and process modifications (e.g. adjusting the amount or type of alloying element or increasing cooling rates)[43,44]. This difference in processing means that Al-

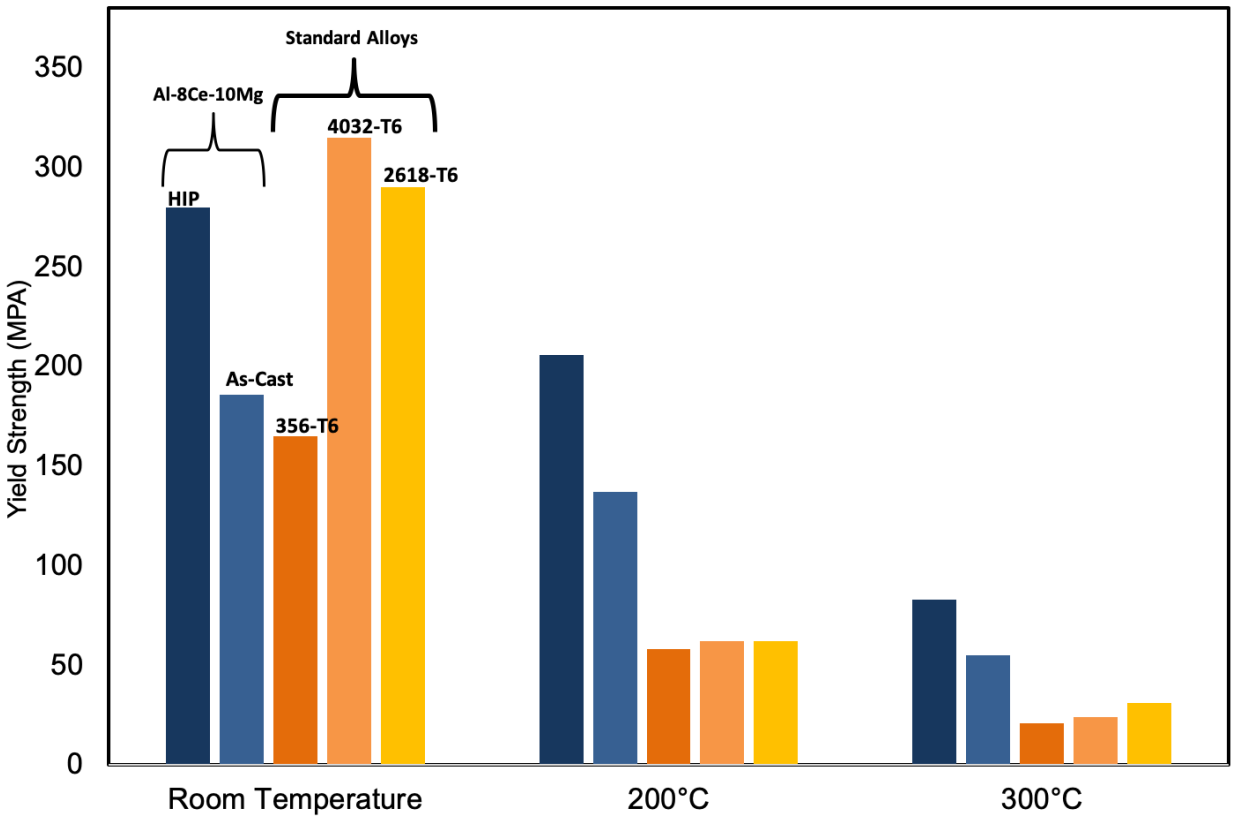

Figure 7.2: Mechanical properties at room and elevated temperatures for an Al-8Ce-10Mg alloy in both and as-cast and HIP treated state compared to traditional cast and wrought alloys, detailing the increase in mechanical yield stress retention at elevated temperatures of Al-Ce alloys.

LREE alloys can in some cases be used without the need for heat-treatment.

The underlying mechanism for stabilization of the intermetallic phase rests in the maximum solubility of Ce in the solid-solution matrix phase a face-centered cubic (FCC) Al. As predicted by thermodynamic modeling[44], this value is about 1.06×10^{-4} wt % at the eutectic temperature (640.5°C) and decreases rapidly to below 1×10^{-6} wt % at 450°C. Below 400°C, the solubility can be considered, for all practical purposes, nonexistent. In contrast, the maximum solubility observed for the traditional Al alloying elements are as follows: copper, ~5.65 wt % at 550°C; silicon, ~1.56 wt % at 577°C; and Mg, ~17 wt % at 450°C, which are several orders of magnitude higher than Ce in Al. Kinetics also contributes to the microstructural stabilization in Al-LREE alloys. The large size of Ce atoms results in a reduced diffusion coefficient when compared to other alloying elements. The diffusion coefficient for Ce in the FCC Al matrix at 500°C is 5.7×10^{-14} cm^2/s compared to copper (6.0×10^{-10} cm^2/s), silicon ($1.3x10^{-9}$), or Mg (1.4×10^{-9} cm^2/s) at identical temperatures. Moreover, strong vacancy binding to Ce atoms[141] further stabilizes the $Al_{11}Ce_3$ intermetallic as this impedes the dominate transport mechanism for solute atoms within the matrix. As a result, mobility of Ce is very limited, effectively halting the dissolution and coarsening of fine precipitates. The combined effects of low solubility and slow diffusion form a system very resistant to morphological change at elevated temperature and promotes mechanical and microstructural stability of the Al-LREE intermetallic phase.

Expanding Al-LREE alloys into higher order compositions such as ternary and quaternary has shown excellent promise as well. For example, A family of new alloys of great interest is the Al-Ce-Mg system. The eutectic nature of Al-LREE alloys combined with the limited interaction between Ce and Mg, means new composition limits can be attained. In current commercial aluminum alloys Mg is limited to roughly 5% due to castability and concerns. Al-LREEs alloys have shown tolerance for up to 10 wt% Mg, nearly twice that of the most common commercial aluminum alloys, like A535[105]. Increasing the amount of Mg that can be used in producing the alloy, increases the amount of solid solution strengthening possible. Since solid solution strengthening of Al with Mg occurs during casting at sufficient cooling rates, the ability of Al-LREE alloys to tolerate high Mg levels greatly increases the viability of producing a heat-treat free alloy.

Comparing Al-LREE alloys to current industrial high-performance Al is instructive for understanding their advantages and disadvantages. Firstly, in the as-cast state, room temperature performance of Al-8Ce-10Mg (all values are in wt%) alloys show yield strength higher than the Mg-containing, heat-treated A356 industrial alloys. The clearest distinguishing feature of Al-8Ce-10Mg is the retention of mechanical strength at elevated temperature. Figure 7.2 reveals that at 200 °C Al-8Ce-10Mg possesses more than double the yield strength of competing materials. This same trend holds to 300 °C where Al-Ce-Mg alloys remain nearly twice as strong as current high-performance commercial alloys.

Compared to common Al alloys which coarsen and rapidly lose strength once continuously exposed to elevated temperatures, Al-LREE alloys can retain the majority of their strength after exposure to upwards of 0.9 homologous temperature for extended periods of time[142]. Additionally, since both the formation of the Al-LREE intermetallic phases and the partitioning of Mg into solid solution occur during solidification post casting heat-treatments can be eliminated or minimized.

7.5 Thermal Treatment of Aluminum Alloys

At every step in the production pathway for Al alloys, from master alloy ingot to finished part, time and energy are required. While primary Al ingot production accounts for the largest portion of Al alloy embodied energy, there are many downstream opportunities to reduce energy use and speed production. Examination of the production timeline for an Al part within a foundry, shown in Figure 7.3, finds somewhere between 10-30 hours spent in a low-efficiency heat treatment furnace. Which as discussed are typically no more than 25% thermally efficient. This time spent in a furnace is required for most aluminum alloys as traditional Al alloys derive strength from a two-step solution and aging heat treatment (Figure 7.4a). During the solution heat treatment, solute elements dissolve into the matrix and then are retained in a supersaturated solid solution by quenching the alloy to room temperature This procedure enables the controlled formation of finely dispersed precipitates via age hardening, commonly at 100–200°C. The size and distribution of these precipitates is tailored via the heat treatment to control an alloy's mechanical properties. However, this same solubility, which enables optimization of mechanical properties, also limits stability at high temperatures.

Another energy intensive process pervasive throughout the high-performance Al industry, hot

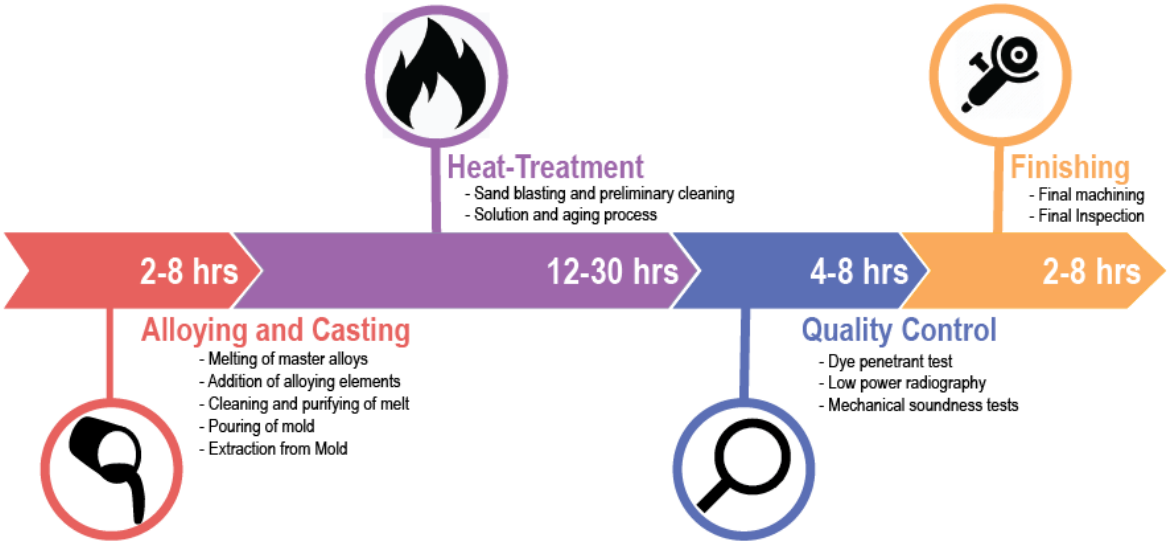

Figure 7.3: Production timeline for heat-treated aluminum alloys within a foundry

isostatic pressing (HIP), is used to mitigate casting defects improving the fatigue behavior and homogeneity across heats of Al components (Figure 7.4b). This method relies on a pressure vessel which is loaded with castings before being pressurized and held at elevated temperature[143]. The combined pressure and temperature of the process is designed to be high enough to overcome material flow stress, the point at which a material will maintain a constant strain rate in the plastic deformation regime. This isostatic pressure at temperature acts to close internal pores and rapidly redistribute solute elements into the matrix, while retaining component dimensions[143,144]. The solute redistribution leads to phase dissolution and significant coarsening, resulting in inadequate mechanical properties and an inherent requirement for secondary processing steps (i.e. solution and aging heat treatments) that are rate-limiting factors in production. Despite the energy intensity and time commitment, the HIP process is common because it can reduce the quality control burden caused by part to part variances that can be destructive to properties like fatigue and thereby increase production rates and reduce scrap[144].

7.6 Alternative Thermal Processing Routes

The high thermal stability of Al-Ce alloys combined along with the ability to tolerate large amounts of potent solution strengthening Mg leads to the opportunity to investigate new thermal processing techniques for rapidly solutionizing Mg without affecting the Al-LREE intermetallics. As discussed, Mg content of Al-Ce alloys is not limited by castability like in traditional alloys, but at high Mg levels between 7-10 wt% cooling rates experiences during casting of large parts can lead to partitioning of Mg. Figure 7.5a shows the result of a slowly cooled Al-8Ce-10Mg test bar poured in a pre-heated permanent mold. An Al-Mg β phase forms nodular colonies within the matrix and produces two negative effects. Firstly, the Mg content of these phases means that a measurable amount of potential solid solution strengthening within the matrix is lost. Secondly, the microstructure (large, aspherical shape) and incoherency of these phases means they can act as crack nucleation sites during loading, leading to reduction in ductility. Despite their presence, the yield and tensile strengths of Al-Ce-Mg alloys remain high in the as-cast state and may be appropriate for many applications. Solutionization of these phases occurs at a relatively low temperature and may be improve the ductility and strength of the Al-Ce-Mg alloys. HIP treatments without follow on two-step aging treatments (Figure 7.4c) may be a viable option for attain full solution potential of high Mg Al-Ce alloys in a shortened time period[142].

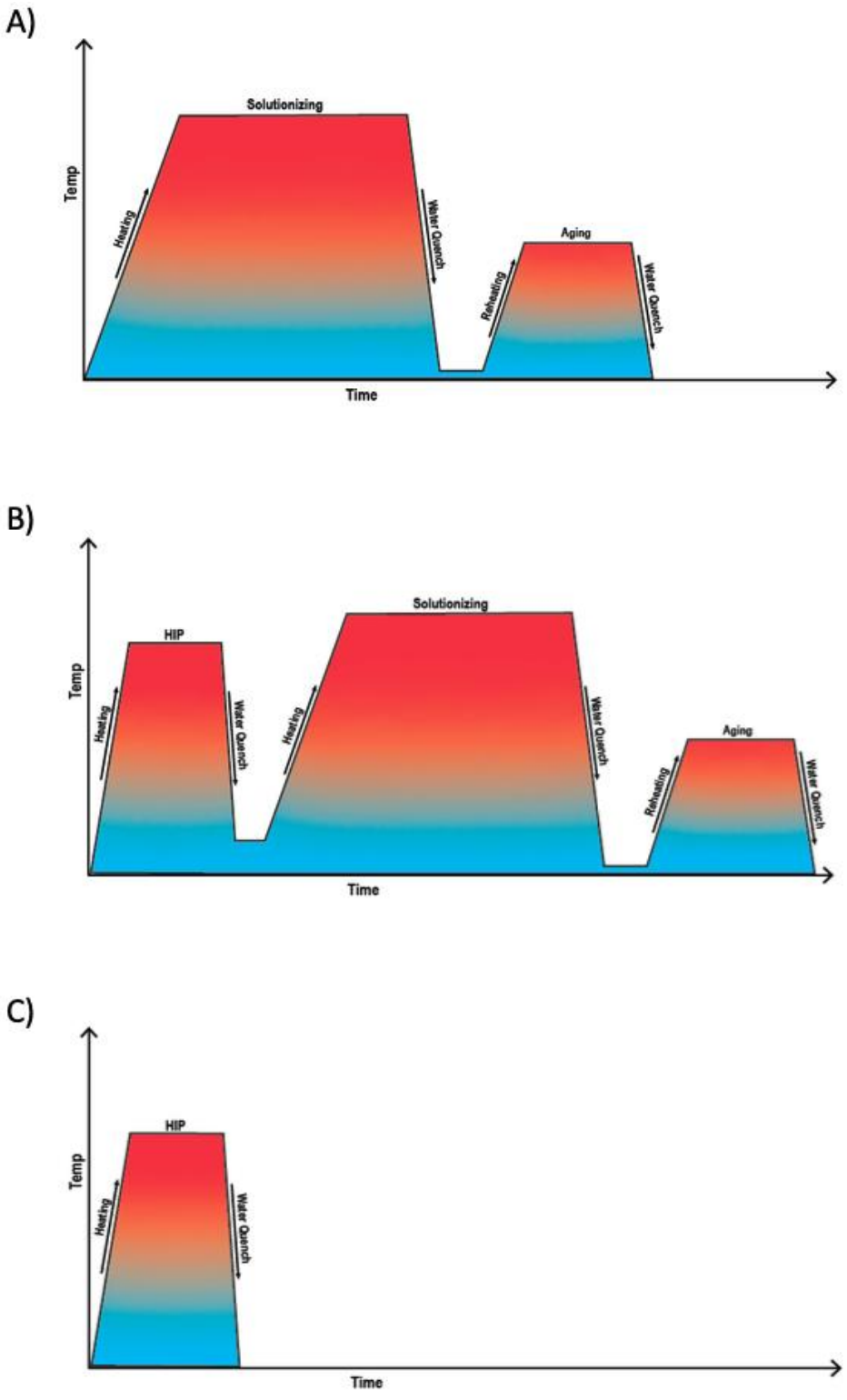

Figure 7.4: Graphical representation of different heat-treatment schedules A) Two-step solid solution heat treatment scheduled B) HIP treatment followed by two-step solid solution heat-treatment C) HIP only heat treatment possible for use with Al-Ce alloys

The application of a HIP without follow on treatment resulted in a homogenized microstructure, improved mechanical strength, and larger elongation to fracture for an Al-8Ce-10Mg alloy. The resulting microstructure (Figure 7.5b-d) shows that the application of a HIP treatment alone is effective at dissolving the Mg-rich phases (Figure 7.5b). Despite the high temperature and pressure of the process the $Al_{11}Ce_3$ intermetallic appears unaffected (Figure 7.5c). Also, no grain growth in observed in the HIPed alloy as grains are pinned on small intermetallic particles. The pinning of grain boundaries prevents growth retaining material strength (Figure 7.5d).

Despite HIPing being an energy dense process, the total time and energy expenditure of the HIP step alone is lower than that of traditional heat treatments[145,146]. The intermediate nature of the energy intensity for a HIP-only processed alloy makes possible energy and time savings in the production of Al-LREE alloys.

7.7 Potential Demand and Energy Savings

The combined benefits of reducing upstream material supply imbalances, decreased manufacturing time, energy savings, and high temperature performance, create a number of driving forces for Al-LREE alloy adoption. In many cases, Al-Ce alloys can be adopted without the need to change manufacturing infrastructure or practices. Design flexibility enabled by the tailorability of material properties and compatibility with several manufacturing methods also makes the adoption of Al-Ce alloys attractive to industries seeking to expand their material offerings or production capacity to include an affordable, high temperature Al alloy.

Recent research into the energy expenditure to manufacture Al engine cylinder heads showed that heat treatment of sand cast components can be as much as 7.74 GJ per metric ton of finished products[112]. Substituting A356 material with an Al-Ce material and eliminating the heat treatment would result in significant energy savings (Figure 7.6A). From a production time perspective, the elimination of heat treatments greatly reduces the manufacturing time per product. Further, the energy savings, infrastructure needs reduction, and labor time gained by not heat-treating mean that capital and operational expenses for foundries can be reduced even while growing manufacturing capacity.

The pathway to impactful energy savings from Al-Ce alloys require large adoption volumes. Market sectors such as automotive, aerospace, and military are all in need of lightweight high temperature materials for various applications and may be key early adopters. For example, engine

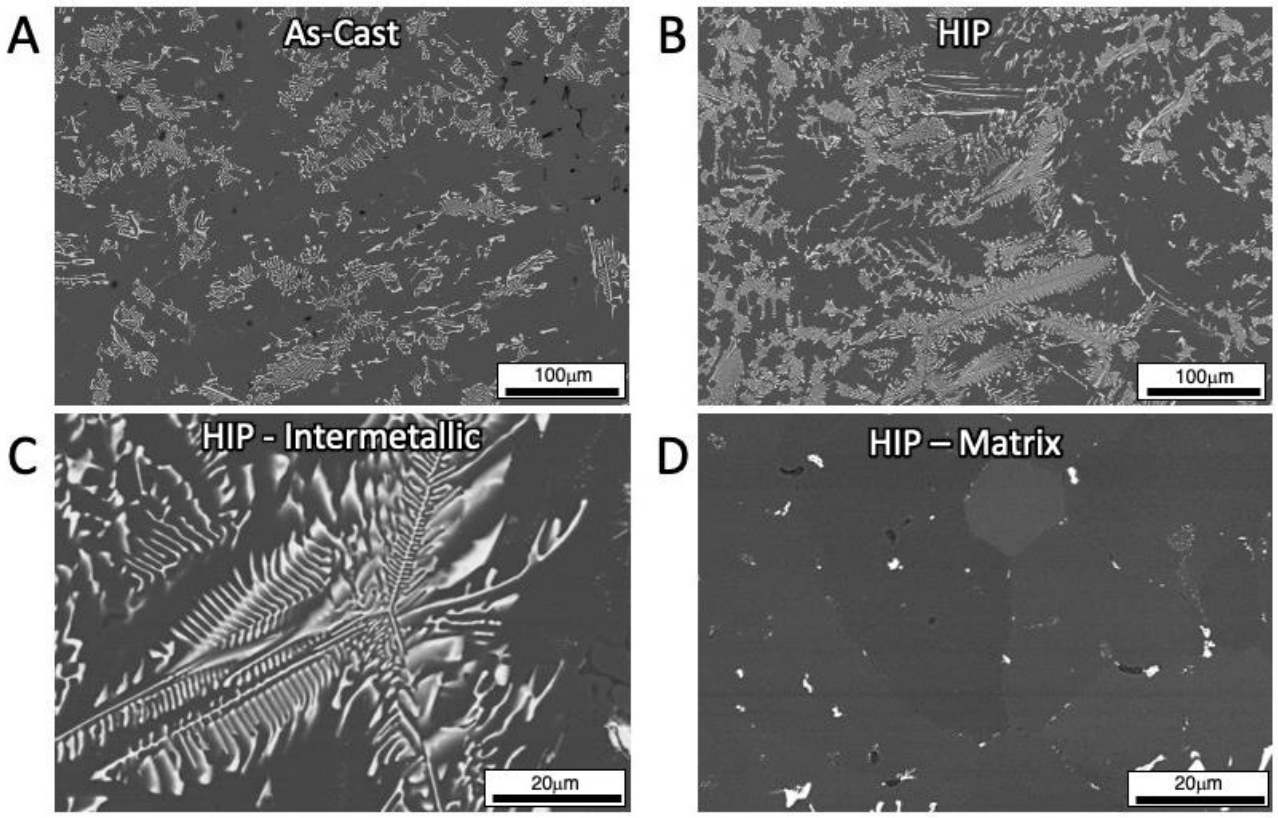

Figure 7.5: Backscattered electron micrographs of A) as-cast Al-8Ce-10Mg, B) HIP condition, C) HIP condition at higher magnification revealing a stable intermetallic structure that does not dissolve or coarsen, and D) the Al matrix with intermetallic particles decorating the grain boundary

components such as heads and blocks that are commonly produced from heat-treated Al-Si alloys could be an early source of large demand for Al-Ce alloys. Recent research into the impact of Al-Ce adoption on the Al industry modeled demand growth of Al-Ce alloys for automotive drivetrain components and anticipated a demand of 280 kt by the year 2055[41]. Combining this data with the expected energy savings per metric ton of produced material would mean that Al-Ce alloys by the year 2050 could be saving as much as ~650,000 MWhr annually through reduction of heat treatments[41,112] (Figure 7.6b). This amount correlates to the energy use of more than 60,000 US homes [147].

Additionally, broad adoption of the Al-LREE family of alloys would have a large impact on the ongoing balance problem of REE materials. Beyond the simple supply and demand mismatch of LREEs is the differing economics of mines around the world. Mines which suffer the most from the current balance problem operate as REE main product mines, with no secondary source of ecnomic value. Many of the world's largest REE deposits are exploited as coproducts of the iron mining process[148]. For example, the Byan Obo mine in China is principally an iron mine and therefore does not need to rely on demand for the more common, less valuable LREE elements to be economical. Meaning Byan Obo can focus efforts on extracting higher value REEs like Nd and Dy and only ramp up LREE separation when demand requires it. The REE main product mines, on the other hand, struggle to develop stable economies of scale considering the low price and overabundance of their largest mine outputs, La and Ce. Many experts agree that in order to diversify the REE supply chain, simply opening mines and developing new processing facilities will not be sufficient[133]. Instead, work must focus on development of new demand for the least valuable REEs. Al-LREEs have the potential to meet the necessary level of demand to motivate new mine and process facility openings by increasing the price of Ce to be more in line with a balanced supply chain. The amount of LREE material needed for an 8wt% Al alloy to meet the predicted demand in just the single application outlined above is 22.4kt annually. A demand of this size represents 24% of combined global Ce and La production in 2018[149]. This amount of new demand for Ce and La will likely be enough to economize new mine operations, stabilize the price of main product Nd and Dy, and promote broader global processing capability.

Demand for Al-LREE alloys is expected to increase rapidly, as the attractive properties of Al-Ce alloys have already spurred interest from manufacturers seeking to take advantage of its material

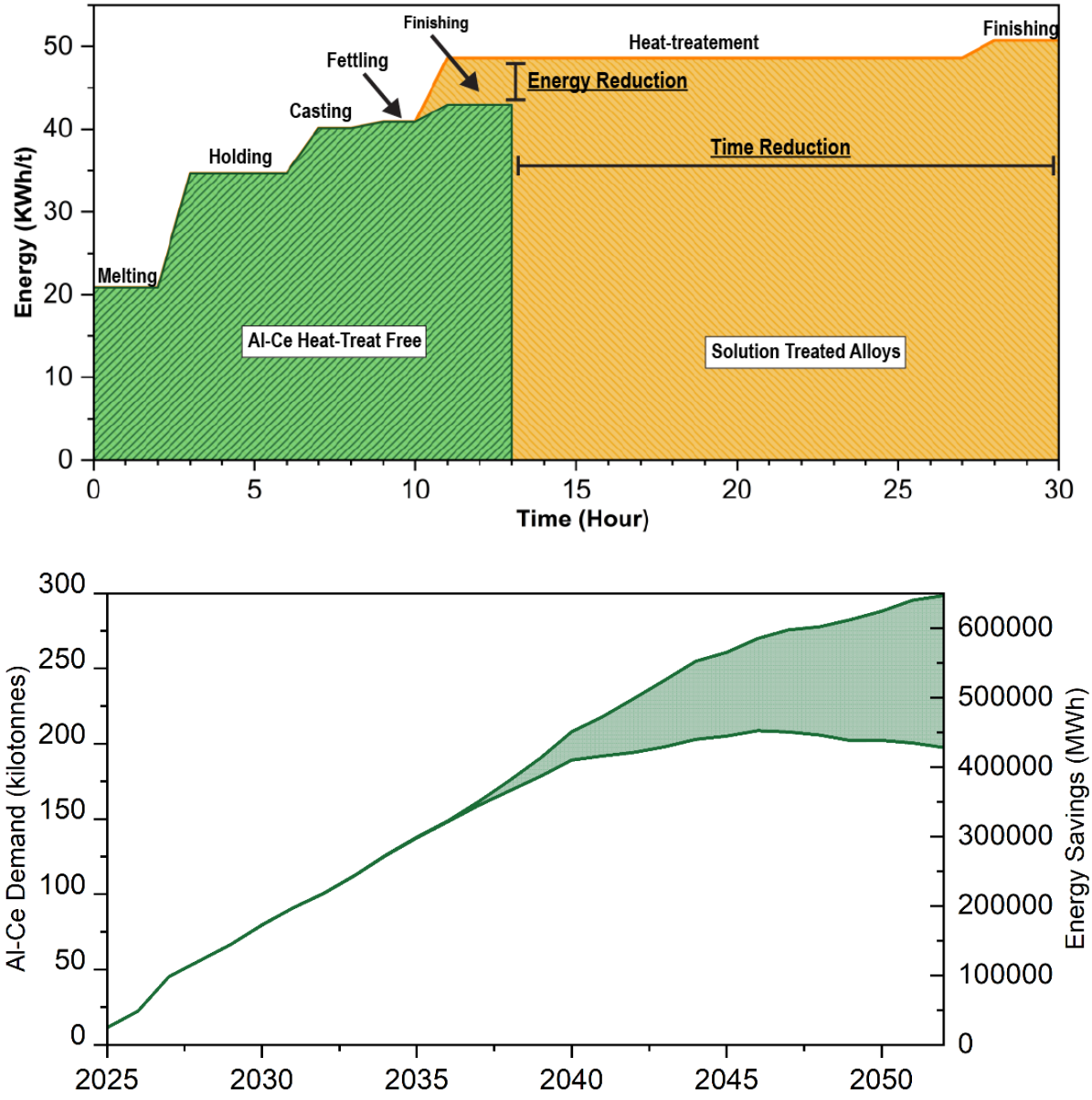

Figure 7.6: A) Plot of potential for decreased energy expenditure and manufacturing time reduction of Al-Ce heat-treat free alloys compared to traditional solution treated alloys. B) Calculated Al-Ce alloy demand for use in power train applications and the associated energy savings from reduced heat treatment requirements.

properties, rapid production timelines, and affordability compared to other high temperature Al alloys. For comparison, the Al-Sc family of alloy is one of the most well-known systems of high temperature Al alloys. However, these alloys have several shortcomings. Chiefly, they are prohibitively expensive due to their containing scandium. This limits their application to specialty and niche demand uses like military and sports equipment[150,151]. Furthermore, Al-Sc alloys have different heat-treatment requirements than more common Al-Cu or Al-Si alloys[152]. To reach optimal performance the alloys must be aged at relatively high temperatures[152]. This incompatibility means that Al-Sc alloys, despite being a very low volume product, require dedicated foundry heat-treatment infrastructure to produce. A dedicated low volume production line imparts additional burdens on production timelines beyond those seen by demand increases from more conventional alloys. Other common high temperature alloys are not nearly as costly as Al-Sc but suffer instead from difficulties in manufacturing. For example, RR350 is a moderately expensive alloy relative to A356. However the major issue with using RR350 is the difficulty in processing[153]. It has very low castabtlity and thus can only be produced in small quantities by a select number of Al casting houses. Al-LREE alloys do not suffer from these problems being both affordable and easy to process.

The most significant limitation on the Al-LREE alloys is a possible supply chain issue for early adopters. Since Ce and La account for the largest fraction, typically about 50%, of REE, it must be separated during the mining process prior to the high value REEs such as Nd and Dy. A lack of demand in the current market has reinforced the mine operators' habit of depositing Ce and La back into tailings after the high value REEs are extracted. Due to their high abundance, domestic and foreign mines are likely able to adjust to near-term increases in Ce demand resulting from increased demand for Al-Ce alloys, but the supply chains from mining companies to Al producers are not yet established and may take time to develop. Additionally refined Ce and La are considered a hazardous materials by US DOT and only limited quantities can be transported in its pure metallic form making shipping costs high to receive large quantities[154]. Methods are being developed to overcome this hurdle which may further reduce the production burden of Ce metal increasing propagative benefit potential.

7.8 Conclusion

Identifying and exploiting propagative benefits in supply chains and manufacturing is difficult. In

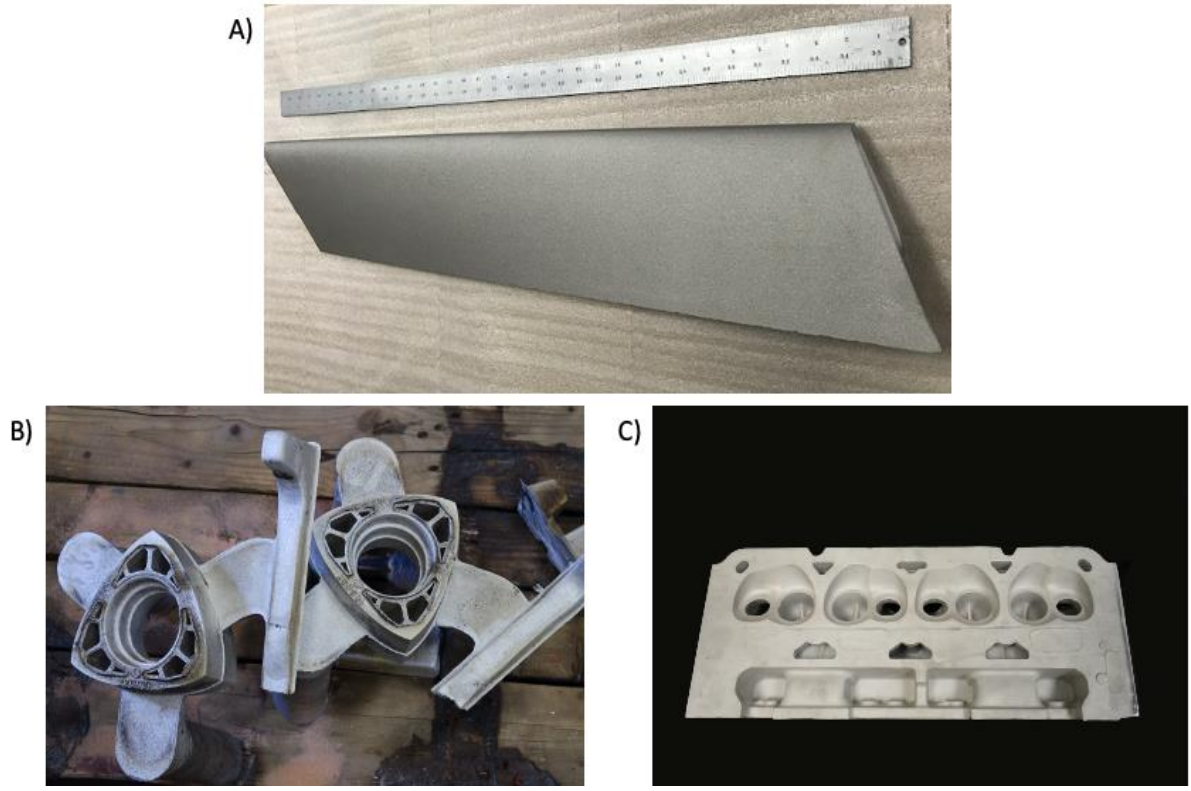

Figure 7.7: A) A central hub spoke for a distributed hydrokinetic energy turbine. The first commercial product made from Al-Ce alloys. B) Casting of a rotary engine piston for testing of Al-Ce alloy castability in complex, small feature expendable mold castings. C) Large casting of a cylinder head from Al-Ce alloys for testing and verification.

some cases, realizing these benefits may require large changes like overhauling existing production methods. Al-LREE alloys show promise for taking advantage of nascent value in the REE supply chain and compounding that value onto aluminum alloy markets. Demand growth potential for Al-LREE is high, and this makes the likelihood of finding new applications for the low value byproduct LREEs of main product mines high as well. The ability for Al-LREE alloys to be flexibly manufactured means that the energy reduction benefits of Al-LREE alloys can be realized across the spectrum of Al alloy products without sacrificing on mechanical performance or weight savings. Additionally, the broad applicability will induce higher demand for Al-LREE alloys and, in turn, abundant LREEs, making REE mining economics more attractive adding stability to this critical material supply chain.

7.9 Acknowledgements

This research was sponsored by the Critical Materials Institute, an Energy Innovation Hub funded by the U.S. Department of Energy (DOE), Office of Energy Efficiency and Renewable Energy, Advanced Manufacturing Office, and Eck Industries. This research was supported in part by an appointment to the Oak Ridge National Laboratory HERE and SULI program. This work was performed under the auspices of the U.S. DOE with ORNL under contract DE-AC05-00OR22725 and with LLNL under Contract DE-AC52-07NA27344.

8. Conclusions

8.1 Per Chapter Conclusions

8.1.1 Castabilty of an Aluminum Cerium Alloys

Al-Ce alloys have the possibility of replacing heavier steel and cast-irons for use in high-temperature applications. Al-Ce alloys are castable along a broad range of cerium content, and are compatible with modern casting practices, requiring no changes to present foundry infrastructure. Mechanical properties are as high as 252 MPa for tensile and 128 MPa for yield strength. Though high temperature mechanical properties are not represented here, the combination of thermodynamic properties and stability following heat-treatment suggest that Al-Ce-X alloys hold great promise for high-temperature mechanical properties.

Compositional variation is possible with the Al-Ce-X alloy family; Mg and Si both have the possibility to be alloyed with Al-Ce to create a highly tailorable microstructure and mechanical properties. The impediment of silicon on castability is a negative, but it is theorized that by decreasing the silicon content good castability can be returned while maintaining the room-temperature strength of the Al-Ce-Si-Mg alloy.

8.1.2 Developing and Al-Ce Alloy Design Paradigm

Cerium strengthened aluminum alloys exhibit highly desirable behavior for many applications: high ductility, robust room-temperature mechanical properties, exceptional high-temperature mechanical property retention, high tolerance to casting defects, and excellent castability across a broad range of compositions. In fact, the cast materials approach the mechanical properties of traditional wrought alloys. The microstructure remains stable to above 500 °C, corresponding to a homologous temperature (T/TMelt) greater than 0.84, which rivals the stability observed in heat tolerant materials such as superalloys.

Given the high availability and low cost of cerium metal, these alloys are economically viable for large volume industries such as the transportation sector, where their properties make them ideally suited for vehicle light weighting. Elimination or reduction of heat-treatment amplifies the economic and environmental benefits of light weighting in the transportation sectors. Adoption of these alloys by industry will not only impact current technologies but will provide the basis with which to develop the next generation of high temperature aluminum alloys. Finally, by creating demand for Ce, which is overproduced, the economics of rare-earth mining improve. In a typical

deposit, one-third to one-half of the rare-earth content by weight is cerium, so converting a by-product into a co-product will help stabilize global production and encourage diversification of the rare-earth supply chain.

8.1.3 Efficacy of Using Mischmetal as a Primary Alloying Addition

Despite the differences between the Al-12Ce and Al-12MM alloys it is expected that by combining aluminum with MM instead of cerium would result in a very similar alloy family and could be a route to reducing supply risk and cost. Aluminum alloy producers may be able to diversify their supply chain by leveraging the similarities between cerium and the other light rare earth elements to provide a flexible sourcing of LREE compounds for producing high temperature aluminum-LREE alloys.

8.1.4 Resistance of Al-Ce-Mg alloys to Loss of Mechanical Strength following Extended Exposure to Elevated Temperatures

Al-Ce-Mg alloys have the potential to be a good choice for material deign where elevated temperature stability is an important factor. Al-Ce alloys offer a mechanical property stability above that of traditional commercial alloys. Al-Ce shows up a 50% improvement over Al-Si and a 30% improvement over Al-Cu alloys at 250 °C and a 90% improvement at 400 °C over both Al-Si and Al-Cu alloys. Al-Ce alloys are not without their shortfalls however, and ductility of Al-Ce-Mg alloys remains a concern. Solutions which might be possible are lowering the amount of Mg present in the alloys to limit embrittlement and balance properties.

Additionally, the proposition of an aluminum alloy which can survive temporary excursion to well above the proposed operating temperature is interesting. This property of Al-Ce alloys is in comparison to traditional options which as shown above might suffer catastrophic reductions in material properties which would create a source of part failure.

Overall the results show clearly that Al-Ce alloys are a viable option for taking the place of current aluminum alloys in many stationary and dynamic elevated temperature applications thanks to their retention of high amounts of material mechanical properties when compared to their traditional counterparts.

8.1.5 Resistance of Al-Ce Alloys to Aqueous Corrosion

Improving corrosion resistance and manufacturing flexibility of Al alloys is among the most important properties for continued growth in Al alloy adoption. Presented in this report is data and analysis which makes it clear that Ce has potential to improve corrosion properties of Al alloys in several ways:

- Ce used a primary addition to Al alloys created the potential for producing an alloy that combines excellent elevated temperature stability and strength with near Al-Si alloy levels of corrosion resistance.
- Minor additions of Ce below 1% can greatly improve the corrosion resistance of current Al alloys through blocking grain boundary dissolution and alloy sensitization processes.
- Measured additions of Ce and Ce containing alloys to scrap supply streams may be a pathway to easing restrictions on particular scrap metal in the production of Al alloys that are sensitive to Cu impurities deleterious to high corrosion resistance.

Overall Ce appears to be an option for reducing corrosion of Al alloys whether as a minor or main addition. However, in the case of Ce as a scavenging addition, further work is needed to fully understand how Ce effects the mechanical properties of alloys to which it is added as a minor addition, specifically how additions of Ce can be made without sacrificing measurable portions of alloy ductility. Regardless of the shortfalls of Ce as a minor addition, the results included in this report show Ce alloys present a viable pathway to realizing a new family of cost effective, corrosion resistant, manufacturable, elevated temperature Al alloys should their development continue.

8.1.6 Increase in Mechanical Properties of Al-Ce-Mg Alloys Through High Pressure Processing Routes

Identifying and exploiting propagative benefits in supply chains and manufacturing is difficult. In some cases, realizing these benefits may require large changes like overhauling existing production methods. Al-LREE alloys show promise for taking advantage of nascent value in the REE supply chain and compounding that value onto aluminum alloy markets. Demand growth potential for Al-LREE is high, and this makes the likelihood of finding new applications for the low value byproduct LREEs of main product mines high as well. The ability for Al-LREE alloys to be flexibly manufactured means that the energy reduction benefits of Al-LREE alloys can be realized

across the spectrum of Al alloy products without sacrificing on mechanical performance or weight savings. Additionally, the broad applicability will induce higher demand for Al-LREE alloys and, in turn, abundant LREEs, making REE mining economics more attractive adding stability to this critical material supply chain.

8.2 Broader Impacts

The development of a viable new aluminum alloy system for use as a high-temperature, lightweight, corrosion resistant option in the expanded application of aluminum alloys will have various positive implications for the growth of aluminum alloys. These include further replacement of ferrous materials in applications such as diesel engines, extended lifetime of aluminum in marine environments, and reduction of energy footprint for the aluminum industry on a mass normalized basis. Additionally, using cerium as the main alloying addition in a new family of allows will have upstream benefits to the production economics of REEs, an important strategic concern for the US as they move toward a more renewable and sustainable energy landscape. Finally, a new family of aluminum alloys based on using a highly stable intermetallic formed during solidification creates opportunities for development of new advanced processes for manufacturing of aluminum alloys.

8.3 Future Work

Al-Ce casting alloys have been established as a real candidate for expanding the library of aluminum alloys available to the scientific community for research and to industry for production. However, there is still a large amount of work to be done for Al-Ce casting alloys to be fully understood. Firstly, new models of complex, higher order systems must develop to accelerate selection of alloys with attractive properties. To do this many alloy systems must be explored experimentally with high throughput methods to understand phase spaces and characterize possible material properties. Additionally, pilot scale trials must continue to further develop any new manufacturing methods which uniquely benefit Al-Ce alloys.

Finally, work to understand Al-Ce alloys must be expanded beyond casting and additive manufacturing to other fields of advanced manufacturing such as powder metallurgy and rapid cooled casting to further take advantage of cooling rate and other effects on material properties.

References

(1) Tisza, M.; Lukács, Z. High Strength Aluminum Alloys in Car Manufacturing. *IOP Conf. Ser. Mater. Sci. Eng.* **2018**, *418*, 012033. https://doi.org/10.1088/1757-899X/418/1/012033.

(2) Long, R. S.; Boettcher, E.; Crawford, D. Current and Future Uses of Aluminum in the Automotive Industry. *JOM* **2017**, *69* (12), 2635–2639. https://doi.org/10.1007/s11837-017-2554-9.

(3) Stojanovic, B.; Bukvic, M.; Epler, I. Application of Aluminum and Aluminum Alloys in Engineering. *Appl. Eng. Lett. J. Eng. Appl. Sci.* **2018**, *3* (2), 52–62. https://doi.org/10.18485/aeletters.2018.3.2.2.

(4) Jayakrishna, K.; Kar, V. R.; Sultan, M. T. H.; Rajesh, M. Materials Selection for Aerospace Components. In *Sustainable Composites for Aerospace Applications*; Elsevier, 2018; pp 1–18. https://doi.org/10.1016/B978-0-08-102131-6.00001-3.

(5) Mondolfo, L. F. *Aluminum Alloys: Structure and Properties*; Elsevier, 2013.

(6) Fleischer, R. L. High-Strength, High-Temperature Intermetallic Compounds. *J. Mater. Sci.* **2016**, *22* (7), 2281–2288. https://doi.org/10.1007/BF01082105.

(7) Liu, M.; Čížek, J.; Chang, C. S. T.; Banhart, J. Early Stages of Solute Clustering in an Al–Mg–Si Alloy. *Acta Mater.* **2015**, *91*, 355–364. https://doi.org/10.1016/j.actamat.2015.02.019.

(8) Marsh, S. P.; Glicksman, M. E. Kinetics of Phase Coarsening in Dense Systems. *Acta Mater.* **1996**, *44* (9), 3761–3771. https://doi.org/10.1016/1359-6454(95)00451-3.

(9) Ratke, L.; Voorhees, P. W. *Growth and Coarsening: Ostwald Ripening in Material Processing*; Springer Science & Business Media, 2013.

(10) Hernandez-Sandoval, J.; Garza-Elizondo, G. H.; Samuel, A. M.; Valtiierra, S.; Samuel, F. H. The Ambient and High Temperature Deformation Behavior of Al–Si–Cu–Mg Alloy with Minor Ti, Zr, Ni Additions. *Mater. Des.* **2014**, *58*, 89–101. https://doi.org/10.1016/j.matdes.2014.01.041.

(11) Hildeman, G. J.; Jr, R. E. S. Aluminum Powder Alloy Product for High Temperature Application. US4464199A, August 7, 1984.

(12) Binnemans, K.; Jones, P. T.; Müller, T.; Yurramendi, L. Rare Earths and the Balance Problem: How to Deal with Changing Markets? *J. Sustain. Metall.* **2018**, 1–21. https://doi.org/10.1007/s40831-018-0162-8.

(13) *ASM Handbook, Volume 02 - Properties and Selection: Nonferrous Alloys and Special-Purpose Materials*; ASM International, 1990.

(14) Fishman, T.; Myers, R. J.; Rios, O.; Graedel, T. E. Implications of Emerging Vehicle Technologies on Rare Earth Supply and Demand in the United States. *Resources* **2018**, *7* (1), 9. https://doi.org/10.3390/resources7010009.

(15) *Critical Materials Strategy*; United States Department of Energy, 2011.

(16) Li, K.; Xue, D. A new set of electronegativity scale for trivalent lanthanides. *Phys. Status Solidi B* **2007**, *244* (6), 1982–1987. https://doi.org/10.1002/pssb.200642493.

(17) Bunzli, J.-C. G.; Pecharsky, V. K. *Handbook on the Physics and Chemistry of Rare Earths: Including Actinides*; Elsevier, 2019.

(18) Davis, J. R. *Aluminum and Aluminum Alloys*; ASM International, 1993.

(19) Gegel, G. A. Maerial and Process Consultancy, 2016.

(20) Luo, A. A. Magnesium: Current and Potential Automotive Applications. *JOM* **2002**, *54* (2), 42–48. https://doi.org/10.1007/BF02701073.

(21) Kaufman, J. G.; Rooy, E. L. *Aluminum Alloy Castings: Properties, Processes, and Applications*; ASM International, 2004.

(22) Mondolfo, L. F. *Aluminum Alloys: Structure and Properties*; Elsevier, 2013.

(23) Booth-Morrison, C.; Dunand, D. C.; Seidman, D. N. Coarsening Resistance at 400 °C of Precipitation-Strengthened Al–Zr–Sc–Er Alloys. *Acta Mater.* **2011**, *59* (18), 7029–7042. https://doi.org/10.1016/j.actamat.2011.07.057.

(24) Fuller, C. B.; Seidman, D. N.; Dunand, D. C. Mechanical Properties of Al(Sc,Zr) Alloys at Ambient and Elevated Temperatures. *Acta Mater.* **2003**, *51* (16), 4803–4814. https://doi.org/10.1016/S1359-6454(03)00320-3.

(25) DeHoff, R. *Thermodynamics in Materials Science, Second Edition*; CRC Press, 2006.

(26) ASM Handbook Volume 15: Casting - ASM International http://www.asminternational.org/search/-/journal_content/56/10192/05115G/PUBLICATION;jsessionid=8D39962EFDB60497CDBFCEC0431A79A1 (accessed Jan 15, 2016).

(27) Flemings, M. C.; Niyama, E.; Taylor, H. F. Fluidity of Aluminum Alloys: An Experimental and Quantitative Evaluation. *AFS Trans.* **1961**, *69*, 625–635.

(28) Davis, J. R. *Aluminum and Aluminum Alloys*; ASM International, 1993.

(29) Chakrabarti, D. J.; Laughlin, D. E. Phase Relations and Precipitation in Al–Mg–Si Alloys with Cu Additions. *Prog. Mater. Sci.* **2004**, *49* (3–4), 389–410. https://doi.org/10.1016/S0079-6425(03)00031-8.

(30) Bergsma, S. C.; Kassner, M. E.; Li, X.; Wall, M. A. Strengthening in the New Aluminum Alloy AA 6069. *Mater. Sci. Eng. A* **1998**, *254* (1–2), 112–118. https://doi.org/10.1016/S0921-5093(98)00701-1.

(31) Kang, Y. B. Aluminum-Cerium Binary Phase Diagram (2008 Kang Y.B.) http://mio.asminternational.org/apd/index.aspx (accessed Mar 30, 2016).

(32) Zhong, Y. Aluminum-Magnesium Binary Phase Diagram (2005 Zhong Y.) http://mio.asminternational.org/apd/index.aspx (accessed Mar 30, 2016).

(33) Samuel, A. M.; Gauthier, J.; Samuel, F. H. Microstructural Aspects of the Dissolution and Melting of Al2Cu Phase in Al-Si Alloys during Solution Heat Treatment. *Metall. Mater. Trans. A* **1996**, *27* (7), 1785–1798. https://doi.org/10.1007/BF02651928.

(34) Rogl, P. Aluminum-Cerium-Silicon Ternary, Isothermal Section (1991 Rogl P.) http://mio.asminternational.org/apd/datasheet.aspx?dbKey=grantami_apd&record=558932&history=524351&locate=False (accessed Mar 31, 2016).

(35) S. Garde, C.; Takeuchi, T.; Nakano, Y.; Takeda, Y.; Ota, Y.; Miyauchi, Y.; Sugiyama, K.; Hagiwara, M.; Kindo, K.; Honda, F.; Settai, R.; Ōnuki, Y. Electrical and Magnetic

Properties of R_3Al_{11} (R = La, Ce, Pr, and Nd). *J. Phys. Soc. Jpn.* **2008**, *77* (12), 124704. https://doi.org/10.1143/JPSJ.77.124704.

(36) Collins, J. A. *Failure of Materials in Mechanical Design: Analysis, Prediction, Prevention*; John Wiley & Sons, 1993.

(37) Knipling, K. E.; Dunand, D. C.; Seidman, D. N. Criteria for Developing Castable, Creep-Resistant Aluminum-Based Alloys – A Review. *Z. Für Met.* **2006**, *97* (3), 246–265. https://doi.org/10.3139/146.101249.

(38) Knipling, K. E.; Seidman, D. N.; Dunand, D. C. Ambient- and High-Temperature Mechanical Properties of Isochronally Aged Al–0.06Sc, Al–0.06Zr and Al–0.06Sc–0.06Zr (at.%) Alloys. *Acta Mater.* **2011**, *59* (3), 943–954. https://doi.org/10.1016/j.actamat.2010.10.017.

(39) Brooks, C. R.; Brooks, C. R. *Heat Treatment, Structure and Properties of Nonferrous Alloys*; American Society for metals Metals Park, OH, 1982; Vol. 4.

(40) Ratke, L.; Voorhees, P. W. *Growth and Coarsening: Ostwald Ripening in Material Processing*; Springer Science & Business Media, 2013.

(41) Nguyen, R. T.; Imholte, D. D.; Rios, O. R.; Weiss, D.; Sims, Z.; Stromme, E.; McCall, S. K. Anticipating Impacts of Introducing Aluminum-Cerium Alloys into the United States Automotive Market. *Resour. Conserv. Recycl.* **2019**, *144*, 340–349. https://doi.org/10.1016/j.resconrec.2019.02.009.

(42) Glazoff, M. V.; Zolotorevsky, V. S.; Belov, N. A. *Casting Aluminum Alloys*; Elsevier, 2010.

(43) Sims, Z. C.; Weiss, D.; McCall, S. K.; McGuire, M. A.; Ott, R. T.; Geer, T.; Rios, O.; Turchi, P. a. E. Cerium-Based, Intermetallic-Strengthened Aluminum Casting Alloy: High-Volume Co-Product Development. *JOM* **2016**, *68* (7), 1940–1947. https://doi.org/10.1007/s11837-016-1943-9.

(44) Sims, Z. C.; Rios, O.; Weiss, D.; Turchi, P. E.; Perron, A.; Lee, J. R.; Li, T.; Hammons, J.; Bagge-Hansen, M.; Willey, T. M.; others. High Performance Aluminum-Cerium Alloys for High-Temperature Applications. *Mater. Horiz.* **2017**. https://doi.org/10.1039/c7mh00391a.

(45) Sims, Z. C.; Rios, O.; McCall, S. K.; Van Buuren, T.; Ott, R. T. Characterization of near Net-Shape Castable Rare Earth Modified Aluminum Alloys for High Temperature Application. In *Light Metals 2016*; Springer International Publishing, 2016; pp 111–114.

(46) Hunt, A. *Element Recovery and Sustainability*; Royal Society of Chemistry, 2013.

(47) Iyer, A. V.; Lim, H.; Rios, O.; Sims, Z.; Weiss, D. An Economic Model and Experiments to Understand Aluminum-Cerium Alloy Recycling. *JOM* **2018**, *70* (4), 547–552. https://doi.org/10.1007/s11837-018-2764-9.

(48) Kołodyńska, D.; Fila, D.; Gajda, B.; Gęga, J.; Hubicki, Z. Rare Earth Elements—Separation Methods Yesterday and Today. In *Applications of Ion Exchange Materials in the Environment*; Inamuddin, Ahamed, M. I., Asiri, A. M., Eds.; Springer International Publishing: Cham, 2019; pp 161–185. https://doi.org/10.1007/978-3-030-10430-6_8.

(49) King, A. H.; Eggert, R. G.; Gschneidner, K. A. Chapter 283 - The Rare Earths as Critical Materials. In *Handbook on the Physics and Chemistry of Rare Earths*; Bünzli, J.-C. G.,

Pecharsky, V. K., Eds.; Including Actinides; Elsevier, 2016; Vol. 50, pp 19–46. https://doi.org/10.1016/bs.hpcre.2016.08.001.

(50) Czerwinski, F. Thermal Stability of Aluminum Alloys. *Materials* **2020**, *13* (15), 3441. https://doi.org/10.3390/ma13153441.

(51) Roy, S.; Allard, L. F.; Rodriguez, A.; Porter, W. D.; Shyam, A. Comparative Evaluation of Cast Aluminum Alloys for Automotive Cylinder Heads: Part II—Mechanical and Thermal Properties. *Metall. Mater. Trans. A* **2017**, *48* (5), 2543–2562. https://doi.org/10.1007/s11661-017-3986-0.

(52) Roy, S.; Allard, L. F.; Rodriguez, A.; Watkins, T. R.; Shyam, A. Comparative Evaluation of Cast Aluminum Alloys for Automotive Cylinder Heads: Part I—Microstructure Evolution. *Metall. Mater. Trans. A* **2017**, *48* (5), 2529–2542. https://doi.org/10.1007/s11661-017-3985-1.

(53) Sims, Z. C.; Weiss, D.; McCall, S. K.; McGuire, M. A.; Ott, R. T.; Geer, T.; Rios, O.; Turchi, P. A. E. Cerium-Based, Intermetallic-Strengthened Aluminum Casting Alloy: High-Volume Co-Product Development. *JOM* **2016**, *68* (7), 1940–1947.

(54) Liu, Y.; Michi, R. A.; Dunand, D. C. Cast Near-Eutectic Al-12.5 wt.% Ce Alloy with High Coarsening and Creep Resistance. *Mater. Sci. Eng. A* **2019**, *767*, 138440. https://doi.org/10.1016/j.msea.2019.138440.

(55) Gao, M. C.; Ünlü, N.; Shiflet, G. J.; Mihalkovic, M.; Widom, M. Reassessment of Al-Ce and Al-Nd Binary Systems Supported by Critical Experiments and First-Principles Energy Calculations. *Metall. Mater. Trans. A* **2016**, *36* (12), 3269–3279. https://doi.org/10.1007/s11661-005-0001-y.

(56) Sims, Z. C.; Rios, O.; McCall, S. K.; Buuren, T. V.; Ott, R. T. Characterization of Near Net-Shape Castable Rare Earth Modified Aluminum Alloys for High Temperature Application. *Light Met. 2016* **2016**, 107–114.

(57) Henderson, H. B.; Stromme, E. T.; Kesler, M. S.; Sims, Z. C.; Chesser, P.; Richardson, B.; Thompson, M. J.; Love, L.; Peter, W.; Morris, E.; others. Additively Manufactured Single-Use Molds and Reusable Patterns for Large Automotive and Hydroelectric Components. *Int. J. Met.* **2019**, 1–9.

(58) Mahidhara, R. K. Elevated-Temperature Coarsening Behavior in Aluminum Alloys. *J. Mater. Eng. Perform.* **1997**, *6* (1), 102–105. https://doi.org/10.1007/s11665-997-0038-8.

(59) Apergis, E.; Apergis, N. The Role of Rare Earth Prices in Renewable Energy Consumption: The Actual Driver for a Renewable Energy World. *Energy Econ.* **2017**, *62*, 33–42. https://doi.org/10.1016/j.eneco.2016.12.015.

(60) Plotkowski, A.; Rios, O.; Sridharan, N.; Sims, Z.; Unocic, K.; Ott, R. T.; Dehoff, R. R.; Babu, S. S. Evaluation of an Al-Ce Alloy for Laser Additive Manufacturing. *Acta Mater.* **2017**, *126*, 507–519.

(61) Stromme, E. T.; Henderson, H. B.; Sims, Z. C.; Kesler, M. S.; Weiss, D.; Ott, R. T.; Meng, F.; Kassoumeh, S.; Evangelista, J.; Begley, G.; Rios, O. Ageless Aluminum-Cerium-Based Alloys in High-Volume Die Casting for Improved Energy Efficiency. *JOM* **2018**, *70* (6), 866–871. https://doi.org/10.1007/s11837-018-2861-9.

(62) Ryen, Ø.; Holmedal, B.; Nijs, O.; Nes, E.; Sjölander, E.; Ekström, H.-E. Strengthening Mechanisms in Solid Solution Aluminum Alloys. *Metall. Mater. Trans. A* **2006**, *37* (6), 1999–2006. https://doi.org/10.1007/s11661-006-0142-7.

(63) Gao, L.; Ou, X.; Ni, S.; Li, K.; Du, Y.; Song, M. Effects of Θ′ Precipitates on the Mechanical Performance and Fracture Behavior of an Al–Cu Alloy Subjected to Overaged Condition. *Mater. Sci. Eng. A* **2019**, *762*, 138091. https://doi.org/10.1016/j.msea.2019.138091.

(64) Kim, K.; Roy, A.; Gururajan, M. P.; Wolverton, C.; Voorhees, P. W. First-Principles/Phase-Field Modeling of Θ′ Precipitation in Al-Cu Alloys. *Acta Mater.* **2017**, *140*, 344–354. https://doi.org/10.1016/j.actamat.2017.08.046.

(65) Starke, E. A. The Causes and Effects of "Denuded" or "Precipitate-Free" Zones at Grain Boundaries in Aluminum-Base Alloys. *JOM* **1970**, *22* (1), 54–63. https://doi.org/10.1007/BF03355628.

(66) Ibrahim, M.; Samuel, A.; Doty, H.; Samuel, F. Effect of Aging Conditions on Precipitation Hardening in Al-Si-Mg and Al-Si-Cu-Mg Alloys. *Int. J. Met.* **2017**, *11* (2), 274–286. https://doi.org/10.1007/s40962-016-0057-z.

(67) Starink, M. J.; Zahra, A.-M. B′ and β Precipitation in an Al–Mg Alloy Studied by DSC and TEM. *Acta Mater.* **1998**, *46* (10), 3381–3397. https://doi.org/10.1016/S1359-6454(98)00053-6.

(68) Scotto D'Antuono, D.; Gaies, J.; Golumbfskie, W.; Taheri, M. L. Grain Boundary Misorientation Dependence of β Phase Precipitation in an Al–Mg Alloy. *Scr. Mater.* **2014**, *76*, 81–84. https://doi.org/10.1016/j.scriptamat.2014.01.003.

(69) *A Handbook of Lattice Spacings and Structures of Metals and Alloys*; Elsevier, 1958. https://doi.org/10.1016/C2013-0-08243-6.

(70) Okamoto, H. Al-Mg (Aluminum-Magnesium). *J. Phase Equilibria Mater. Park* **1998**, *19* (6), 598.

(71) Terzi, S.; Salvo, L.; Suery, M.; Dahle, A. K. Coarsening Mechanisms during Isothermal Holding of a Dendritic Al-10wt%Cu Alloy. *Trans. Indian Inst. Met.* **2009**, *62* (4–5), 447–449. https://doi.org/10.1007/s12666-009-0060-7.

(72) Koch, G. H.; Brongers, M. P. H.; Thompson, N. G.; Virmani, Y. P.; Payer, J. H. Chapter 1 - Cost of Corrosion in the United States. In *Handbook of Environmental Degradation of Materials*; Kutz, M., Ed.; William Andrew Publishing: Norwich, NY, 2005; pp 3–24. https://doi.org/10.1016/B978-081551500-5.50003-3.

(73) Revie, R. W. *Corrosion and Corrosion Control: An Introduction to Corrosion Science and Engineering*; John Wiley & Sons, 2008.

(74) *Defense Management: Observations on Changes to the Reporting Structure for DOD's Corrosion Office and Its Implementation of GAO Recommendations*; U.S. Government Accountability Office, 2019.

(75) Yunovich, M.; Thompson, N. G. Corrosion of Highway Bridges: Economic Impact and Control Methodologies. *Concr. Int.* **2003**, *25* (1), 52–57.

(76) Glazoff, M. V.; Zolotorevsky, V. S.; Belov, N. A. *Casting Aluminum Alloys*; Elsevier, 2010.

(77) Vasudevan, A. K.; Doherty, R. D. *Aluminum Alloys--Contemporary Research and Applications: Contemporary Research and Applications*; Elsevier, 2012.

(78) Davis, J. R. *Corrosion of Aluminum and Aluminum Alloys*; ASM International, 1999.

(79) *Rare Earth-Based Corrosion Inhibitors*; Elsevier, 2014. https://doi.org/10.1016/C2013-0-16231-9.

(80) Aluminum Anodizing. In *Corrosion: Fundamentals, Testing, and Protection*; Cramer, S. D., Covino, B. S., Eds.; ASM International, 2003; pp 736–740. https://doi.org/10.31399/asm.hb.v13a.a0003680.

(81) Zhigang, F.; Cao, J.; Guan, Y. *Corrosion Control Technologies for Aluminum Alloy Vessel*; Springer Singapore, 2020. https://doi.org/10.1007/978-981-15-1932-1.

(82) Twite, R. L.; Bierwagen, G. P. Review of Alternatives to Chromate for Corrosion Protection of Aluminum Aerospace Alloys. *Prog. Org. Coat.* **1998**, *33* (2), 91–100. https://doi.org/10.1016/S0300-9440(98)00015-0.

(83) Bethencourt, M.; Botana, F. J.; Calvino, J. J.; Marcos, M.; RodrÍguez-Chacón, M. A. Lanthanide Compounds as Environmentally-Friendly Corrosion Inhibitors of Aluminium Alloys: A Review. *Corros. Sci.* **1998**, *40* (11), 1803–1819. https://doi.org/10.1016/S0010-938X(98)00077-8.

(84) Gharbi, O.; Thomas, S.; Smith, C.; Birbilis, N. Chromate Replacement: What Does the Future Hold? *Npj Mater. Degrad.* **2018**, *2* (1), 1–8. https://doi.org/10.1038/s41529-018-0034-5.

(85) Mansfeld, F.; Wang, Y. Development of "Stainless" Aluminum Alloys by Surface Modification. *Mater. Sci. Eng. A* **1995**, *198* (1–2), 51–61. https://doi.org/10.1016/0921-5093(95)80058-3.

(86) Nie, Z. R.; Jin, T.; Fu, J.; Xu, G.; Yang, J.; Zhou, J. X.; Zuo, T. Y. Research on Rare Earth in Aluminum. *Mater. Sci. Forum* **2002**, *396–402*, 1731–1736. https://doi.org/10.4028/www.scientific.net/MSF.396-402.1731.

(87) Cardinale, A. M.; Macciò, D.; Luciano, G.; Canepa, E.; Traverso, P. Thermal and Corrosion Behavior of as Cast Al Si Alloys with Rare Earth Elements. *J. Alloys Compd.* **2017**, *695*, 2180–2189. https://doi.org/10.1016/j.jallcom.2016.11.066.

(88) Nabawy, A. M.; Samuel, A. M.; Alkahtani, S. A.; Abuhasel, K. A.; Samuel, F. H. Role of Cerium, Lanthanum, and Strontium Additions in an Al – Si – Mg (A356) Alloy. *Int. J. Mater. Res.* **2016**, *107* (5), 446–458. https://doi.org/10.3139/146.111360.

(89) Ravi, M.; Pillai, U. T. S.; Pai, B. C.; Damodaran, A. D.; Dwarakadasa, E. S. A Study of the Influence of Mischmetal Additions to Ai-7si-0.3mg (Lm 25/356) Alloy. *Metall. Mater. Trans. A* **1996**, *27* (5), 1283–1292. https://doi.org/10.1007/BF02649865.

(90) Binnemans, K.; Jones, P. T. Rare Earths and the Balance Problem. *J. Sustain. Metall.* **2015**, *1* (1), 29–38. https://doi.org/10.1007/s40831-014-0005-1.

(91) Binnemans, K.; Jones, P. T.; Müller, T.; Yurramendi, L. Rare Earths and the Balance Problem: How to Deal with Changing Markets? *J. Sustain. Metall.* **2018**, *4* (1), 126–146. https://doi.org/10.1007/s40831-018-0162-8.

(92) Sedriks, A. J.; Green, J. A. S.; Novak, D. L. Corrosion Behavior of Aluminum-Boron Composites in Aqueous Chloride Solutions. *Metall. Trans.* **1971**, *2* (3), 871–875. https://doi.org/10.1007/BF02662748.

(93) Harrison, T. J. INTERGRANULAR CORROSION PROTOCOL DEVELOPMENT FOR 7075-T651 EXTRUSION. 7.

(94) Gschneidner, K. A.; Calderwood, F. W. The AI-Ce (Aluminum-Cerium) System. **1988**, *9* (6), 4.

(95) Massalski, T. B. The Al−Cu (Aluminum-Copper) System. *Bull. Alloy Phase Diagr.* **1980**, *1* (1), 27–33. https://doi.org/10.1007/BF02883281.

(96) Boyer, H. E. Heat Treating of Nonferrous Alloys. *Metallogr. Microstruct. Anal.* **2013**, *2* (3), 190–195. https://doi.org/10.1007/s13632-013-0074-8.

(97) Sims, Z. C.; Rios, O.; McCall, S. K.; Van Buuren, T.; Ott, R. T. Characterization of near Net-Shape Castable Rare Earth Modified Aluminum Alloys for High Temperature Application. In *Light Metals 2016*; Springer, 2016; pp 111–114.

(98) Arrabal, R.; Mingo, B.; Pardo, A.; Mohedano, M.; Matykina, E.; Merino, M. C.; Rivas, A. Microstructure and Corrosion Behaviour of A356 Aluminium Alloy Modified with Nd. *Mater. Corros.* **2015**, *66* (6), 535–541. https://doi.org/10.1002/maco.201407674.

(99) Meng, L.; Zheng, X. L. Overview of the Effects of Impurities and Rare Earth Elements in Al−Li Alloys. *Mater. Sci. Eng. A* **1997**, *237* (1), 109–118. https://doi.org/10.1016/S0921-5093(97)00096-8.

(100) Nie, Z. R.; Jin, T.; Fu, J.; Xu, G.; Yang, J.; Zhou, J. X.; Zuo, T. Y. Research on Rare Earth in Aluminum. In *Aluminium Alloys 2002 - ICAA8*; Materials Science Forum; Trans Tech Publications Ltd, 2002; Vol. 396, pp 1731–0. https://doi.org/10.4028/www.scientific.net/MSF.396-402.1731.

(101) Dabalà, M.; Armelao, L.; Buchberger, A.; Calliari, I. Cerium-Based Conversion Layers on Aluminum Alloys. *Appl. Surf. Sci.* **2001**, *172* (3–4), 312–322. https://doi.org/10.1016/S0169-4332(00)00873-4.

(102) Song, Y. L.; Liu, Y. H.; Wang, S. H.; Yu, S. R.; Zhu, X. Y. Effect of Cerium Addition on Microstructure and Corrosion Resistance of Die Cast AZ91 Magnesium Alloy. *Mater. Corros.* **2007**, *58* (3), 189–192. https://doi.org/10.1002/maco.200603988.

(103) Zhang, X.; Wang, Z.; Zhou, Z.; Xu, J. Effects of Cerium and Lanthanum on the Corrosion Behavior of Al-3.0 Wt.%Mg Alloy. *J. Mater. Eng. Perform.* **2016**, *25* (3), 1122–1128. https://doi.org/10.1007/s11665-016-1948-0.

(104) Wang, H.; Jiang, B.; Yi, D.; Wang, B.; Liu, H.; Wu, C.; Shen, F. Microstructure, Corrosion Behavior and Mechanical Properties of a Non-Isothermal Ageing Treated Cast Al–4.5Cu–3.5Zn–0.5Mg Alloy. *Mater. Res. Express* **2020**, *7* (1), 016547. https://doi.org/10.1088/2053-1591/ab638a.

(105) *Properties and Selection of Aluminum Alloys*; Anderson, K., Weritz, J., Kaufman, J. G., Eds.; ASM International, 2019. https://doi.org/10.31399/asm.hb.v02b.9781627082105.

(106) Yan, J.; Heckman, N. M.; Velasco, L.; Hodge, A. M. Improve Sensitization and Corrosion Resistance of an Al-Mg Alloy by Optimization of Grain Boundaries. *Sci. Rep.* **2016**, *6* (1), 26870. https://doi.org/10.1038/srep26870.

(107) Jain, S.; Lim, M. L. C.; Hudson, J. L.; Scully, J. R. Spreading of Intergranular Corrosion on the Surface of Sensitized Al-4.4Mg Alloys: A General Finding. *Corros. Sci.* **2012**, *59*, 136–147. https://doi.org/10.1016/j.corsci.2012.02.018.

(108) Zhang, R.; Qiu, Y.; Qi, Y.; Birbilis, N. A Closer Inspection of a Grain Boundary Immune to Intergranular Corrosion in a Sensitised Al-Mg Alloy. *Corros. Sci.* **2018**, *133*, 1–5. https://doi.org/10.1016/j.corsci.2018.01.009.

(109) Zhang, R.; Knight, S. p.; Holtz, R. l.; Goswami, R.; Davies, C. h. j.; Birbilis, N. A Survey of Sensitization in 5xxx Series Aluminum Alloys. *CORROSION* **2015**, *72* (2), 144–159. https://doi.org/10.5006/1787.

(110) Öztürk, İ.; Hapçı Ağaoğlu, G.; Erzi, E.; Dispinar, D.; Orhan, G. Corrosion Behavior of B and Ti Grain-Refined Sr-Modified A356. *J. Mater. Eng. Perform.* **2018**, *27* (10), 5197–5204. https://doi.org/10.1007/s11665-018-3657-3.

(111) Kuchariková, L.; Liptáková, T.; Tillová, E.; Kajánek, D.; Schmidová, E. Role of Chemical Composition in Corrosion of Aluminum Alloys. *Metals* **2018**, *8* (8), 581. https://doi.org/10.3390/met8080581.

(112) Salonitis, K.; Jolly, M.; Pagone, E.; Papanikolaou, M. Life-Cycle and Energy Assessment of Automotive Component Manufacturing: The Dilemma Between Aluminum and Cast Iron. **2019**, 23.

(113) Grieb, B. The Al-Ce-Fe System (Aluminum-Cerium-Iron). *Bull. Alloy Phase Diagr.* **1989**, *10* (6), 669–671. https://doi.org/10.1007/BF02877642.

(114) Yang, T.; Wu, C.; Su, X.; Tu, H.; Liu, Y.; Peng, H.; Wang, J. The 450 and 600 °C Isothermal Sections of the Al-Ce-Zn (0-33.3 at.%Ce) Ternary System. *J. Phase Equilibria Diffus.* **2015**, *36* (3), 198–208. https://doi.org/10.1007/s11669-015-0372-8.

(115) Belov, N. A.; Khvan, A. V. The Ternary Al–Ce–Cu Phase Diagram in the Aluminum-Rich Corner. *Acta Mater.* **2007**, *55* (16), 5473–5482. https://doi.org/10.1016/j.actamat.2007.06.009.

(116) Belov, N. A.; Khvan, A. V. Structure and Phase Composition of Alloys of the Al-Ce-Cu System in the Region of the Al-Al8CeCu4 Quasi-Binary Join. *Russ. J. Non-Ferr. Met.* **2007**, *48* (1), 45–50. https://doi.org/10.3103/S1067821207010099.

(117) Wang, H.; Wei, W. Coordinating Technological Progress and Environmental Regulation in CO2 Mitigation: The Optimal Levels for OECD Countries & Emerging Economies. *Energy Econ.* **2020**, *87*, 104510. https://doi.org/10.1016/j.eneco.2019.104510.

(118) *Critical Materials Strategy*; United States Department of Energy, 2011.

(119) Binnemans, K.; Jones, P. T. Rare Earths and the Balance Problem. *J. Sustain. Metall.* **2015**, *1* (1), 29–38. https://doi.org/10.1007/s40831-014-0005-1.

(120) Capuzzi, S.; Timelli, G. Preparation and Melting of Scrap in Aluminum Recycling: A Review. *Metals* **2018**, *8* (4), 249. https://doi.org/10.3390/met8040249.

(121) Menzie, W. D.; Barry, J. J.; Bleiwas, D. I.; Bray, E. L.; Goonan, T. G.; Matos, G. *The Global Flow of Aluminum from 2006 through 2025*; Open-File Report; USGS Numbered Series 2010–1256; U.S. Geological Survey, 2010; pp 3–4.

(122) Li, Y.; Yue, Q.; He, J.; Zhao, F.; Wang, H. When Will the Arrival of China's Secondary Aluminum Era? *Resour. Policy* **2020**, *65*, 101573. https://doi.org/10.1016/j.resourpol.2019.101573.

(123) Nobrega, J. H. C. Sustainability in Manufacturing Processes: Practices Performed in Metal Forming, Casting, Heat Treatment, Welding and Electrostatic Painting. *Int. J. Sustain. Dev.* 15.

(124) Wong, V. W.; Tung, S. C. Overview of Automotive Engine Friction and Reduction Trends–Effects of Surface, Material, and Lubricant-Additive Technologies. *Friction* **2016**, *4* (1), 1–28. https://doi.org/10.1007/s40544-016-0107-9.

(125) Lee, W.; Schubert, E.; Li, Y.; Li, S.; Bobba, D.; Sarlioglu, B. Overview of Electric Turbocharger and Supercharger for Downsized Internal Combustion Engines. *IEEE Trans. Transp. Electrification* **2017**, *3* (1), 36–47. https://doi.org/10.1109/TTE.2016.2620172.

(126) World Aluminium — Mass Flow Statistics http://www.world-aluminium.org/statistics/massflow/ (accessed May 1, 2020).

(127) U.S. Geological Survey. *Mineral Commodity Summaries 2001-2018*, 2001st–2018th ed.; Reston, VA, 2001.

(128) Du, X.; Graedel, T. E. Uncovering the End Uses of the Rare Earth Elements. *Sci. Total Environ.* **2013**, *461–462*, 781–784. http://dx.doi.org/10.1016/j.scitotenv.2013.02.099.

(129) Haque, N.; Hughes, A.; Lim, S.; Vernon, C. Rare Earth Elements: Overview of Mining, Mineralogy, Uses, Sustainability and Environmental Impact. *Resources* **2014**, *3* (4), 614–635. https://doi.org/10.3390/resources3040614.

(130) Gambogi, J. Rare Earths. In *2015 Minerals Yearbook*; Reston, VA, 2018.

(131) Goonan, T. G. *Rare Earth Elements: End Use and Recyclability*; Scientific Investigations Report; USGS Numbered Series 2011–5094; U.S. Geological Survey: Reston, VA, 2011; Vol. 2011–5094. https://doi.org/10.3133/sir20115094.

(132) Lokanc, M.; Eggert, R.; Redlinger, M. *The Availability of Indium: The Present, Medium Term, and Long Term*; NREL/SR--6A20-62409, 1327212; 2015; p NREL/SR--6A20-62409, 1327212. https://doi.org/10.2172/1327212.

(133) Binnemans, K.; Jones, P. T.; Müller, T.; Yurramendi, L. Rare Earths and the Balance Problem: How to Deal with Changing Markets? *J. Sustain. Metall.* **2018**, *4* (1), 126–146. https://doi.org/10.1007/s40831-018-0162-8.

(134) Sprecher, B.; Daigo, I.; Murakami, S.; Kleijn, R.; Vos, M.; Kramer, G. J. Framework for Resilience in Material Supply Chains, With a Case Study from the 2010 Rare Earth Crisis. *Environ. Sci. Technol.* **2015**, *49* (11), 6740–6750. https://doi.org/10.1021/acs.est.5b00206.

(135) Haynes, W. M. Abundance of Elements in the Earth's Crust and the Sea. In *CRC Handbook of Chemistry and Physics*; CRC Press, 2014.

(136) *Mineral Yearbook 2020: Litihum*; USGS.

(137) Kesler, M. S.; Neveau, M. L.; Carter, W. G.; Henderson, H. B.; Sims, Z. C.; Weiss, D.; Li, T. T.; McCall, S. K.; Glicksman, M. E.; Rios, O. Liquid Direct Reactive Interface Printing of Structural Aluminum Alloys. *Appl. Mater. Today* **2018**, *13*, 339–343. https://doi.org/10.1016/j.apmt.2018.10.005.

(138) Plotkowski, A. J. Additive Manufacturing Methods Using Aluminum-Rare Earth Alloys and Products … US20180080103A1, March 22, 2018.

(139) Raghavan, V. Al-Ce-Mg (Aluminum-Cerium-Magnesium). *J. Phase Equilibria Diffus.* **2007**, *28* (5), 453–455. https://doi.org/10.1007/s11669-007-9136-4.

(140) Sjölander, E.; Seifeddine, S. The Heat Treatment of Al–Si–Cu–Mg Casting Alloys. *J. Mater. Process. Technol.* **2010**, *210* (10), 1249–1259. https://doi.org/10.1016/j.jmatprotec.2010.03.020.

(141) Simonovic, D.; Sluiter, M. H. F. Impurity Diffusion Activation Energies in Al from First Principles. *Phys. Rev. B* **2009**, *79* (5), 054304. https://doi.org/10.1103/PhysRevB.79.054304.

(142) Weiss, D. Improved High-Temperature Aluminum Alloys Containing Cerium. *J. Mater. Eng. Perform.* **2019**, *28* (4), 1903–1908. https://doi.org/10.1007/s11665-019-3884-2.

(143) Swinkels, F. B.; Wilkinson, D. S.; Arzt, E.; Ashby, M. F. Mechanisms of Hot-Isostatic Pressing. **1983**. http://dx.doi.org/10.22028/D291-23986.

(144) Atkinson, H. V.; Davies, S. Fundamental Aspects of Hot Isostatic Pressing: An Overview. *Metall. Mater. Trans. A* **2000**, *31* (12), 2981–3000. https://doi.org/10.1007/s11661-000-0078-2.

(145) Atkinson and Davies - Fundamental Aspects of Hot Isostatic Pressing An .Pdf.

(146) Mashl, S. J.; Hebeisen, J. C.; Apelian, D.; Wang, Q. Hot Isostatic Pressing of A356 and 380/383 Aluminum Alloys: An Evaluation of Porosity, Fatigue Properties and Processing Costs. *SAE Trans.* **2000**, *109*, 27–33.

(147) Hojjati, B.; Wade, S. H. U.S. Household Energy Consumption and Intensity Trends: A Decomposition Approach. *Energy Policy* **2012**, *48*, 304–314. https://doi.org/10.1016/j.enpol.2012.05.024.

(148) Campbell, G. A. Rare Earth Metals: A Strategic Concern. *Miner. Econ.* **2014**, *27* (1), 21–31. https://doi.org/10.1007/s13563-014-0043-y.

(149) *Rare Earths — Market Report*; Roskill, 2019.

(150) Emsley, J. Unsporting Scandium. *Nat. Chem.* **2014**, *6* (11), 1025–1025. https://doi.org/10.1038/nchem.2090.

(151) Yan, P.; Zhang, G.; Yang, Y.; Mclean, A. Characterization and Pre-Concentration of Scandium in Low-Grade Magnetite Ore. *JOM* **2019**, *71* (12), 4666–4673. https://doi.org/10.1007/s11837-019-03541-5.

(152) Røyset, J.; Ryum, N. Scandium in Aluminium Alloys. *Int. Mater. Rev.* **2005**, *50* (1), 19–44. https://doi.org/10.1179/174328005X14311.

(153) Sabau, A. S.; Mirmiran, S.; Glaspie, C.; Li, S.; Apelian, D.; Shyam, A.; Allen Haynes, J.; Rodriguez, A. F. Hot-Tearing Assessment of Multicomponent Nongrain-Refined Al-Cu

Alloys for Permanent Mold Castings Based on Load Measurements in a Constrained Mold. *Metall. Mater. Trans. B* **2018**, *49* (3), 1267–1287. https://doi.org/10.1007/s11663-018-1204-0.

(154) *Electronic Code of Federal Regulations (ECFR)*.

Appendices

Appendix 1: Composition of Commercial Alloys Cast During

Table A-1: Compositions of Alloys used throughout report

Alloy	Al	Si	Fe	Cu	Mn	Mg	Ni	Zn	Ti	Sn	Be	B	Ag	Zr	Li	Others each	Others total
A206	Bal	0.5	<0.10	4.2-5.0	0.20-.50	0.15-.35	<0.05	<0.1	0.15-0.30	<0.05						0.05	0.15
A356	Bal	6.5-7.5	<0.2	<0.20	0.18	0.20-.45		<0.1	0.18							0.05	0.15
HP A356	Bal	7.0	<0.1	<0.01	<0.01	0.35		<0.01	0.08								
535.2	Bal	<0.1	<0.1	<0.05	0.1-.25				0.1-.25		0.003-0.007	0.002				0.05	0.15
2055	Bal	0.07	0.1	3.2-4.2	0.1-0.5	0.2-0.6		0.3-0.7	0.1				0.2-0.7	0.05-0.15	1-1.3	0.05	0.15
2618	Bal	0.1-0.25	0.9-1.3	1.9-2.7		1.6	1	0.1	0.04-.10							0.05	0.15
4032	Bal	11-13.5	<1.0	0.5-1.3		0.8-1.3	0.5-1.3	<0.25								0.05	0.15

* all values in weight percent

Appendix 2: Mechanical Properties of Thermally Exposed Samples

Table A-2: Mechanical Properties of Al-Ce-Mg alloys compared to traditional alloy before and after thermal exposure.

Alloy	Thermal Exposure	Tensile (Mpa)	Yield (Mpa)	%E	Yield Retention
A206-T7	As-Treated	434.4	344.8	2.5	-
	250C 500 Hours	335.1	231.0	6.9	67.00%
	250C 1000 hours	333.7	235.8	5.6	68.40%
	400C 500 hrs	283.4	139.3	14.4	40.40%
	400C 1000 hrs	283.4	135.1	17.1	39.20%
A356-T6	As-Treated	227.5	165.5	3.5	-
	250C 500 Hours	127.6	55.2	25.0	33.33%
	250C 1000 hours	127.6	55.2	30.3	33.33%
	400C 500 hrs	131.0	48.3	24.9	29.17%
	400C 1000 hrs	136.5	54.5	24.6	32.92%
Al8Ce10Mg	As-Cast	207.5	162.7	0.8	-
	250C 500 Hours	191.7	160.0	1.8	98.31%
	250C 1000 hours	186.9	151.7	1.0	93.22%
	400C 500 hrs	233.1	186.2	1.6	114.41%
	400C 1000 hrs	222.7	195.8	1.7	120.34%

Appendix 3: Additional Images of Salt Fog Corroded Samples

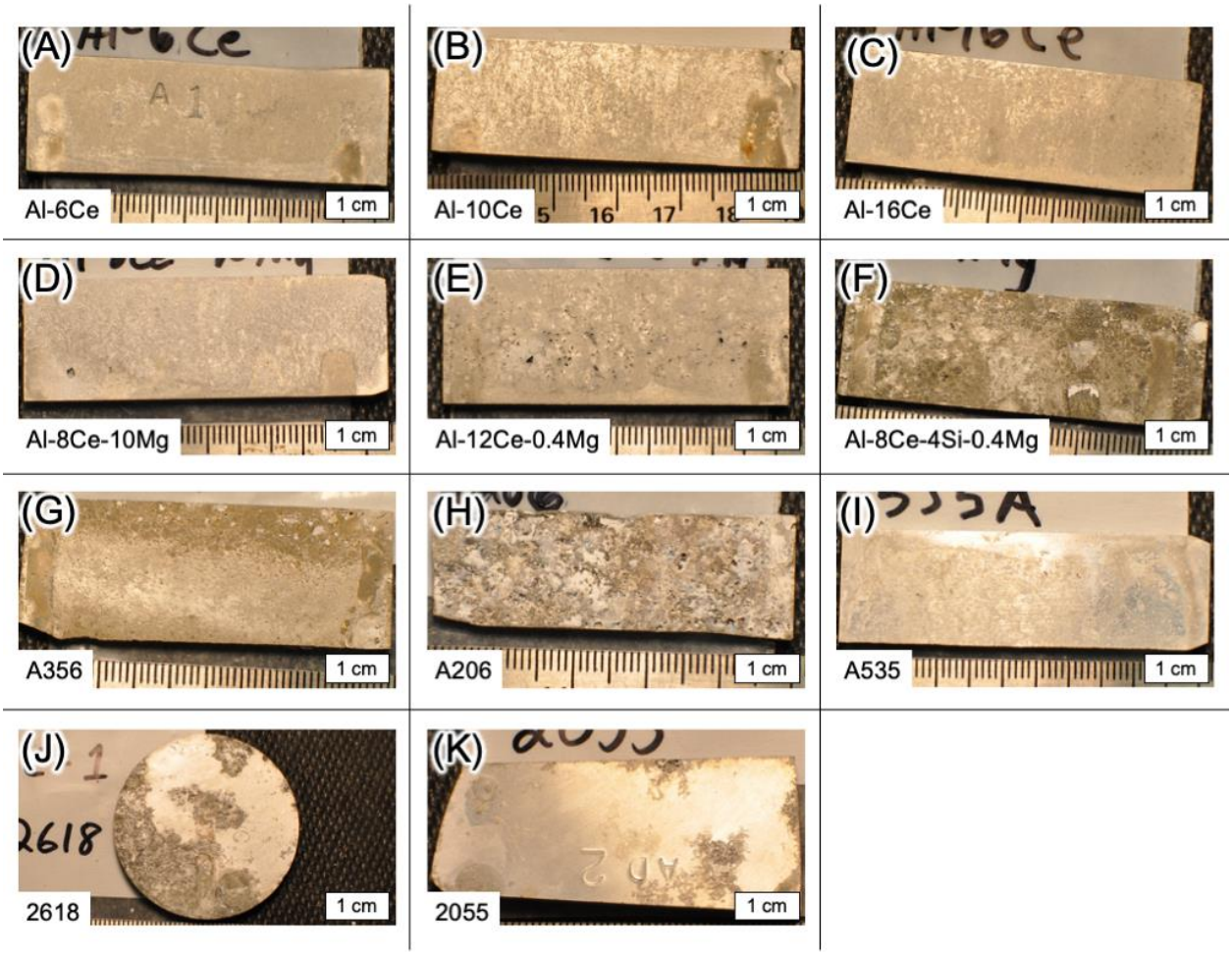

Figure A.1: Collection of images taken after sample exposure to salt fog for 1000hrs follwed by a rinse and cleaning with ultrasound.

Vita

Zachary Sims grew up in Greeneville, TN where he attended high school at Greeneville High School home of the Greeneville Green Devils. Following high school, he moved to Knoxville, TN to attend the University of Tennessee Knoxville. After receiving his bachelor's degree in physics in 2014, Zachary took a position at ORAU as an intern working in the Correlated Electron Material Group at Oak Ridge National Laboratory under the guidance of Athena Safa-Sefat. Shortly following this appointment, he transitioned to working with Orlando Rios in the Deposition Science and Technology Group on the development of Al-Ce alloys in late 2014. He remained in this position for roughly a year and a half until starting his Ph.D. work in the Bredesen Center at the University of Tennessee Knoxville in 2016. At the same time as beginning his Ph.D. work, Zachary became married to Melinda, his now wife of 4 years. After the completion of his Ph.D. work, Zachary will move to Livermore California where he will begin work as a Lawrence Fellow at Lawrence Livermore National Laboratory.